The essential role of the plasma sheath in plasma-liquid interaction and its applications – a perspective

Patrick Vanraes[1,*], Annemie Bogaerts[1]

[1]*PLASMANT, Department of Chemistry, University of Antwerp, Universiteitsplein 1, 2610 Wilrijk-Antwerp, Belgium*
*Corresponding author. Email: patrick.vanraes@uantwerpen.be

Abstract

Based on current knowledge, a plasma-liquid interface looks and behaves very differently from its counterpart at a solid surface. Local processes characteristic to most liquids include a stronger evaporation, surface deformations, droplet ejection, possibly distinct mechanisms behind secondary electron emission, the formation of an electric double layer and an ion drift-mediated liquid resistivity. All of them can strongly influence the interfacial charge distribution. Accordingly, the plasma sheath at a liquid surface is most likely unique in its own way, both with respect to its structure and behavior. However, insights into these properties are still rather scarce or uncertain, and more studies are required to further disclose them. In this Perspective Article, we argue why more research on the plasma sheath is not only recommended, but crucial to an accurate understanding of plasma-liquid interaction. First, we analyze how the sheath regulates various elementary processes at the plasma-liquid interface, in terms of the electrical coupling, the bidirectional mass transport and the chemistry between plasma and liquid phase. Next, these three regulatory functions of the sheath are illustrated for concrete applications. Regarding the electrical coupling, a great deal of attention is paid to the penetration of fields into biological systems, due to their relevance for plasma medicine, plasma agriculture and food processing. Further, we illuminate the role of the sheath in nuclear fusion, nanomaterial synthesis and chemical applications. As such, we hope to motivate the plasma community for more fundamental research on plasma sheaths at liquid surfaces.

1. Introduction

In 1928, Langmuir introduced the term *plasma* to describe the body of an ionized gas where the free electrons and ions occur in about equal numbers [1]. This balance corresponds to a nearly negligible space charge, which is now known as the plasma criterion of quasi-neutrality. Already in 1923, Langmuir distinguished this quasi-neutral zone from the thin layer with an appreciable space charge formed at any plasma boundary, for which he used the term *sheath* [2]. For instance, at the interface between a plasma and a solid object on a floating potential, the free electrons reach the surface by diffusion on a much smaller time scale than the ions. Therefore, the object obtains a negative surface charge, while a thin region around it gets depleted from electrons and thus forms a positively charged plasma sheath. Consequently, an electric field is built up in the sheath, repelling electrons back into the plasma and accelerating positive ions towards the negatively charged surface.

In many applications, this leads to undesirable effects, like damage to the plasma reactor wall by sputtering or an increased heat flux [3]. In other applications, such as plasma etching, sputtering and ion implantation, the sheath plays a central role, because it determines the energy and angular distributions of the incident ions, which are largely responsible for the surface modification [4, 5]. The sheath generally contributes to the interfacial physical and chemical processes working during any type of plasma treatment of materials, further illustrating its technical importance. Moreover, its properties govern the plasma boundary conditions, as well as the emission of particles from the surface into the plasma volume, which both influence the overall plasma behavior. All these effects have motivated numerous investigations since the dawning of plasma physics. The study of the plasma sheath has developed accordingly into a fully-fletched subdomain.

Nonetheless, very few attention has been paid to the plasma sheath in research on plasma-liquid interaction. This remarkable observation is readily substantiated with a quick exploration using any scientific search engine. Combining the search terms “plasma-liquid interactions” and “plasma sheath” or “Debye sheath” in Google Scholar, for example, provides a total of only 36 publications at this moment of writing, as opposed to nearly 1000 results with the former term alone. Yet, even with these publications, a careful analysis of the plasma sheath at a liquid surface is still lacking in scientific literature. A profound understanding is urgently needed, because of the rapidly increasing interest in the fundamentals of plasma-liquid interaction, for applications ranging from water treatment [6-10], nanomaterial synthesis [10-13], polymer solution treatment [10, 14-16] and chemical analysis [10, 17, 18] to food processing [19-21], plasma agriculture [22-24] and plasma medicine [25-32]. The latter three applications namely also fall under this overarching research field, because biological tissue is naturally surrounded by a liquid layer. They deserve a special mentioning as important drivers of the field, with promising applications for sterilization [33, 34], for enhanced seed germination and plant growth [22-24], and for skin, wound, dental and cancer treatment [25-32]. Modeling and optimizing the plasma treatment in these processes requires the appreciation of the sheath under the corresponding conditions.

With the present Perspective Article, we aim to provoke a higher level of awareness regarding the importance of the plasma sheath at a liquid surface, by exploring the peculiarities for the situation at a liquid surface. First, Section 2 emphasizes the general importance of the sheath for plasma-liquid

interaction. After discussing the fundamental considerations (Section 2.1), we explore the role of the sheath in the bidirectional mass transport (Section 2.2) and the chemistry (Section 2.3) at a plasma-liquid interface. Doing so, we argue why the fundamental study of the sheath at a liquid surface is not only interesting, but essential for an accurate understanding of plasma-liquid interaction, as well as for a faster progress in the various applications. Afterwards, we discuss the variability of sheaths, with special attention to anode sheaths (Section 2.4). Next, Sections 3 to 5 illustrate this claim for a few selected processes. We start with the role of the sheath as an electric field regulator for food processing, plasma agriculture and plasma medicine (Section 3). According to the second example, the sheath can also serve as a mass transport regulator at liquid metal walls in a nuclear fusion reactor (Section 4). Thirdly, we zero in on the effect of the sheath on the chemistry in nanomaterial synthesis and other applications (Section 5). Subsequently, Section 6 deals with several insights and gaps in knowledge regarding liquid-related sheath properties, including electron emission from a liquid surface (Section 6.1) and droplet formation at the interface (Section 6.2). Finally, Section 7 concludes this review with a summary of the newly obtained insights and recommendations for future research. Accordingly, we hope to increase awareness on the essential role of the sheath in plasma-liquid interaction, as well as to provide a starting platform for advanced models and theories describing the underlying physics.

2. The general importance of the plasma sheath in plasma-liquid interaction

2.1 Fundamental considerations

In Section 2, we argue why the plasma sheath deserves a place in the spotlight in both fundamental and applied research on plasma-liquid interaction. Since this perspective builds further on the insights obtained in our previous review paper [35], there will be several occasions in this section where we refer to it, for more detailed information. For a structured discussion, we limit Sections 2.1 till 2.3 to ion sheaths with a positive space charge at a negatively charged surface. Such sheaths are, for instance, encountered at a cathode or at a material on a floating potential, submerged in a plasma. Section 2.4 will deal with the situation at a liquid anode and the ways in which sheaths can differ.

From a fundamental point of view, the plasma sheath at a liquid surface is more than simply a theoretical curiosity. Similar to the case at a solid surface, it determines the boundary conditions of the plasma phase. According to the fluid dynamics continuity equations, this includes the mass and energy transport across the boundary. More specifically, the sheath plays an active role in these equations, as it generally accelerates positive ions towards the surface, increasing the heat flux into the material, which on its turn influences the emission of particles and heat into the plasma. Besides that, the sheath governs the boundary conditions for Maxwell's equations, which do not only dictate the local potential drop across the sheath, but also affect the behavior of the plasma and the liquid due to their electrical coupling. In simplified terms, the sheath thus forms an essential part in the equivalent circuit of the entire plasma reactor. A change in its properties will therefore determine the electrical potential distribution over the plasma and liquid phases. More specifically, rapid fluctuations of the sheath potential regulate the field penetration into the liquid phase. We will explain and illustrate this in Section 3 in more detail for field-

induced processes in biological materials. For a more fundamental discussion on the electrical coupling in plasma-liquid systems, we refer to our pervious review [35].

Further, the plasma sheath regulates the mechanisms behind secondary electron emission from a surface in multiple ways. First of all, it defines the local electric field, which is largely responsible for the kinetic energy distributions of the charged plasma species bombarding the material. The fast incident ions can subsequently transfer their energy to bound electrons in the surface through a kinetic electron emission mechanism [36-38]. Secondly, the electric field at the interface can modify the local electronic structure of the material. The sheath field is namely closely related to the local field of the electrical double layer in the liquid, which can reach towards the order of 10^9 V/m at submerged electrodes and electrocatalysts [39-41]. This approaches the threshold of 3.0×10^9 V/m for dielectric breakdown of water without bubble formation [42]. Local fields as low as 10^7 V/m have been observed to induce a refractive index change, which could be attributed to reorientation of the water molecules or the excitation of their OH stretch vibration [43, 44]. Such effects may translate themselves into the bending of the band scheme or the shifting of individual surface levels. Note in this regard that an amorphous semiconductor model is frequently used to explain laser-induced breakdown in dielectric liquids (see e.g. [45-52]). In our previous review paper, we have promoted this view for plasma initiation in the liquid phase and plasma-liquid interaction [35]. Recently, Delgado et al. adopted a similar band structure model for the plasma-water interface, to explain their experimental study on secondary electron emission at a water electrode [53]. For a field aiming towards the liquid phase, band bending or the surface level shifts lower the energy required for the release of electrons. The sheath may therefore give rise to field-enhanced ion-induced secondary electron emission, as further explained in Section 6.1.

As a side note for the case of hydrated electrons at the air-water interface, a reduction of the vertical binding energy with a few tenths of an eV may actually already be naturally present relative to the bulk species. This is suggested by simulation results independently obtained with several quantum mechanical methods (see e.g. [54-58]). As a possible explanation, interfacial solvated electrons may be subject to a strong naturally present local field. Remarkably large field strength values have namely been obtained in several computational studies for the vapor-water interface: 10^8 V/m with quasichemical theory [59], 8×10^8 V/m with classical molecular dynamics simulations [60], 10^9 V/m with density functional theory [61], and 1.5×10^{10} V/m with ab initio molecular dynamics simulation [62]. These high values were mostly attributed to the arranged orientation of water molecules at the water surface, in analogy with recent electrical field measurements for the water-oil interface of aqueous microdroplets by means of stimulated Raman excited fluorescence microscopy [63].

Thirdly, a sufficiently large number of emitted electrons alters the electron density and thus the space charge in the sheath. On its turn, this adjusts the sheath properties. In this way, a feedback loop emerges between the sheath and the electron emission. The possible mechanisms behind electron emission from a liquid surface are also more elaborately discussed in our previous review [35].

Additionally, the liquid surface structure adapts to the presence of the sheath field in a myriad of ways (see Figure 1). The microscopic structure is expected to diverge from the more familiar gas-liquid interface, due to the appearance of the net surface charge. Analogous to a liquid adjacent to a solid

electrode or surface, an electrical double layer forms in contact with the plasma sheath. Such reorganization of the liquid determines which condensed species are directly exposed to the incoming plasma particles. This may strongly influence the mass transport across the interface. In contrast to solids, liquids generally conduct electricity through ion drift, giving their surface a distinct resistive behavior. In Section 3.3, we will discuss an experimental indication that this may lead to a more diffuse type of plasma than usually observed at a solid surface, so-called resistive barrier discharge. Moreover, the liquid surface can deform by the Coulomb attraction from the sheath, to generate capillary waves or Taylor cones [35, 64-68]. When these deformations become extreme or get combined with other violent plasma processes, such as sputtering, droplets will be released towards the gas phase. Likewise, droplet emission is also expected when the sheath generates a sufficiently strong heat flux onto the liquid to initiate local boiling. Many liquids generally display stronger evaporation than solids, modifying the composition of the contacting gas phase. Similar to electron emission, these liquid-specific phenomena affect the electric field and space charge distribution over the surface, creating a feedback loop between them and the sheath. Since these processes are absent for solids, the plasma sheath at a liquid surface is expected to have a unique character and behavior, depending on the liquid properties. In other words, classical sheath models are likely inapplicable to the plasma-liquid interface. The fundamental study of plasma sheaths at liquids is therefore highly required, in order to scrutinize how this multitude of factors affects the plasma-liquid interactions. Our previous review introduces the general role of evaporation, droplet ejection and surface deformation in further detail [35].

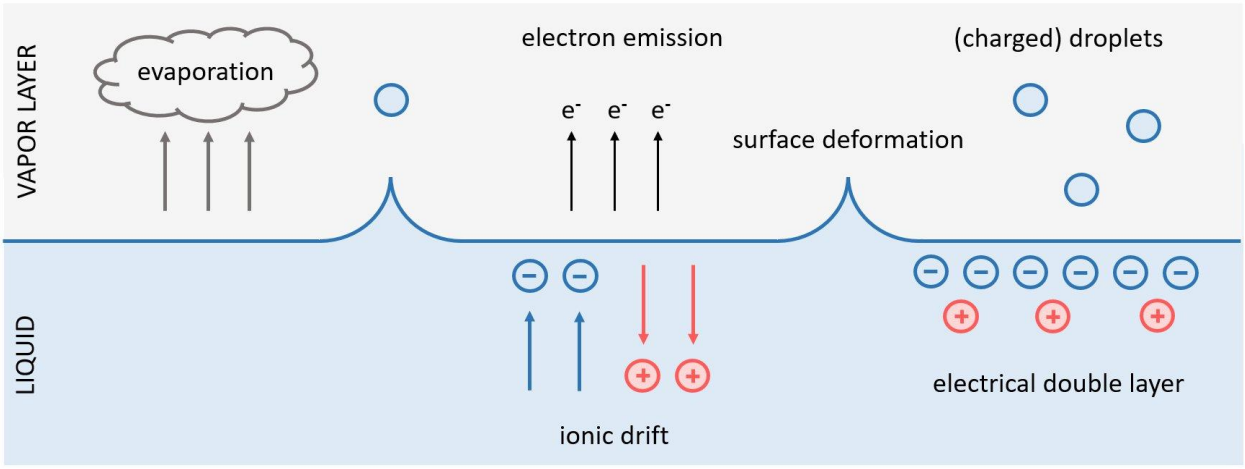

Figure 1. Schematic summary of the processes at a plasma-liquid interface which are expected to affect the plasma sheath. Reversely, the sheath also affects these processes, creating a feedback loop.

2.2 Bidirectional mass transport across the plasma sheath

Apart from the fundamental considerations in Section 2.1, a detailed understanding of the plasma sheath over a liquid is also crucial for an efficient and goal oriented optimization of the numerous related technologies. A large portion of these methods are predicated on transferring reactive plasma species into the liquid phase. Atmospheric air plasma, for instance, produces several types of reactive oxygen

species, such as ozone, hydroxyl radicals and hydrogen peroxide. When brought into the liquid phase, these species readily react with the solvent or solutes, changing the molecular structure. Organic pollutants in water can be decomposed in this manner, ideally down to CO_2 and H_2O as harmless end products. This makes plasma one of the advanced oxidation techniques considered for water treatment. Similarly, plasma treatment has been proposed for the decomposition of pesticides on the surface of seeds before germination [24, 69]. Next to that, reactive oxygen species can be used to kill bacteria for sterilization purposes, in food processing or plasma medicine. Plasma-generated reactive oxygen and nitrogen species often contribute to the liquid chemistry as well. They are especially crucial in plasma treatment of cancerous tumors [25, 30-32] and in plasma agriculture for fertilizer synthesis [22, 23]. Besides this, plasma gases other than air have been applied for polymer solution treatment, as a preparation step before spin coating [10, 14-16]. The Plasma-Liquid Interactions Roadmap from 2016 [68] puts a strong emphasis on these types of applications, where the plasma forms a means to induce chemical reactions in the liquid.

Correspondingly, the primary reactive species in the solvent need to be either generated directly in the liquid phase, or transferred into the liquid from the gaseous phase. Regarding the former pathway, absorption of plasma-produced UV photons by the solvent or solutes is generally considered as the main mechanism (see e.g. [68]). For the latter pathway, the reactive plasma species need to cross the sheath before they enter the liquid phase. Especially the transport of ions and electrons is expected to be affected by the sheath, due to the presence of the electric field. Their collisions with neutrals additionally amend the overall plasma species transmission. At atmospheric pressure and room temperature, ions have a mean-free path l smaller than 1 μm, which is significantly smaller than the expected sheath thickness [68]. The ions will anisotropically transfer their kinetic energy to the neutrals in the thin sheath section with a thickness l right above the liquid surface. Charge transfer reactions between the ions and neutrals additionally produce hot neutrals traveling towards the surface. Accordingly, the pressure and temperature of the neutrals in this layer are better expressed as tensors, instead of scalars. This likely affects their interaction with and transport into the liquid surface.

Analogously, the sheath mediates the reverse transfer of liquid species into the plasma as well, as summarized in Figure 2. For instance, a local electric field of a few kV/cm perpendicular to the liquid surface increases the evaporation rate of water [70, 71], while a parallel field causes a decrease [72]. Solutes may also be emitted into the gas phase in their entirety or in fragments, in which the sheath may play an important role. Electrical discharge is even able to extract non-volatile species from a solvent, in agreement with numerous experiments using a wide variety of plasma sources (see e.g. [17, 18]). This observation has laid the foundation for plasma-liquid systems in analytical chemistry. An example with a rich research history is the electrolyte cathode atmospheric glow discharge (ELCAD), where an electrolytic sample serves as the cathode of a diffuse plasma [73-76]. ELCAD allows the detection of aqueous trace metal ions, implying the transfer of the metal species from the liquid to the plasma phase. In theory, the metal species can be emitted into the plasma as ions or atoms, but the relative dominance and underlying physics of these mechanisms are still unclear. Inspiration can be taken from the mechanisms proposed for ion desorption by lasers, for which several uncertainties remain as well (see e.g. [77]).

The transfer of liquid species into the plasma phase is, however, relevant too for all other applications. Traces of compounds in the gas phase may namely contribute significantly to the overall plasma features [17, 78-82], affecting the desired effect. The decomposition of organic pollutants in a plasma reactor for water treatment can, for instance, occur for an important part in the gaseous phase. A detailed study on this topic has been performed by Ognier et al., who used an AC powered coaxial DBD reactor for the decomposition of four volatile compounds (acetic acid, phenol, ethanol and 1-heptanol) [83]. When the plasma was switched on, the mass transfer increased for each pollutant from the liquid to plasma, proportionally to the corresponding Henry law constant. According to the measurements, minimally 95% of the pollutant decomposition took place in the gas phase.

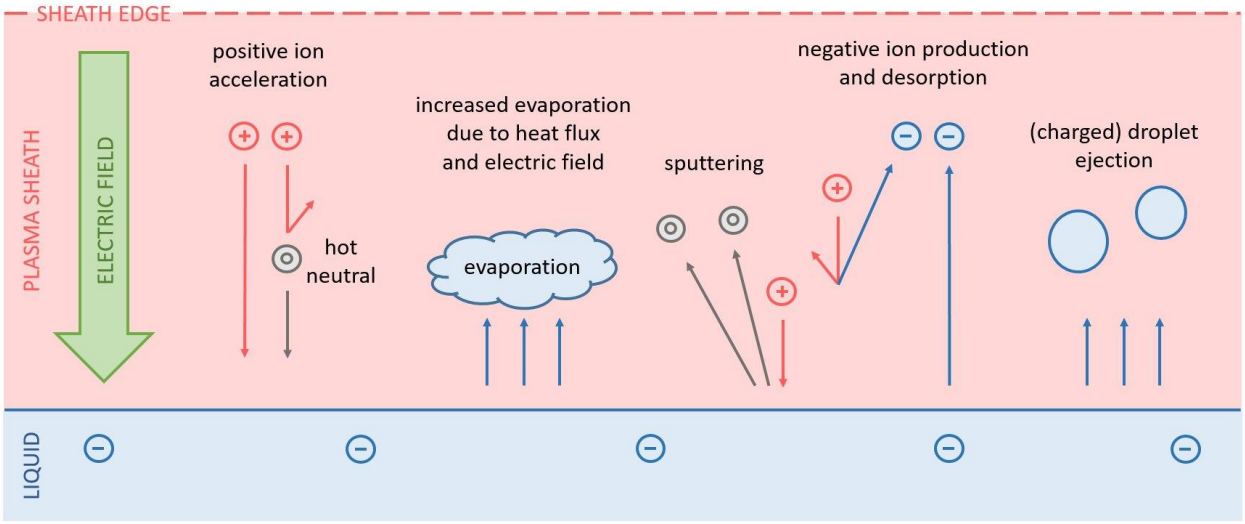

Figure 2. Schematic summary of the aspects of the bidirectional mass transport across the plasma sheath that are mostly affected by the presence of the electric field.

This effect is often neglected, but deserves special attention in applications, for a comprehensive insight into the overall process. In order to reach the plasma phase, liquid species have to cross the sheath, which acts as a barrier for positively charged droplets or ions, and facilitates the extraction of negative particles. This filter function of the sheath will be illustrated in Section 4 for fusion reactors with liquid walls. Further, the electric field strength at the liquid surface regulates the incident ion energy and heat flux, which determine the extent of sputtering, desorption, evaporation and droplet ejection. Therefore, an accurate description of the plasma sheath is required to understand the bidirectional mass transport through it. Current models ignore this effect, for example by assuming species transmission as dictated by Henry's law (see e.g. [84-89]). The validity of Henry's law at a plasma-liquid interface is, however, highly questionable, exactly due to all of the aforementioned plausible mechanisms. Even if the mass transport of certain solutes across the interface appears sensitive to their Henry's law constants, as in the experiments of Ognier et al. [83], the law itself may be violated, in the sense that the constants need to be recalibrated. For example, the Henry's law constants might depend on the local electric field.

2.3 Plasma sheath chemistry

Kinetic models neglecting the plasma sheath are at risk for another oversimplification. Such models simulate the chemical reactions in the system by means of separate chemistry sets, each corresponding to one region in the reactor. Obviously, at least two regions must be distinguished: the gaseous plasma and the liquid phase. In recent years, a few computational groups, including ours, have developed plasma-liquid models that limit their chemistry sets to these two zones (see e.g. [84-88]). The sets are coupled with one another through the boundary conditions at the plasma-liquid interface, describing the mass transport across the surface with, for instance, Henry's law and Raoult's law. Although such straightforward approach allows to obtain a first estimation of the reactive species densities, it disregards the chemistry in two crucial zones. First of all, the liquid surface is known to host its own chemistry, acting as a catalyst for both gaseous and liquid reactants [90, 91]. This surface chemistry is expected to significantly depend on the surface charge, which is closely related to the sheath properties. Moreover, the reactions of gaseous or liquid species at a solid surface or electrode can tremendously change under an applied electric field, as well-known from electrochemistry and surface science [92-95]. A similar influence may therefore take place at the plasma-liquid interface.

Secondly, the plasma sheath forms another zone with a unique chemistry. Its difference with the chemistry in the plasma bulk has several causes. To start with, a sheath is generally poor in electrons, which eliminates a large part of the electron impact reactions at low kinetic energies [96, 97]. Some sheaths or sheath regions, on the contrary, contain a negative space charge region where the reverse effect can occur. Examples are the anode sheath (see Section 2.4) and the thin Aston dark space at the cathode in a glow discharge [96]. Additionally, the strong electric field accelerates the electrons to far higher kinetic energies than in the bulk plasma, bringing their chemistry in a higher kinetic regime. The ion chemistry similarly shifts to a higher kinetic regime as well, allowing endothermic reactions which do not take place in the plasma bulk [98]. Based on experimental research, the energetic collisions of positive ions in the sheath are, for example, an important source of negative ions, even in low pressure plasmas [99-101]. At a non-evaporative solid surface, a fully collision-free sheath is observed only at pressures below 1 Pa [102, 103]. At a liquid surface, a substantially larger portion of liquid species is expected in the sheath as compared to the bulk plasma, due to evaporation, desorption and sputtering processes. In principle, these differences do not necessarily imply reactions of a different nature in comparison to the plasma bulk, as they only mean a shift of the chemistry to a different regime in the sheath. Following this line of thought, it seems reasonable to describe both regions with the same gas chemistry set, as long as it covers a sufficiently wide range of conditions for the electron and ion energies, as well as the species densities.

There are, however, two factors that might cause an essential contrast in chemistry between the plasma sheath and plasma bulk (see Figure 3). As the first factor, the sheath may be populated with numerous microdroplets, acting as catalysts or miniscule reaction vessels. That is, reactions can be accelerated by orders of magnitude in microdroplets relative to their liquid bulk counterparts, as demonstrated in several investigations [104-107]. Interestingly, the droplets allow a voltage-dependent chemistry acceleration and a reversible electrochemical derivation [108]. This makes the plasma sheath an interesting reaction environment for microdroplets, with a promising application for chemical synthesis. When coupled with

mass spectrometry, these features also allow an in situ mechanistic study and capture of key radical intermediates, applicable for chemical analysis purposes [108]. Moreover, the aforementioned remark on the distinct surface chemistry at a liquid surface remains valid for a droplet boundary. All of these droplet-related chemical principles should be strongly dependent on the presence of an electric field. Therefore, microdroplets can lead to an essentially different chemistry in the plasma sheath with respect to the plasma bulk.

As a second factor, a strong electric field like the one in the sheath can alter the rate and pathway of reactions also in the absence of any droplets. In fact, the electric field dependence of chemical reactions involving charged functional groups is heavily pronounced in the gas phase, in comparison to its muted effect in solution due to dielectric screening [109]. For an introduction to such field effects, we recommend the Tutorial by Shaik et al. [110]. This Tutorial explains the impact of the field on a reaction by means of its orientation relative to the axis of the bond to be broken and the so-called reaction axis. The latter is defined as the direction along which electron pairing undergoes reorganization from reactant-like to product-like bonding. A field along the bond axis facilitates bond breaking. A field along the reaction axis catalyzes the reaction. Moreover, forbidden-orbital mixing can be removed and stereo-selectivity can be controlled with a field component perpendicular to the reaction axis [110]. Since polar molecules orient themselves along a strong electric field, a net modification of their chemistry may be expected in a plasma sheath.

In other words, the sheath chemistry is expected to diverge significantly from the bulk plasma chemistry, due to the dissimilar particle densities and charge carrier kinetic energies, and due to the presence of microdroplets and field-dependent reactions. The products created in the sheath need to travel less of a distance to enter the plasma bulk or the liquid surface than particles crossing the entire sheath thickness. They are therefore of prime interest for a description of the species and charge transport through the plasma-liquid interface. Moreover, the sheath forms an electrostatic and chemical barrier for plasma and liquid species coming from the bulk phases. As such, the question arises how much the bulk species contribute to the fluxes onto the liquid surface or into the plasma, in comparison to the species generated in the sheath.

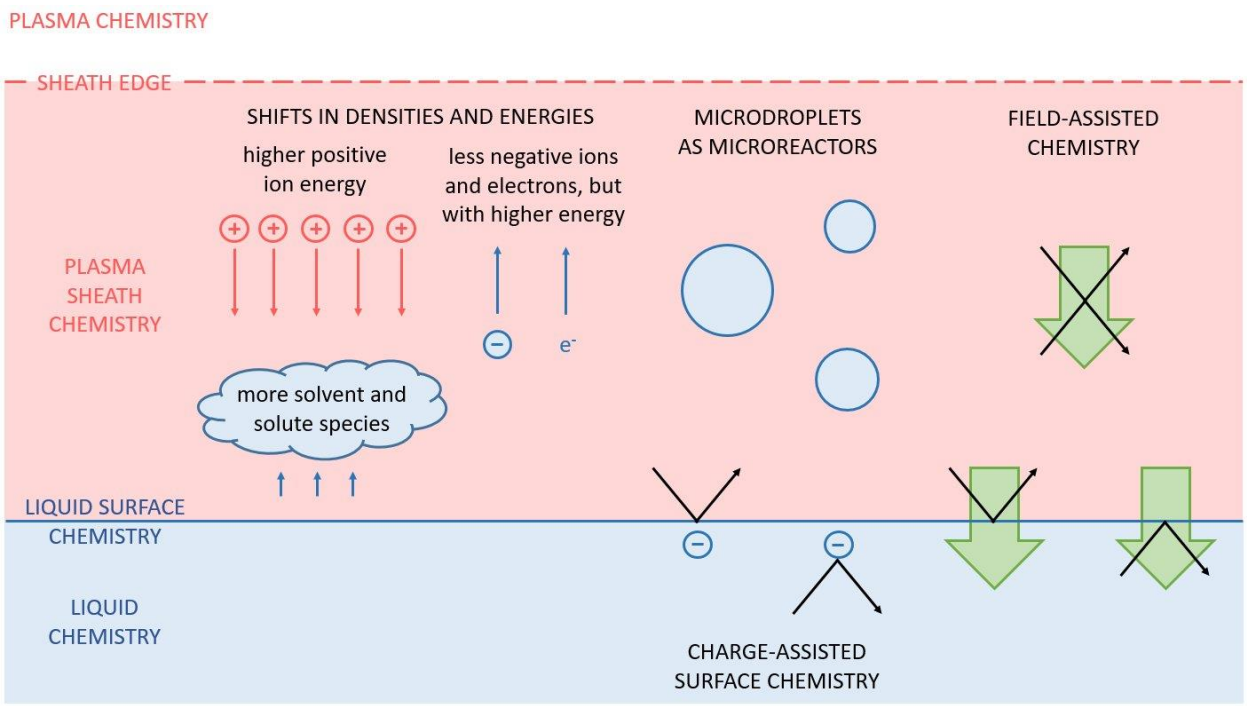

Figure 3. Schematic summary of the aspects in the plasma sheath chemistry and liquid surface chemistry that are mostly affected by the presence of the electric field. The thin black arrows denote reactions and the green downward arrows represent the electric field.

The answer will of course strongly depend on the pressure and ionization degree of the plasma. For low pressure plasmas with solid boundaries, ion-neutral reactions in the sheath become noticeable at 1 Pa for increasing pressure, based on studies of the incident ion energy distribution functions [102, 103]. Below 1 Pa, the sheath is often considered collisionless for ions. However, collisions and reactions between the neutral species will still occur with a high frequency. At atmospheric pressure, the sheath is strongly collisional for both ions and neutrals, providing numerous opportunities for any particle to react while crossing the sheath. An interesting study in this regard has been performed by Liu et al., using a one-dimensional fluid model with a chemistry set of 17 species and 60 reactions, for the simulation of a radio-frequency atmospheric-pressure He-O_2 plasma with solid boundaries [111]. From a detailed analysis of the particle transport in the sheath region, the wall fluxes were found to originate from a 3 to 300 µm thin boundary layer contacting each electrode, i.e. only a fraction of the sheath thickness of 472 to 489 µm. As such, the chemistry in the thin boundary layer supplied the species incident to the surface. More studies are required to test this hypothesis for other plasma sources. Unfortunately, the research domain of plasma sheath chemistry has remained remarkably inactive up to now, also for gas discharges with solid boundaries. With the present Perspective Article, we therefore hope to motivate the plasma community to breathe new life into this topic. For this purpose, a few examples are discussed in Section 5 on how the sheath can regulate the chemistry for nanomaterial and chemical synthesis, by varying the ion or electron kinetic energy at a liquid cathode or anode, respectively.

2.4 Sheath variability and anode sheaths

In general, the sheath features depend on the plasma and liquid properties, as well as any externally applied fields. At low pressure, for instance, collisionless ion sheaths at a positively biased solid surface can be described with a one-dimensional steady-state two-fluid model, from which a sheath thickness l is deduced as [112]

$$l = \frac{\lambda_D \sqrt{2}}{3} \left(\frac{2e\Delta\phi}{T_e} \right)^{3/4} \quad (1)$$

where λ_D is the Debye length, e the elementary charge, T_e the electron temperature and $\Delta\phi$ the sheath potential drop determined from the global current balance. Equation 1 implies the sheath scale to be several Debye lengths thick if $e\Delta\phi \gg T_e$. Its deduction is based on the Bohm criterion, which states that ions need to enter the sheath from the plasma with a velocity of at least the ion sound speed $c_s = \sqrt{k_B T_e / m_i}$, with k_B the Boltzmann constant and m_i the mass of the ions. However, a waterproof analytical formulation of the sheath is mathematically complicated in this way, which formed the subject of a heated discussion at the start of this century [113-116]. The transition point where the Bohm criterion needs to be applied namely does not coincide with the sheath edge, i.e. the boundary between the sheath and the quasi-neutral plasma as defined by Langmuir [113, 117]. In order to avoid inconsistencies, the equations for the sheath and plasma can be coupled to one another with the method of matched asymptotic expansions, by introducing an additional transition region between the plasma and the sheath [118-120]. Alternatively, patching methods may be applied to force the equations together at the transition point [114, 121]. Considering that ion sheaths at solid surfaces are the most intensely studied types of plasma sheaths, this illustrates the challenging character of this research domain.

As another example of this complexity, the distinct types of plasma sheaths formed at a biased solid electrode at low pressure have been identified only recently. Figure 4 shows the qualitative electrical potential profile of five types, including the well-known ion sheath. Electron sheaths are thin regions of negative space charge, emerging near a positively biased electrode for a sufficiently small effective surface area of the sheath edge [112]. Double sheaths additionally possess a positive space charge region at the side of the quasi-neutral plasma. They can arise under various conditions, related to the electrode configuration or due to secondary electron emission [112, 122-127]. An anode glow emerges from an electron sheath when the potential difference between the electrode and the plasma rises, enhancing the ionization rate in the sheath by accelerated electrons. Due to the inertia of the ions, they leave the sheath much slower than the electrons, causing a positive space charge at the side of the electrode. The higher electron energy in this region results in a larger number of excitations, making it glow. When the bias voltage, or alternatively the pressure, is further increased, the positive space charge region expands, leading to an abrupt fireball onset. A fireball is a transient phenomenon, after which the sheath and plasma potential are adjusted. For an excellent overview of these different types of sheaths at low pressure, we refer to the recent review of Baalrud et al. [112].

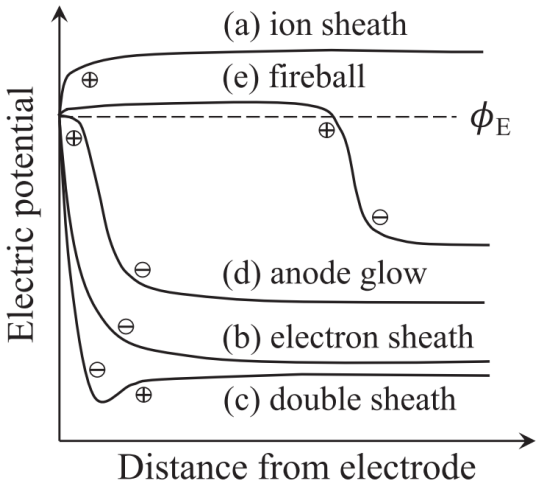

Figure 4. Electrostatic potential profile of five plasma sheath types that can form at a biased solid electrode. Regions of negative and positive space charge are denoted by minus and plus signs, respectively. Reprinted from [112] in Plasma Sources Science and Technology 29(5): p. 053001 (2020). © IOP Publishing. Reproduced with permission. All rights reserved.

An important subsequent question is how these insights need to be translated for sheaths at higher pressures. In this regard, we also highly recommend the assessment made by Baalrud et al. in [112]. They have suggested a similarity between fireballs at low pressure and anode spots or anode glow at atmospheric pressure, taking into account the nearly identical reactor geometry and power system used to generate them. The two phenomena namely involve a self-organized, highly-luminous and localized secondary discharge generated near biased electrodes in a plasma. The underlying mechanisms may therefore display similarities as well. However, Baalrud et al. point out a clear contrast between their usual theoretical description. On the one hand, kinetic effects associated with details of the velocity distribution functions, i.e. beyond the assumptions in fluid or thermodynamics models, are essential in the fireball model. On the other hand, spots in atmospheric pressure plasmas seem well represented by means of fluid models, such as the ones including reaction-diffusion or drift-diffusion descriptions. According to these models, spots are formed due to a thermal instability coupled with the boundary condition of the electrode temperature, a parameter absent in the fireball model. As such, Baalrud et al. propose to investigate the transition between the low and high pressure regimes, in order to elucidate these differences. Analogously, they bring forward the same considerations for the transition from a low-pressure ion sheath to a complex cathode spot structure at higher pressures.

At a liquid surface, the situation may be very different, due to the processes presented in Figure 1. Therefore, the sheath models for solid surfaces may be inaccurate or perhaps even invalid at a liquid surface. Currently, assessing the differences is a matter of speculation, because several properties of the plasma-liquid interface are still poorly understood. Sections 6.1 and 6.2 will illustrate this for electron emission and droplet generation at the liquid surface, which can involve evaporation, surface deformation, the electrical double layer and ion drift in the liquid phase. A validated fundamental knowledge on these processes is crucial to obtain a trustworthy description of the plasma sheath in plasma-liquid interaction. The present uncertainties regarding the sheath are also demonstrated by

comparing a few recent models for plasma interaction with a water anode. Figure 5 displays some characteristics of the anode sheath at the water surface according to an analytical model developed by Rumbach et al. [128], a one-dimensional particle-in-cell Monte Carlo collision (PIC-MCC) model with liquid chemistry by Gopalakrishnan et al. [129], and a one-dimensional PIC-MCC model by Levko et al. describing plasma species in both the gas and liquid phase with computational macro-particles [130]. Although the three models show some agreement with each other and with the experimental study by Rumbach et al. [131], they predict a different sheath structure. The model by Levko et al. calculated a positive space charge region in contact with the surface, based on the interaction between an anode-directed streamer in humid nitrogen and de-ionized water. This corresponds with an anode spot, as often observed over a water anode (see e.g. [132-141]). The model by Gopalakrishnan et al. instead found an electron sheath without a positive space charge in argon over an electrolyte electrode. The model by Rumbach et al. simply assumed an electron sheath at the aqueous anode, as displayed in Figure 5.

This dissimilarity may be the result of the different operational conditions or the distinct computational methods, which would be interesting to investigate with a dedicated comparative study. In any case, it clearly shows that the currently available data on sheath properties cannot simply be generalized for all combinations of plasma-liquid interaction. A key question will be what type of plasma sheath is formed at the liquid. Obviously, the sheath type will strongly influence the plasma-liquid electrical coupling, the species transport across the interface and the sheath chemistry.

For an anode sheath, the schemes in Figures 2 and 3 need to get modified accordingly. As an important difference with cathode sheaths, the electric field strength in the gas phase near an anode is often estimated to be weaker. For an anode sheath at a liquid, values ranging from 10^4 to 10^6 V/m are reported (see e.g. [128-130, 138, 142]), corresponding to an electron impact energy up to 10 eV with the surface. Contrarily, ion sheaths at a water cathode are often thought to contain a field around 10^7 V/m [68, 73, 143]. The latter value originates from the measured cathode voltage drop, which usually lies within the interval from 400 to 700 V (see e.g. [73, 143-149]), and the implicit assumption of a sheath thickness around 40 to 70 µm. According to the plasma-liquid interaction Roadmap by Bruggeman et al., the ions bombarding a liquid cathode surface are therefore expected to obtain a kinetic energy of a few eV, up to perhaps tens of eV at most, based on an ion mean free path smaller than 1 µm at atmospheric pressure [68]. This stands in contrast with values around 100 eV mentioned elsewhere (see e.g. [150, 151]). A strikingly lower field strength of 2 - 4 × 10^5 V/m has been observed in the cathode sheath of an atmospheric air plasma between two streams of tap water, implying two orders of magnitude lower ion energies [152, 153]. These are exciting observations, demanding further investigation, because the ion energy distribution provides essential insight into the possible electron emission mechanisms. Fields in the order of 10^5 V/m namely seem to contradict the current theories of ion-induced secondary electron emission, as discussed in more detail in Section 6.1. Next to that, the field strength in the sheath strongly determines the likeliness and prevalence of the processes depicted in Figures 2 and 3. Obtaining accurate values for it is therefore of primary importance.

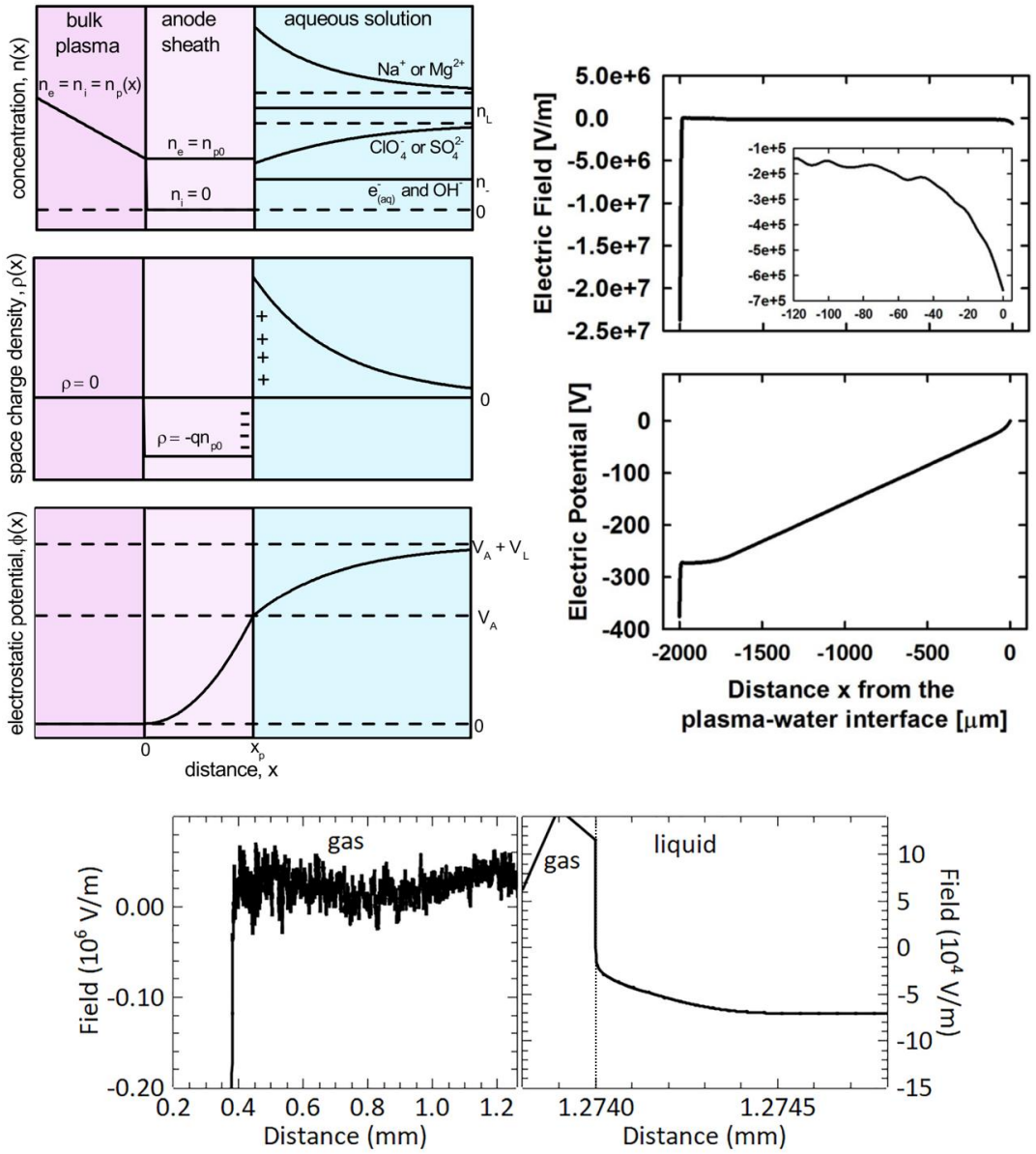

Figure 5. Anode sheaths at a water surface according to three different models. (top left) The assumed qualitative gradient of charged species and the resulting space charge density and electrostatic potential across the electrolyte surface normal in the model by Rumbach et al. (top right) The electric field and electric potential calculated with the model by Gopalakrishnan et al. in the Ar plasma phase over an electrolyte anode. The cathode fall voltage is around 100 V. The electric field in the bulk plasma region remains nearly constant around the value -1.5×10^5 V m^{-1}. The inset shows the field strength increase in the electron sheath. (bottom) The electron field profile obtained with the model by Levko et al. along the liquid surface normal of de-ionized water in contact with a humid nitrogen plasma under steady-state, with a cathode voltage of -2 kV. (top left) Reprinted figure with permission from [128] in Physical Review E 95(5): p. 053203 (2017). Copyright 2017 by the American Physical Society. (top right) Reprinted from [129] in Journal of Physics D: Applied Physics 49(29): p. 295205 (2016). © IOP Publishing. Reproduced with permission. All rights reserved. (bottom) Reprinted from [130], with the permission of AIP Publishing.

3. The sheath as an electric field regulator for food processing, plasma agriculture and plasma medicine

3.1 Plasma-induced electric fields for electrostatic disruption

The previous sections discussed the relevance of the plasma sheath for plasma-liquid applications in general, in terms of the electrical coupling between the plasma and liquid phases (Section 2.1), the species transport through the sheath (Section 2.2) and the sheath chemistry (Section 2.3). In Sections 3 to 5, we zero in on a few specific applications, where the sheath plays a particular role to obtain the desired effect. The list of these examples is far from complete, but serves as an extra emphasis on the importance of the sheath in plasma-liquid interactions and as a motivation for more research on this topic. The current Section 3 puts the looking glass over the electric field penetration into the condensed phase, which is tightly linked to the electrical coupling function of the plasma sheath.

Any object under plasma treatment is subject to ions, electrons, photons, neutral species, and the local electric field of the sheath at the contact surface. The latter may, on itself, cause modifications in the material, apart from or in synergy with the plasma particles. Its effect in the treatment process should therefore also be analyzed, for a complete understanding of the observed effects. In the domain of plasma-liquid applications, this has mainly attracted the attention of researchers working on the treatment of biological material. Indeed, electric fields are known for a long time to affect biological organisms. To explain the observed effects, several mechanisms have been proposed in literature. Throughout Section 3, we zoom in on these mechanisms, for fields ranging over the orders of 10^{-1} till 10^{5} V/cm in amplitude, and 10^{-12} till 10^{2} s in duration. Doing so, we want to illustrate how crucial it is to know the exact parameters of the field penetrating into the condensed phase. Although the focus lies on biological materials, a part of the presented knowledge also applies to liquid matter in general. More specifically, Section 3.3 deals with field penetration into the liquid phase, and its relationship with the plasma sheath. Section 3.6 presents field-induced effects on a molecular level, which may also occur in non-biological plasma-liquid systems.

As a first example, electrostatic disruption of the cell membrane was introduced by Mendes et al. to explain *E. coli* inactivation under atmospheric pressure glow discharge treatment [154]. This mechanism assumes the cell membrane to acquire a sufficiently large electrostatic charge, so the resulting outward electrostatic stress exceeds its tensile strength. An estimation of the required membrane potential gives several to tens of volts [154]. Electrostatic disruption has frequently been suggested to explain immediate cell death under plasma treatment [155-159]. Outside the plasma community, however, field-induced inactivation of microorganisms or biological tissue is more commonly attributed to electropermeabilization, which forms the topic of Section 3.2.

3.2 Plasma-induced electric fields for electroporation

The membrane of cells under treatment can be understood as a capacitor filled with a low dielectric constant material [160]. In the presence of an electric field, the intra- and extracellular ions move along the field direction, accumulating free charges at the opposite sides of the membrane. This process plays

an important role in signal transduction between the cell's interior and exterior [160, 161]. For a rising field strength, the transmembrane potential increases, up to a certain threshold value of usually around 0.2 to 1.0 V [160, 162, 163]. At and above this threshold, pores are formed in the membrane, either reversibly or irreversibly, an effect known as electroporation (see Figure 6). In the case of temporary pores, mass transfer occurs between the intra- and extracellular solutions, including water molecules, minerals and larger particles, depending on the pore size. Such reversible perforations have a lifetime of several milliseconds to hours [164, 165]. Permanent pores, on the other hand, correspond to the rupturing of the cell wall. Accordingly, reversible and irreversible electroporation can result in apoptosis (delayed, programmed cell death) and necrosis (immediate, unprogrammed cell death).

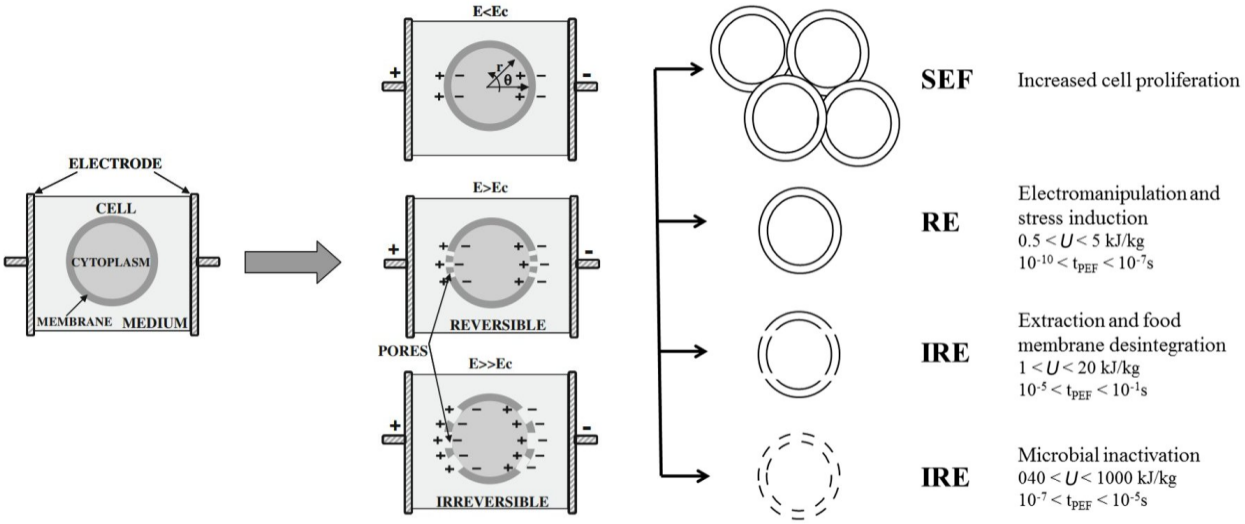

Figure 6. Schematic description of electroporation. A biological cell is located in an electric field E. For a field below the critical value $\mathrm{E_c}$, charge separation occurs in the intra- and extracellular liquids, but the cell membrane remains intact. Beyond this threshold, reversible pores develop in the membrane, represented with the dashed line (RE: reversible electroporation). For increasing field strength, the pores become irreversible, corresponding to the rupturing of the cell wall (IRE: irreversible electroporation). In contrast, keeping the field strength at sublethal values can stimulate the growth of cells (SEF: stimulating electric fields). When biological material is treated with pulsed electric fields, these processes occur over a certain range of the treatment time t_{PEF} (in s) and the total specific energy U (in kJ/kg), as indicated at the right. (left part) Reprinted by permission from Springer Nature from [162] in Food Engineering Reviews 2(2): p. 109-130 (2010). (right part) Adapted from [160]: L. Galván-D'Alessandro and R.A. Carciochi, Fermentation, Vol.4(1), p. 1, 2018; licensed under a Creative Commons Attribution (CC BY) license.

Based on this mechanism, electric fields can be used to inactivate hazardous or undesirable micro-organisms in biological materials. In practice, this type of treatment is most frequently performed with pulsed electric field (PEF) technology. PEF has found widespread application for food processing [166-170], and has been proposed as a novel method for enhanced seed germination [69, 171-174], wound healing [175-178] and cancer treatment [179-181]. Note that, coincidently or not, these resemble some of the most popular applications in plasma agriculture and plasma medicine. For food processing and wound healing, the inactivation of micro-organisms due to electroporation is generally considered as the

main underlying mechanism [168-170, 176-178]. For seed and cancer treatment, in contrast, the positive impact has frequently been attributed to reversible electroporation in the multicellular tissue [108, 179-181]. Reversible electroporation namely enables the extraction of intracellular molecules and the infusion of water or foreign materials into and within the cell, which may benefit the subsequent germination process in the case of seeds, or the healing process in the case of tumors. Such a mechanism may also be used for gene delivery in wound or cancer treatment, a technique known as gene electrotherapy [175, 180]. An alternative is electrochemotherapy, where the membranes of the malignant cells are permeabilized for the infusion of cytotoxic drugs [182, 183]. Interestingly, a few recent studies have tested the combination of pulsed electric fields with plasma treatment of tumors [182, 184-188]. In an in vitro study with a three-dimensional cell model, pulsed electric fields were found to greatly potentiate the cytotoxic effect of plasma-activated phosphate-buffered saline [184]. Reversely, a second study demonstrated a reduction in the required pulsed electric field intensity after a pretreatment of two cell lines with plasma-activated medium [187]. In a third investigation by our group, such medium in combination with electric field treatment caused cell death, while the field alone turned out to be nonlethal [186]. In another study on direct cell culture medium treatment with the kINPen plasma jet, the killing potential increased when the cells were pre-treated 3 to 5 min in advance with pulsed electric fields [188]. In yet another investigation using direct treatment with the kINPen, more cells were killed when the plasma process preceded the pulsed electric field [182]. In a sixth investigation, the sequence of treatment did not seem to play a significant role [185]. However, a parallel combination turned out to be more effective than a serial application with a 15 min pause in between both regimes. Interestingly, cell membrane permeabilization was induced by pulsed electric fields, but not by plasma.

This shifts forward the question whether plasma treatment alone can cause electroporation under different circumstances. Obviously, electroporation can only take effect for a sufficiently large electric field applied over the cells, in agreement with Figure 6. For this reason, several sources in literature have proposed a comparison between plasma-liquid interaction and pulsed electric field treatment with respect to the electric field (see e.g. [189-192]). A strongly simplified reasoning could go as follows. On the one hand, plasma treatment of biological materials is generally performed by means of atmospheric pressure plasma jets and dielectric barrier discharges. Atmospheric pressure plasma jets can generate fields in the order of 10 kV/cm in a propagating plasma bullet, with local values approaching 100 kV/cm [193-195]. The field at the head of a propagating streamer filament in a dielectric barrier discharge can reach even higher, ranging from tens to around 200 kV/cm [192, 196-198]. On the other hand, pulsed electric field treatment is often described in terms of a few operating conditions, one of which is called the applied electric field. It refers to the voltage applied over two metal electrodes in contact with the cell culture medium, divided by the inter-electrode distance. The critical value $\mathrm{E_c}$ of this parameter required for electroporation is typically found to range in the order of 0.1 to 10 kV/cm [166, 199-202]. For animal cells, for instance, values around 0.4 to 0.5 kV/cm are often cited [203, 204]. Comparing these values with the local ones found for the plasma sources, it appears as if electroporation is accessible with plasma treatment. As a necessary condition according to this logic, the cells should be positioned sufficiently close to the location where the electric field is considered, e.g. the plasma sheath. However, a high field strength is an insufficient condition for electroporation, because its time-dependency needs to be added in the equation as well. We will discuss this further in Section 3.3.

Still, electroporation has been proposed as an important mechanism in plasma treatment of various biological systems, based on numerous experimental observations. Ouf et al. studied the inactivation of *A. niger* spores in wastewater from the washing process of cherries, grapes and strawberries, by means of a 25 kHz AC powered double atmospheric Ar plasma jet [205]. After the treatment, pores were detected in the spore walls, which they attributed to electroporation. Similarly, Devi et al. treated inoculated *A. parasiticus* and *A. flavus* on groundnuts in a RF powered capacitively coupled plasma reactor at 0.2 mbar [206]. They attributed the disintegration of the fungal spore membrane to a combination of electroporation and plasma etching. Also for plasma treatment of individual unicellular organisms or adherent cell cultures in buffer solution, electroporation is often proposed to explain experimental results. Jinno et al., for instance, investigated the mechanism behind plasma-induced gene transfection, which they partly attributed to the direct effect of the electric field [207]. Such claims are supported by the experiments of Tero et al., who detected pores in the order of 10 to 1000 nm in an artificial cell membrane system at a plasma-liquid interface after irradiation of the solution with plasma [208]. However, direct evidence for plasma-induced electroporation is hard to obtain, since also several other mechanisms can underlie the pore formation, like chemical or biochemical triggers.

3.3 Plasma-induced electric field penetration into the liquid phase

Several points of caution need to be addressed regarding the simplified reasoning in Section 3.2, in the comparison between plasma treatment and pulsed electric fields. First of all, the electric field in the plasma or sheath at a liquid surface refers to local conditions in the gas phase, while the field strength in the liquid phase is expected to be very different. In fact, the liquid is electrically coupled with the plasma phase through the potential at the liquid surface as a boundary condition, rather than by the local electric field. Analogous to the formation of the sheath in the gas phase, an electric double layer will form in the liquid phase. Under steady-state conditions, this double layer blocks the electric field generated by the positive space charge in the sheath and the liquid surface charge by means of dielectric screening. Most of the potential drop over the liquid phase then occurs over the double layer, similar to how the potential drop in the gas phase lies focused in the sheath. As should be noted, the electric double layer in aqueous solutions is very thin in general, in the order of nanometers [39, 41]. The corresponding local electric field can reach up to 10^7 V/cm [39-41], somewhat comparable to the field strength around 10^6 V/cm naturally present at a cell membrane [209]. These local values should not be directly compared with the applied field strength values given in literature for pulsed electric field treatment, as the latter does not take into account the variation of the electric potential in the liquid phase. In summary, the potential drop in the liquid phase is expected to be small under steady-state conditions, with the exception of the electric double layer.

Secondly, the time-dependent behavior of the plasma-induced voltage over the liquid needs to be taken into consideration, especially when its variation occurs faster than the adjustment of the compensating electric double layer. Note that it is indeed the voltage over the liquid that needs to be compared with the one in electric field treatment. Here, the important role of the plasma sheath becomes apparent. Indeed, the voltage over the liquid phase is directly coupled to the sheath potential. Therefore, knowledge

on the temporal evolution of the latter is required to deduce the evolution of the former. This time-dependency is crucial for a full understanding of the electric field-induced processes in biological applications. That is, the critical field E_c for electroporation strongly depends on the applied voltage waveform characteristics. DC fields display the lowest threshold in the order of a few hundreds of V/cm [203]. For AC fields, the peak amplitude E_c can be double this value, yet still well below 1 kV/cm at low frequency, but significantly increasing beyond 10 kHz [210-212]. For pulsed electric fields, E_c decreases with the number of applied pulses and with the pulse width [166, 199-202]. Millisecond pulses generally induce larger pores at moderate field strengths in the order of some hundreds of V/cm, as opposed to the smaller pores induced by microsecond pulses with strong fields in the order of 1 kV/cm [180, 201, 202]. For this reason, the former are often used to stimulate the uptake of large molecules such as nucleic acids into cells, which has laid the foundation of so-called gene electrotransfer [180]. Microsecond pulses, on the other hand, are more fit for the injection of small molecules or ions, forming the basis of electrochemotherapy [180]. An interesting situation emerges when characteristic times, such as the pulse width or voltage rise time, fall below the duration required for the ionic redistribution and thus charging of the cell membrane, which lies in the order of 1 µs (see Figure 7) [180, 213]. In this case, the slow charge redistribution can no longer compensate the external electric field on the sub-microsecond scale. The same reasoning counts for the modification of the electric double layer at the liquid surface. Accordingly, the rapidly changing field can penetrate into the biological tissue, to exert their force on intracellular material, such as organelle membranes [180]. We will discuss this further below.

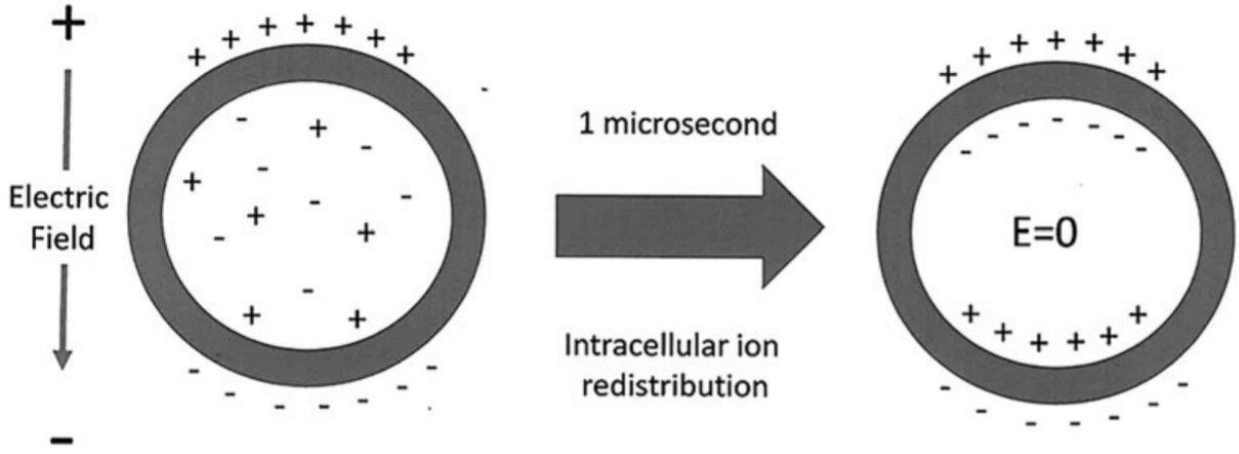

Figure 7. Ion redistribution in the cell cytoplasm during the application of an external electric field. This charging process takes about 1 µs for cells packed together in a tissue. After the redistribution and charging is complete, the local electric field in the cell has diminished, as long as the external field remains present and fixed. However, imposed electric fields with temporal variations shorter than a microsecond can penetrate into the cell and organelles until the ion redistribution comes to a stationary state. Note that this thought experiment can be repeated for the rapid quenching of an external field, and thus also counts for the capacitive discharging of the plasma membrane. Reprinted from [180] in Bioelectricity 1(1): p. 30-34 (2019) with permission. The publisher for this copyrighted material is Mary Ann Liebert, Inc. publishers.

Thirdly, the total treatment time used to obtain reversible electroporation with repetitively pulsed electric field typically ranges from 10^{-10} to 10^{-4} s [160, 170], which lies multiple orders of magnitude below the plasma treatment times of several seconds to minutes. When using a DC or AC voltage for electroporation, the treatment duration is generally limited to the order of 0.1 s, which is still lower than for plasma treatment [210-212]. In practice, long electric field treatment times are often avoided to obtain electroporation, as they lead to ohmic heating and possible thermal damage to the treated biological material [214]. Therefore, the threshold value E_c for conventional electric field treatment may not be an ideal reference for plasma-induced electroporation, where a synergy or counteraction may take place between the pore formation and other longer term effects. For instance, if an electric field deforms a cell from a circular shape into an elliptical one, the field orientation relative to the longer cell axis will influence the threshold for electroporation [215]. Fourthly, electroporation cannot be considered independent from the plasma-induced chemistry. Oxidation of the cell membrane by reactive oxygen and nitrogen species is namely able to facilitate pore formation [216]. According to a computational study where a direct contact is assumed between an air plasma and a cell wall, pores can also be formed by the bombardment of the membrane by ions, electrons and radicals [217].

In other words, the simplified reasoning in Section 3.2 lacks in two crucial aspects regarding the electroporation: the time-dependency of the voltage over the liquid, as well as the potential synergies and counteractions with other plasma-induced effects. Therefore, the role of electroporation in plasma treatment is still not entirely clear up to now. However, multiple recent investigations have added conviction to the belief of its relevance. From a theoretical point of view, strong voltage fluctuations can be expected over the liquid phase in many plasma-liquid systems, due to the rapid pulsed-like nature of the applied electrical discharge source. In plasma medicine, for instance, one of the most commonly studied atmospheric plasma jets for cancer treatment is the kINPen, which is AC powered with a frequency ranging from 0.8 up to tens of MHz [218]. This frequency on its own can generate voltage fluctuations on the sub-microsecond timescale, i.e. below the charging times of the electric double layer and cell membranes in biological tissue. Moreover, the luminescent plasma plume is known to consist of so-called plasma bullets of a high field intensity, which indeed interact with the liquid surface in a sub-microsecond time frame [35, 218-220]. Figure 8 shows that this time frame remains valid for lower power frequencies as well. This may enable the incident electric field to penetrate into the liquid phase and intracellular solution. Still, when the interaction of the plasma bullet with the liquid surface takes place over a few hundreds of nanoseconds, the surface potential fluctuations most likely do so as well. This time frame remains rather close to the characteristic charging times around 1 µs in biological matter, which limits the actual field penetration.

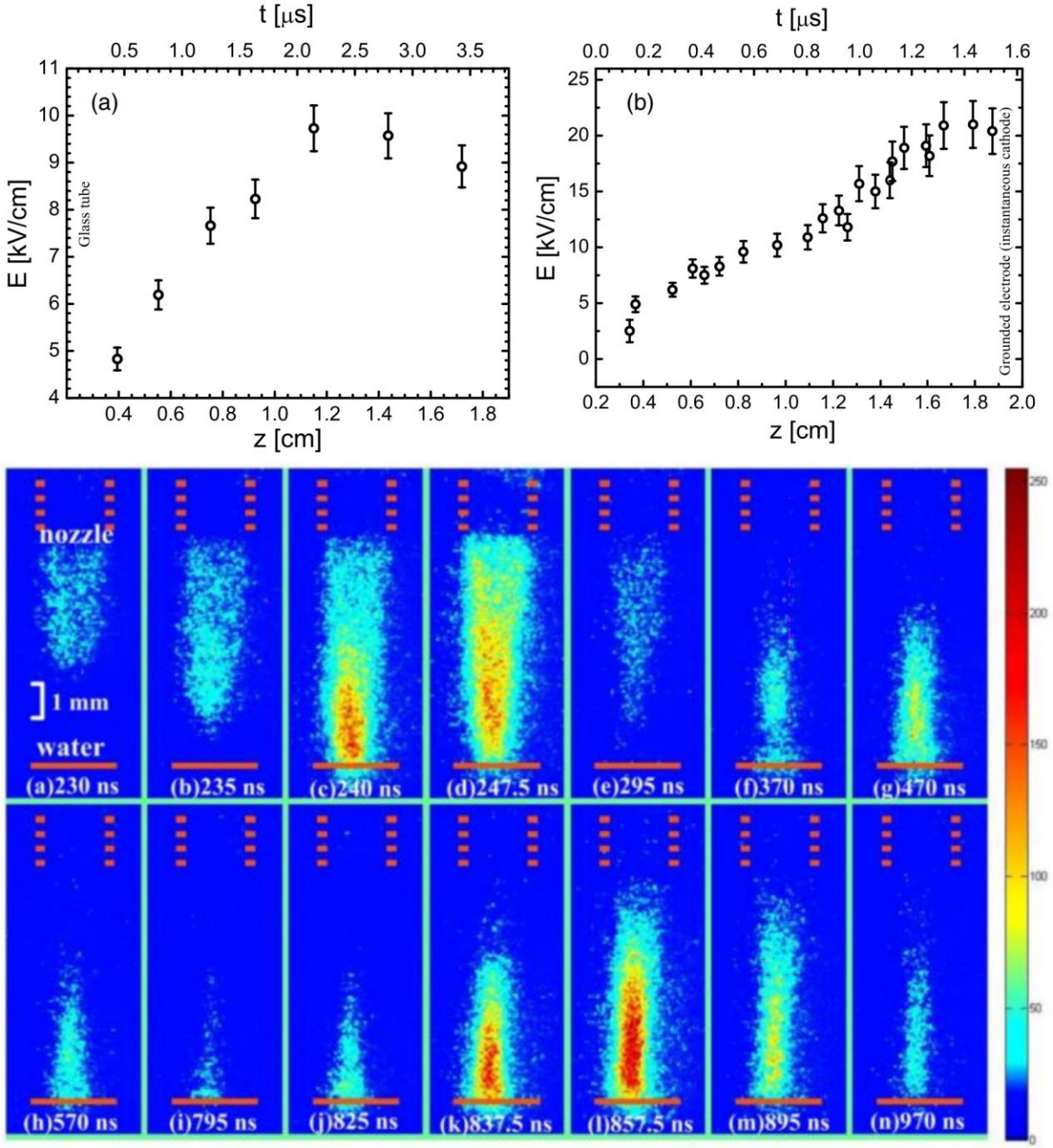

Figure 8. Plasma bullet evolution in three different He plasma jets. (top) The electric field strength E as a function of time and distance from the nozzle, for (left) a jet without a target and (right) a jet at a distance of 2 cm from a grounded active electrode. Both jets are AC powered with a voltage of 4 kV and a frequency of 12.65 kHz. (bottom) Experimental snapshots with an exposure time of 5 ns, showing the propagation of a plasma bullet onto a water surface, for a jet powered with 7 kV pulses of 800 ns at a frequency of 8 kHz. (top) Reprinted from [195] in Journal of Physics D: Applied Physics 47(10): p. 102001 (2014). © IOP Publishing. Reproduced with permission. All rights reserved. (bottom) © 2018 IEEE. Reprinted, with permission, from [221] in IEEE Transactions on Radiation and Plasma Medical Sciences 2(3): p. 223-228 (2018).

Another commonly studied plasma source for biomedical applications is a dielectric barrier discharge, driven by high-voltage pulses or AC power. This discharge type consists of filamentary streamers, which typically interact with an electrode surface on a nanosecond timescale [222, 223]. Since the propagating streamer heads bring with them an intense field, strong fluctuations in the electric potential are also expected at the liquid surface. According to a series of simulation studies by Babaeva et al., this can result in local electric fields well beyond 100 kV/cm in biological tissue under treatment (Figure 9(a)) [192, 198, 224, 225]. Yet, these simulations did not include all of the possible microscopic effects at the liquid surface as presented in Figure 1, i.e. evaporation, microscopic surface deformation and droplet emission. Such effects may be decisive to the plasma-liquid interaction, in agreement with an experimental investigation by Vanraes et al. on a single dielectric barrier micro-discharge filament in contact with a thin water layer (Figure 9(b)) [226]. Time-resolved imaging of the filament namely revealed a continuously present glow-like plasma spot at the liquid electrode, which is generally not observed in the case of solid electrodes. Based on the electrical analysis of the single filament, this unique behavior may be attributed to a so-called resistive barrier discharge, a less known type of plasma with more diffuse features as compared to the usual dielectric barrier discharge [226-228]. The resistive nature of the surface, whether it be purely liquid or biological tissue, may thus play an essential role in the plasma properties, both on a local and general level. More specifically, it likely smooths out the temporal evolution of the surface potential, in comparison to a dielectric barrier discharge with solid electrodes. Correspondingly, the voltage over the liquid phase may fluctuate over a time frame of hundreds of nanoseconds instead of a few or tens of nanoseconds, as suggested by the PMT signal in Figure 9(b) and the measured voltage waveforms [226]. Analogous to the plasma bullets of a plasma jet, this could limit the actual field penetration into the condensed phase.

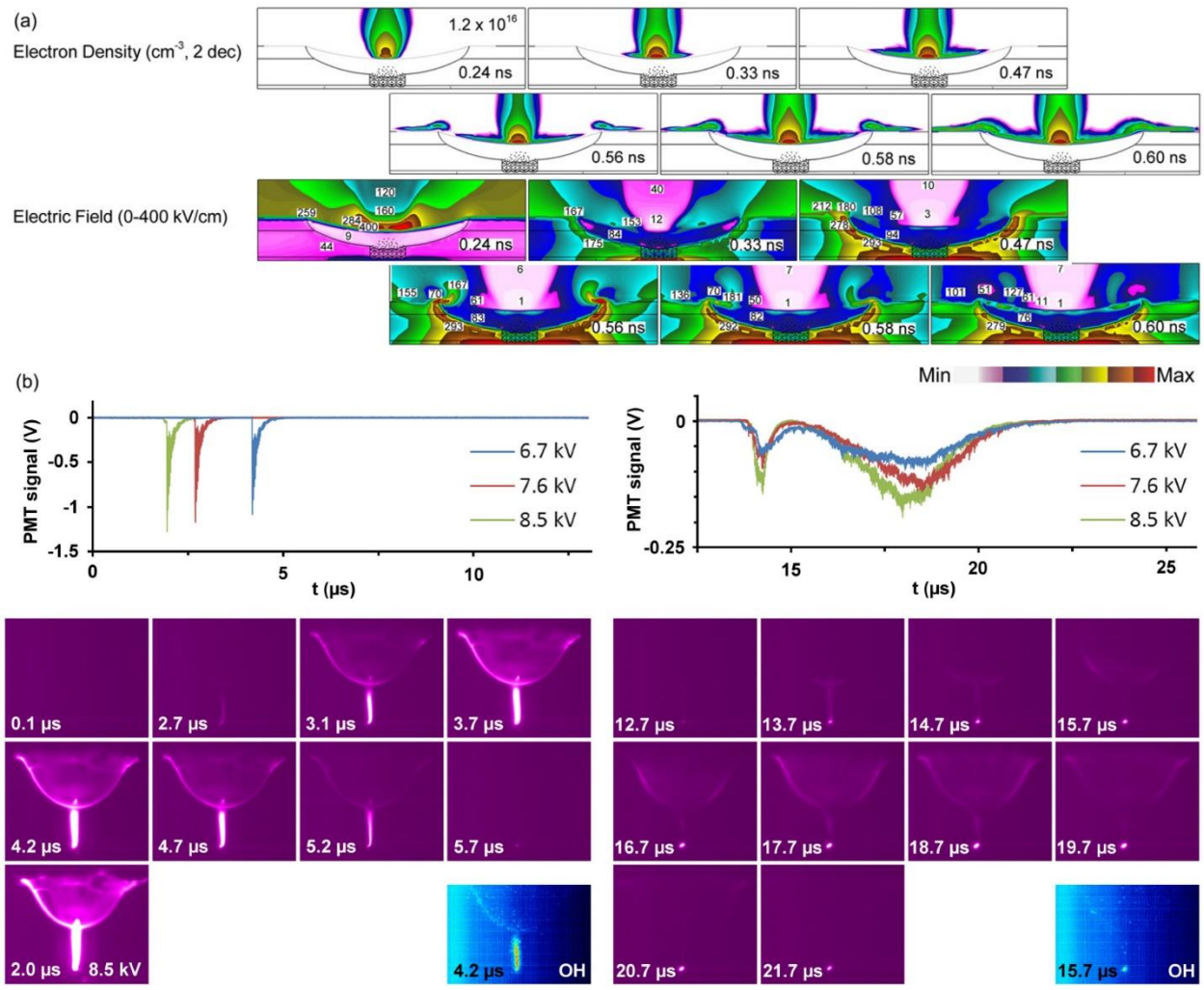

Figure 9. Temporal behavior of a dielectric barrier micro-discharge filament in contact with a liquid electrode. (a) Simulated snapshots of the electron density and electric field around the moment where the filamentary streamer reaches a wound covered in a liquid, having a relative permittivity of $\varepsilon_r = 60$. The maximum values for the snapshot series are $1.2 \times 10^{16}\,\mathrm{cm}^{-3}$ and over 400 kV/cm, respectively. The latter value corresponds to the momentary sheath at the liquid surface. (b) Experimental photomultiplier tube signal and snapshots of an AC powered filament between an upper high voltage needle included in a spherical quartz barrier and a thin water film over a grounded grid, (left) during the negative and (right) positive voltage half cycle. The blue panels present images obtained with an OH filter. The applied voltage amplitude was 6.7 kV, except for the most left bottom panel, where the discharge for 8.5 kV is shown for comparison. (a) Reprinted from [224] in Journal of Physics D: Applied Physics 47(23): p. 235201 (2014). © IOP Publishing. Reproduced with permission. All rights reserved. (b) Reprinted from [226] P. Vanraes, et al., Scientific reports, Vol.8(1): p. 1-11, 2018; licensed under a Creative Commons Attribution 4.0 International License.

3.4 Plasma-induced electric field effects on skin tissue

A process similar to electroporation can also take place in skin, at transdermal voltages beyond 100 V, promoting the tissue's permeability [229, 230]. This can explain the pores seen after skin treatment with an atmospheric plasma jet or dielectric barrier discharge, although plasma etching and Joule heating have been suggested to play a role as well [231, 232]. These pores were found to enhance the skin permeability for oxidative species dissolved in a solution, whereas they are not as effective for the transdermal delivery of gaseous plasma species [233].

Nonetheless, electroporation is but one of the multiple effects electric fields can have on cells and biological tissue. Skin can also absorb species with transdermal DC voltages in the order of 0.1 to 10 V through a process called iontophoresis. This transfer mechanism consists of three components: enhanced passive diffusion, electromigration (EM) and convective solvent flow, also known as electroosmosis (EO) (see Figure 10) [234]. The diffusion component is often neglected due to its comparatively minor contribution to the total species transport [234, 235]. In contrast, electromigration stands for the effective ordered ion movement in the presence of the applied electric field. Since the ions prefer the pathway with the lowest electrical resistance, electromigration mainly transpires through the existing skin pores, such as sweat glands or hair follicles [230, 236-239]. The stratum corneum, on the other hand, usually forms a strong barrier for this type of transport. However, such pathway may become effective in the presence of pore formation, e.g. induced by other mechanisms, such as plasma etching or electroporation. The smaller the ion and the higher its charge, the more effective its electromigration. Therefore, monoatomic ions like Na^+ and Cl^- are transferred faster through this process than the charged peptides and proteins with a lower mobility [234]. Electroosmosis, as the third transport component, stems from the isoelectric point (pI) of the human skin, which lies around 4–4.5, well below the physiological pH of about 7.4. Correspondingly, skin is negatively charged and acts as a cation-selective ion-exchange membrane [234]. As a consequence, the flow of water is favored under an electric field in the anode-to-cathode direction [234, 240-243]. This facilitates the transport of positive ions and counteracts the electromigration of negative ions into the skin, as depicted in Figure 10.

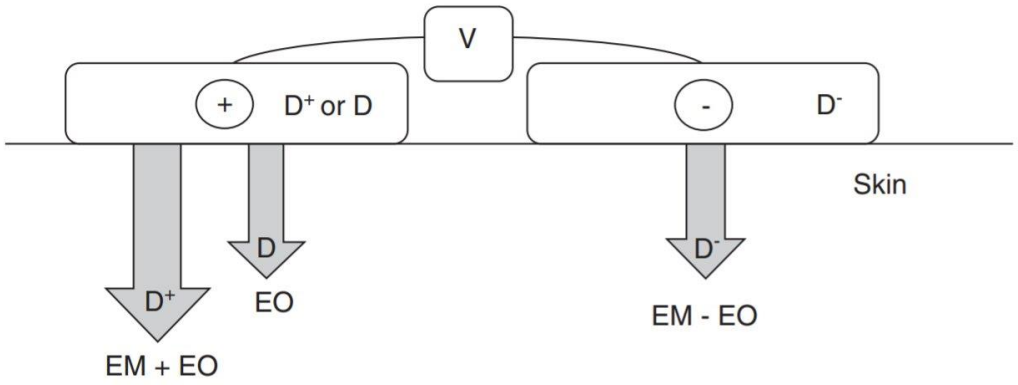

Figure 10. The roles of electromigration (EM) and electroosmosis (EO) in the transport of charged (D^+ and D^-) and neutral (D) molecules during transdermal iontophoresis with an applied DC voltage V under physiological conditions. The size of the grey arrows represents the transport intensity of the considered

species. Reprinted from [234] in Expert opinion on drug delivery 8(5): p. 645-663 (2011) by permission of the publisher (Taylor & Francis Ltd, http://www.tandfonline.com).

Besides the three transport mechanisms contributing during iontophoresis, an increased skin permeability has frequently also been observed after its application *in vitro*. This increased permeability partly corresponds to a disorganization of the stratum corneum. At low current densities, this perturbation remains local, whereas it expands at higher values [244]. Several long-term structural changes have been reported, including a decrease in intercellular lamellar ordering and intralamellar packing. Additionally, iontophoresis increases the electrical conductivity and hydration of the skin tissue. In their strongly recommended review [244], Jadoul et al. distinguish four possible mechanisms for the increased disorder in the stratum corneum:

- An alteration in the ion concentration and ion type can lead to changes in skin integrity. Also the pH can affect the local lipid organization.
- Water is a known dermal conductivity and permeability enhancer, which reduces lamellar ordering. The increased skin hydration may therefore partly explain the observed structural changes in the skin.
- Since the stratum corneum has a higher electrical resistance than the underlying viable skin layers, it forms the place of preference for Joule heating. The general temperature increase by iontophoresis is expected to be minimal, but current flow within localized pathways may lead to confined heating effects and structural perturbations.
- The electric field may also interact in a direct manner with the constituents of the stratum corneum. Electroporation has, for instance, been proposed as a possibility at the low applied voltages in iontophoresis. Although such voltages induce an average electric field that is too low for electroporation, field enhancement at the appendages might enable it at a very localized level. The electric field may also interact directly with the polar groups in the cell membrane lipids. As an example, this mechanism has been held responsible for the non-linearity in the current-voltage relationship of phospholipid bilayers, corresponding to a growing number of structural defects at higher voltages and ultimately a first-order phase transition of the membrane [245]. In such a way, the electric field may force the stratum corneum components to adopt high energy configurations, which enlarge pre-existing channels or create new ones. Consequently, pathways can be created for the electrical current, which may be physically long, but less resistive [246].

Even though the mechanisms of species transport in iontophoresis and electroporation are believed to be different, their effect on the stratum corneum minutes after their application is very similar [244]. In plasma treatment of skin, the combination of both phenomena may occur. Indeed, the plasma-induced voltage over the skin may be understood as the sum of a DC component, resulting in iontophoresis, and a time-dependent component with sub-microsecond fluctuations, responsible for electroporation. This may open the door for synergetic effects.

3.5 Plasma-induced electro-endocytosis

Electric fields can also influence the transport of species between the intracellular and extracellular solutions in less violent ways. Kaneko et al. detected a higher transfection efficiency under plasma-liquid interaction in a cell solution serving as an active electrode in comparison to an identical solution on a floating potential [247]. The observed fluorescent dye injection into the cells could not be explained with electroporation. The authors therefore suggested an enhanced transport through channels which selectively act on the dye, induced either by reactive oxygen species or by the electric field. In several other investigations, plasma treatment turned out to have an important effect on endocytosis, one of the most fundamental physiological functions of cells (see Figure 11) [248, 249]. Jinno et al. investigated the mechanism behind plasma-induced gene transfection and found clathrin-dependent endocytosis to have a dominant contribution [207]. The other part of the species transport was attributed to electroporation, while the permeation did not seem to transpire through ion channels or chemical poration. In follow-up research by the same group, the electric field was discovered to be essential for the gene transfection, with a threshold value around 100 V/cm [250]. Vijayarangan et al., on the other hand, did not notice a significant contribution of poration by the electric field [251]. In their experiments, endocytosis was also revealed as a dominant mechanism for plasma-induced drug delivery into cells. He et al. suggested a similar process for the uptake of gold nanoparticles in cells under plasma treatment, based on their measurements [252].

Note, in this regard, that endocytosis may be induced or enhanced by low electric fields, sometimes referred to as electro-endocytosis [253-256]. A transmembrane voltage below 1 mV may be sufficient to influence endocytosis and endocytic vesicle recycling [255], since field strengths as low as a few V/cm already provide a clearly noticeable effect [253, 254, 256]. The mechanisms behind this process are still under debate, more specifically regarding which type of endocytosis is stimulated by the fields. However, a growing interest can be noticed in recent years in fundamental research on this topic. Perhaps not coincidentally, clathrin-mediated endocytosis has been reported as one of the main underlying principles of gene electrotransfection [254, 257, 258]. Next to that, caveolin/raft-mediated endocytosis and micropinocytosis were demonstrated to be important as well in a study by Rosazza et al. [258], while the caveolin-dependent pathway did not play an obvious role in the experiments by Moisescu et al. [254]. Interestingly, endocytosis may be preceded by the binding of the genetic material to the cell wall. According to the experimental data of Wu and Yuan [259], the presence of divalent cations such as Ca^{2+} and Mg^{2+} enhances gene adsorption to the membrane, thus facilitating the electrotransfer. Based on these insights, the endocytosis observed under plasma treatment might largely be due to relatively weak electric fields penetrating into the biological material, possibly enhanced by iontophoresis. As should be noted, such field-induced effect is somewhat reminiscent to vesicle electroformation, whose underlying mechanism is still under debate (see Figure 11) [260-262]. Artificial vesicles actually form interesting test systems to study the effect of electric fields on the cell membrane. A great deal of inspiration on these effects can be found in numerous review papers (see e.g. [262-266]). Schubert and Römer, as well as Madl et al., for instance, discussed how synthetic membrane systems contribute to the understanding of lipid-driven endocytosis [267, 268]. For more information on electro-endocytosis, we refer to the reviews by Kolosnjaj-Tabi et al. and by Baluška and Wan [255, 256].

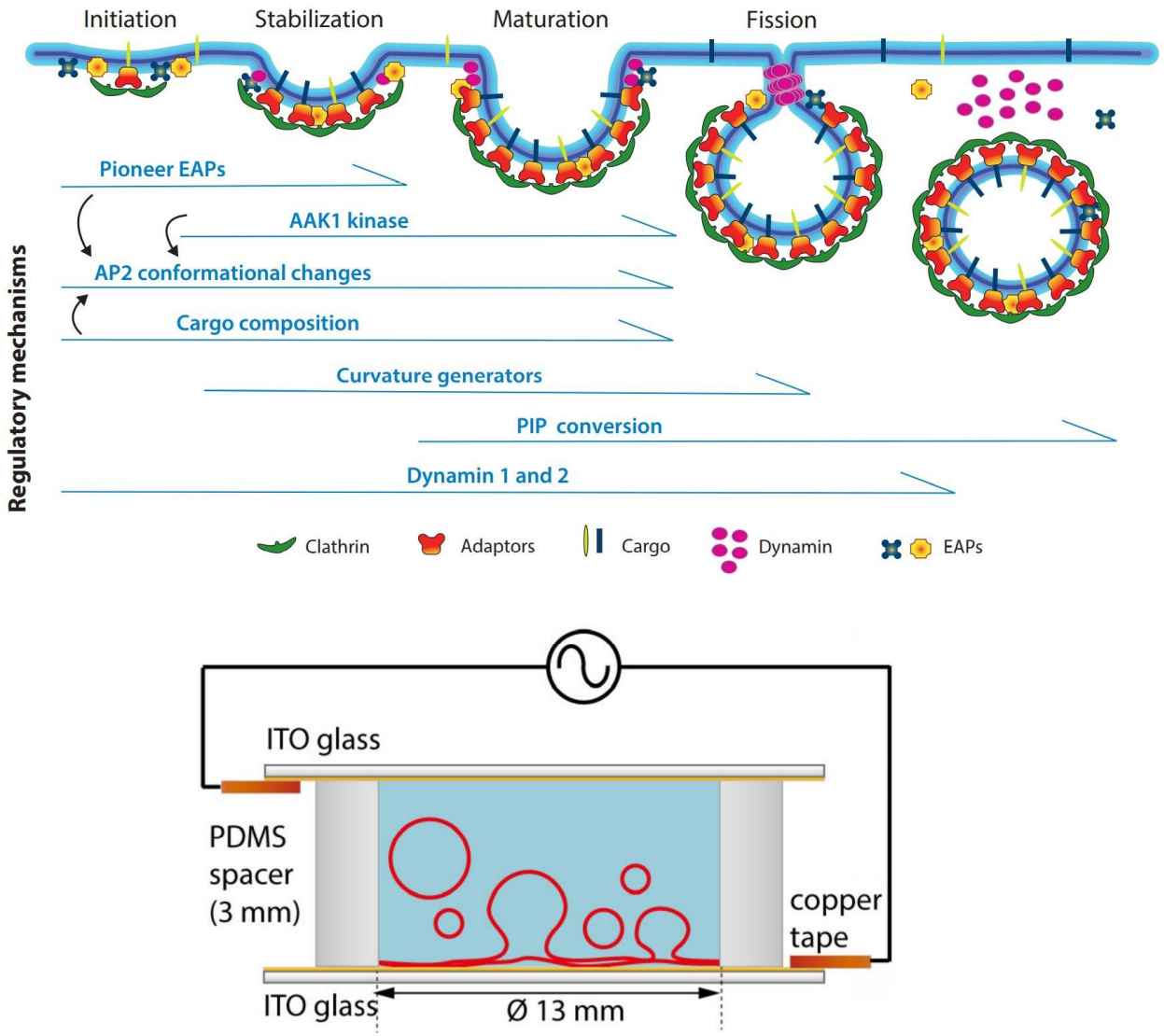

Figure 11. Comparison of (top) clathrin-mediated endocytosis, a mechanism observed in electro-endocytosis, and (bottom) vesicle electroformation on indium tin oxide (ITO) coated glass. As indicated by the horizontal blue line, clathrin-mediated endocytosis is a multistage process, regulated by multiple factors at multiple stages, some of which may be intensified by the field. The electroformation of vesicles can be understood as a field-enhanced version of the natural swelling of a lipid film into vesicles. An electric field stimulates the swelling due to an interplay between electrostatic interaction, bilayer counter ion redistribution, changes in the membrane surface and line tension, as well as electroosmotic processes. (top) Republished with permission of Annual Reviews, Inc., from [249] in Annual review of biochemistry 87, p. 871-896 (2018); permission conveyed through Copyright Clearance Center, Inc. Based on [269]. (bottom) Reprinted from [270]: H. Stein, et al., Frontiers in physiology, Vol.8, p. 63, 2017; licensed under a Creative Commons Attribution (CC BY) license.

3.6 Other effects of plasma-generated fields on biological materials

Electric fields can influence biological materials in many more ways. Figure 12 summarizes some of the most important effects on a cellular level as a function of the electric field strength and pulse duration, based on the recommended review by Kolosnjaj-Tabi et al. [256]. As a tentative rule of thumb, the pulse duration gives an indication of the part of the cellular structure that will be affected by the field. Microsecond pulses have a preferential impact on the cell membrane. Nanosecond pulses, in contrast, shift the aim towards the nuclear matter, by inducing DNA and chromosome damage [271], by altering nuclear processes and by increasing gene expression [272]. Picosecond pulses have recently been made possible with novel high-voltage generators. Their application inhibits the growth of HeLa cells *in vitro* and induces apoptosis, which is believed to follow the mitochondria-mediated route [273, 274]. Note that a shorter pulse in these experiments generally implies a higher field strength. At the lower intensity range around the order of 1 V/cm, the cellular effects become subtler and less destructive. Examples are cell deformation, contraction, elongation, reorientation, alignment and migration. Curiously, cells can also change from one type into another by the electric field, a process known as cellular differentiation. Another peculiar process is cell electrofusion, where the membranes of two cells merge into one [256]. As already mentioned in Section 3.2, electric fields are also able to stimulate cell multiplication, often referred to as proliferation. The current knowledge on the fundamental mechanisms behind these effects is more thoroughly discussed in [256, 275].

One should not forget that the fields can also affect the biological matter on a molecular level. Figure 13 presents a few examples. Similar to iontophoresis in skin tissue (see Section 3.4), electric fields facilitate ionic and molecular transport through biological membranes in other types of biological liquids and tissue via electrophoresis and electroosmosis [275]. Polarizable neutral molecules such as DNA and proteins may be transported and separated in inhomogeneous fields too by dielectrophoresis [276-279]. Further, fields can orientate polar molecules and modify their conformational structure. This is especially relevant for proteins, whose function depends on their quaternary structure. Strong pulsed electric fields in the order of 10 kV/cm are indeed known to inactivate not only microorganisms, but also enzymes [280-283]. Figure 13 shows how they can affect the three-dimensional protein structure. Next to that, DC and AC fields in the order of 10 V/cm or higher may already result in phase transitions, as illustrated with their use for protein crystallization [284]. If such field-induced changes take place in a living organism under plasma treatment, they might obviously have decisive consequences, including different types of cell death. Also in the case of food processing, they may affect the digestion process or the human organism after consumption [283]. Understanding their occurrence and the underlying mechanisms should therefore form a crucial part in the investigation of plasma interaction with biological matter.

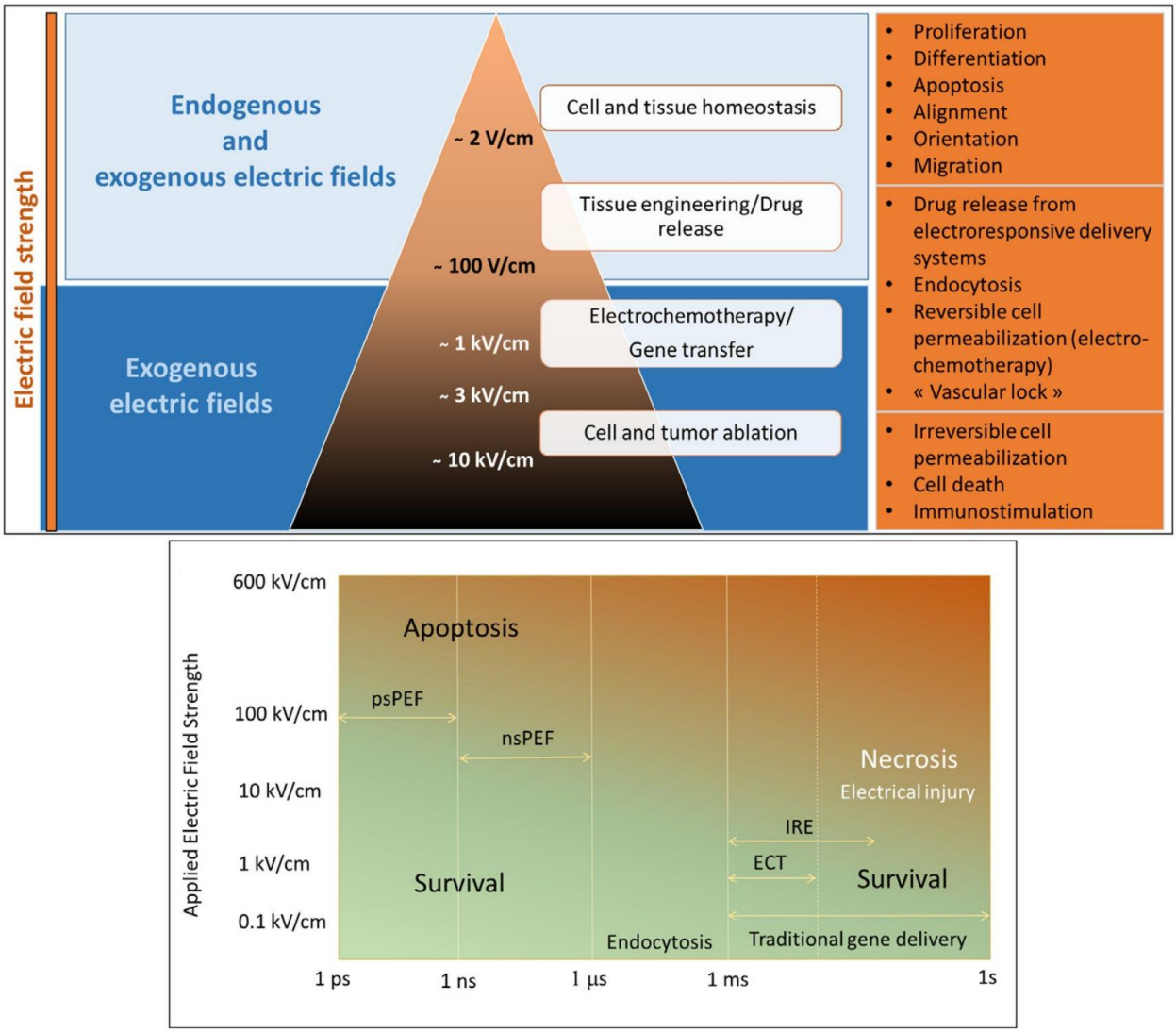

Figure 12. Electric field effects in biological material at a cellular level, (top) as a function of the electric field strength and (bottom) as a function of the field and the pulse duration. The used abbreviations stand for picosecond pulsed electric fields (psPEF), nanosecond pulsed electric fields (nsPEF), irreversible electroporation (IRE) and electrochemotherapy (ECT). (top and bottom) Reprinted from [256] in Advanced drug delivery reviews 138: p. 56-67 (2019), Copyright 2019, with permission from Elsevier. (bottom) Adapted from [285] in Bioelectrochemistry 87: p. 236-243 (2012), Copyright 2012, with permission from Elsevier.

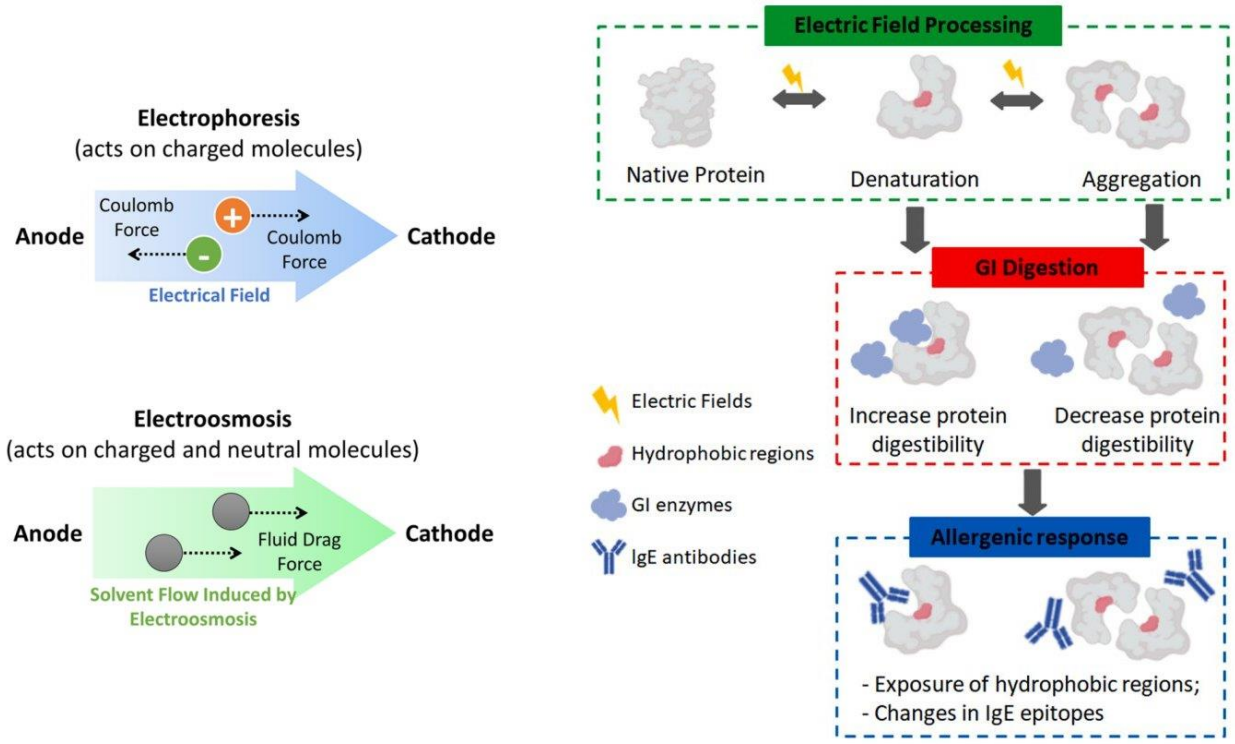

Figure 13. Examples of electric field effects in liquid matter at the molecular level, i.e. (left) transport mechanisms present already at low field intensities and (right) modification of conformational structure at higher intensities. Strong fields can unfold a protein and lead to a higher exposure of an internal hydrophobic pocket. This can lead to either denaturation and a better digestibility by gastro intestinal (GI) enzymes, or a reduced digestibility due to aggregation. These processes can also lead to different immune responses in the human organism. (left) Reprinted by permission from Springer Nature from [275] in Cellular and Molecular Life Sciences 77, p. 2681–2699 (2020). (right) Reprinted from [283] in Food Research International 137: p. 109709 (2020), with permission from Elsevier.

However, these insights are relevant as well for nanomaterial synthesis and chemistry in the liquid phase or at the plasma-liquid interface. Indeed, also for such applications, the plasma-induced electric field can affect the molecular processes in the solution. Moreover, the movement, accumulation and clustering of nanoparticles in a solution can be influenced and controlled with an electric field [266, 286-291]. As should be noted, the same remarks count for magnetic fields (see e.g. [292-295]). A detailed study of the plasma sheath and its relation to the electric and magnetic fields in the liquid will therefore benefit applied research on plasma-liquid interaction in general. In this regard, the sheath dynamics deserves additional attention. It determines the voltage fluctuations over the liquid phase and thus the extent of field penetration, as explained in Section 2.3. Indeed, the amplitude of the penetrating field can only be acquired by means of an accurate sheath model, and to build the latter, more fundamental research needs to be performed.

4. The sheath as a mass transport regulator at liquid metal walls in a nuclear fusion reactor

As already mentioned in Section 1, the presence of a plasma sheath often leads to undesirable effects, like damage to the solid plasma reactor wall by sputtering or an increased heat flux. In order to improve the reactor lifetime, the solid wall may be replaced with a self-repairing liquid one. This approach is currently considered for future nuclear fusion reactors, where damage to the divertor and main chamber plasma facing components (PFCs) forms one of the major concerns [296-298]. In addition to the large heat and ion fluxes, PFCs are exposed to edge-localized modes (ELMs), i.e. explosive magnetohydrodynamic instabilities. On the upside, ELMs provide an effective flushing mechanism for impurities that can otherwise lead to a radiative collapse of the plasma discharge [296]. On the downside, they can cause cracks, blistering, fuzzy, melting and bubbles in the case of solid walls, with an impact that scales with the reactor size [296-298]. Therefore, several ELM control or mitigation techniques have been proposed, including repetitive small pellet injection and resonant 3D magnetic perturbation fields [296, 299].

Additionally, damage to the reactor can be prevented by the use of liquid metal as PFCs, such as liquid lithium, lead lithium alloy (Pb-16Li) and tin [300, 301]. Among these, liquid Li and Pb-16Li can act as deuterium and tritium breeder blankets, due to their retention properties for hydrogen isotopes [300, 302, 303]. As an extra advantage, this results in a diluted Li emission towards the fusion plasma bulk [300, 304]. The plasma sheath over the liquid forms another barrier for the lithium pollution, as displayed in Figure 14. About two thirds of the sputtered Li particles are namely released as ions, which can effectively be accelerated back into the liquid wall by the sheath field [302, 305, 306]. The Li atoms sputtered as neutrals are readily ionized, as shown in several investigations [302, 307-309], which should further limit the undesired lithium pollution. According to a computational analysis by Brooks et al., the effective redeposition of ejected Li from the surface results in a net erosion rate below 1% [310]. However, the simulation of these processes requires advanced modeling methods, because the sheath features vary in time during an ELM [311]. Moreover, the sheath may be influenced by the distinctive properties of the plasma-liquid interface, such as evaporation, surface deformation, droplets and bubbles. This makes the present Perspective Article relevant for nuclear fusion research. Table 1 compares the advantages and disadvantages of solid and liquid PFCs, indicating the need for more investigations on the risks involved with the liquid variant.

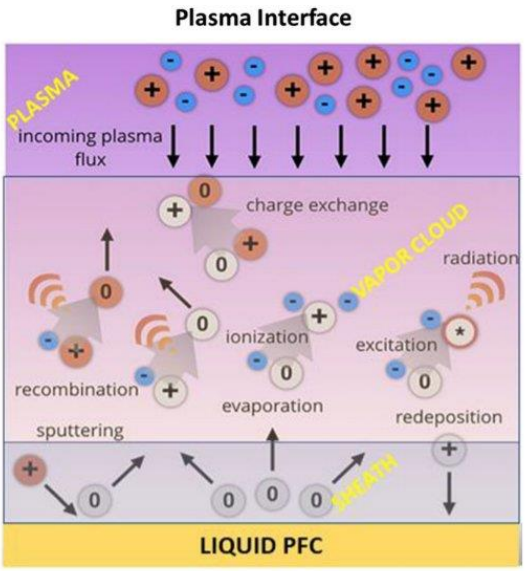

Figure 14. Scheme of the plasma-liquid interface at a liquid plasma facing component in a nuclear fusion reactor, according to Andruczyk et al. [301]. Released liquid species are presented in white. Various processes involving the ions and neutrals need to be considered, such as sheath formation, sputtering, evaporation, adatom effects, ionization, redeposition, migration and surface contamination. Note that the thickness of the sheath relative to the one of the vapor cloud is not *a priori* known, and may vary with the operating conditions, as well as the stage during an ELM. Reprinted by permission from Springer Nature from [301] in Journal of Fusion Energy 39, p. 441–447 (2020).

Table 1. Summary of the advantages and disadvantages of solid and liquid PFCs. The colors indicate the risk, from very low to very high, following the sequence dark green, light green, yellow, orange, and red. Orange and red items could become decisive show stoppers. Reproduced from [298] in Fusion Science and Technology 72(3): p. 211-221 (2017) by permission of the publisher (Taylor & Francis Ltd, http://www.tandfonline.com).

	Solid (e.g. W)	**Liquid**
Lifetime of Plasma Facing Components	PFCs need change-outs	Liquid can be replenished
Maximal steady-state heat flux	5-10 MW/m2	~30 MW/m2 or higher
Resilience to transients (ELMs, disruptions)	Crack formation	Thinning of liquid layer
Tritium retention	Most likely acceptable	Huge hydrogen uptake in Li
Low plasma core contamination (Z_{eff} or radiation)	< 10-5 demonstrated	Not demonstrated
Chemical compatibility in PFC system	None for He; known for water	Critical issue
Embrittlement of structural materials	Irradiation embrittlement	LM embrittlement
Radioactivity at end of plant lifetime	Moderate to high	Low
Accident tolerance (e.g. leaks, air ingress)	Oxidation, little volatilization	Li is potentially problematic
Maintenance and operation	RAMI discussion historically	New
Unknown risks	Low	High

As mentioned above, ELMs may be manipulated by means of magnetic fields, and the same is true for the case with liquid walls. Moreover, magnetic fields enable further control of the mass transport in the sheath. For this reason, the study of a magnetized sheath at a liquid surface is of particular interest to nuclear fusion research. Inspiration can be taken from the parallel research line on magnetized sheaths at solid walls. When B is parallel to the wall, in the absence of collisions and turbulence, the incident particle flux will become zero in the steady state regime [312]. Such situation is relevant for tokamak or stellarator devices, where most surfaces are almost parallel to the magnetic field [313]. The particle-in-cell (PIC) model by Li and Wang predicted such sheath to form with a characteristic time equal to the ion cyclotron time, obtaining a thickness determined by the ion Debye length [314]. For a certain range of the mean-free-path, the sheath splits in two layers of opposite space charge, with the positive one near the wall and the negative one near the plasma, according to the PIC simulations by Moritz et al. [312]. The width of this electric double layer was found to decrease with the magnetic field strength. Other simulation studies, however, demonstrated an opposite process, where the surface collected a positive charge, to repel ions back towards the plasma [315, 316].

In the case of an oblique magnetic field, an additional region appears between the pre-sheath and the Debye sheath, called the magnetic pre-sheath or Chodura layer [112, 312, 317, 318]. Ions from the plasma are first accelerated in the pre-sheath along the magnetic field direction, but reorient towards the wall in the Chodura layer in order to satisfy the Bohm criterion. The effect of the magnetic field and the ion temperature on the sheath was investigated in three independent fluid simulation studies, with some conflicting conclusions. Khoramabadi et al. found the sheath width to decrease with the ion temperature [319], while Liu et al. reported the opposite relationship [320]. Their models agreed on the predicted sheath size reduction as a function of the magnetic field strength, but contradicted with regard to the field orientation. Khoramabadi et al. namely noticed no effect on the sheath parameters by the field component perpendicular to the wall, in contrast to the sheath thickness decrease seen by Liu et al. for a field turning towards this perpendicular direction. The latter effect was also acquired with the model of Pandey et al. [321]. Most fluid models conventionally assume the Boltzmann relation for electron density, which induces inaccuracies. By omitting this assumption, Wang et al. found a floating wall potential reduction and, in the low wall bias range, sheath narrowing [322]. Using a kinetic trajectory simulation model, Chalise and Khanal observed a magnetic field dominant region near the sheath entrance and an electric field dominant region at the wall [323]. Such effects may be useful to manipulate the mass transport through the sheath, but more research is required to obtain insight into the deviations between the models and the sensitivity of the involved parameters.

The situation at a liquid wall with a magnetic field presents some additional challenges in understanding, as well as unique opportunities to regulate the plasma-wall interaction. In electrospraying and electrospinning, for instance, a magnetic field along the symmetry axis of the Taylor cone on the liquid surface can be used to stabilize the cone or to overcome a bending instability of the spraying jet [324-327]. Reversely, charged droplet ejection from the liquid surface may be controlled with an oblique or parallel magnetic field. A similar strategy could be applied to suppress Taylor cone formation or other types of surface deformation. For liquid lithium specifically, a magnetic field parallel with the wall has been proposed as a method to make the lithium flow along the reactor boundaries by means of magnetic

propulsion, an effect discovered at the end of the previous century [328, 329]. Additionally, lithium can be passively pumped by means of thermocapillary [330] and thermoelectric effects [331]. Combined, these mechanisms have motivated the development of thermoelectric magnetohydrodynamics (TE-MHD) [332], which allows to describe stirring of metallic liquids with a magnetic field and an electron beam, consistent with experiments [331, 333]. Although such description seems relevant mainly for very specific systems like fusion reactors, magnetic fields are known to have an effect on liquids in general as well. A strong magnetic field perpendicular to a diamagnetic liquid surface namely deforms the interface by depressing it, referred to as the Moses effect [334, 335]. Paramagnetic liquids, on the other hand, display the reverse Moses effect, where a bump forms on the surface [334, 335]. Both effects are still poorly understood. In this regard, it is useful to keep in mind that liquid lithium is paramagnetic. Water, as a diamagnetic solvent, can also be deformed by this effect. Therefore, magnetic fields may serve as potential regulators of the sheath and the liquid surface in plasma-liquid interaction for a wide range of applications. The study of magnetized plasma sheaths therefore forms an interesting domain for both plasma engineers and scientists. As such, we hope to motivate a collaboration with nuclear fusion scientists and plasma researchers of other fields to further investigate the underlying fundamentals and to develop advanced models for a comprehensive description of magnetized sheaths.

5. The sheath as a chemistry regulator in nanomaterial synthesis and other applications

In Section 2.3, we explained how the chemistry at the plasma-liquid interface strongly depends on the sheath properties. An accurately understanding of this dependency will enable the fine-tuning of target reactions for a specific application. A few examples can already be found in investigations on nanomaterial synthesis. Kaneko and Hatakeyama studied, for instance, the chemical modification of the ionic liquid $[C_8H_{15}N_2]^+[BF_4]^-$ as a function of the incident ion energy [336]. As seen in Figure 15(a), the plasma irradiation of the liquid induced a peak at 297 nm in its UV-vis absorption spectrum, growing with the ion energy for a fixed treatment time. Consequently, the solution changed from pale to dark yellow. When the ionic liquid was used as an anode instead of a cathode, corresponding with electron instead of ion irradiation, the same effect was not observed (see Figure 15(b)). According to the authors, the ion bombardment therefore causes dissociation of the liquid molecules, for which the efficiency improved with ion energy. Following this principle, ion irradiation of ionic liquids may be used for material synthesis, through reactions whose performance can be tuned with a plasma sheath.

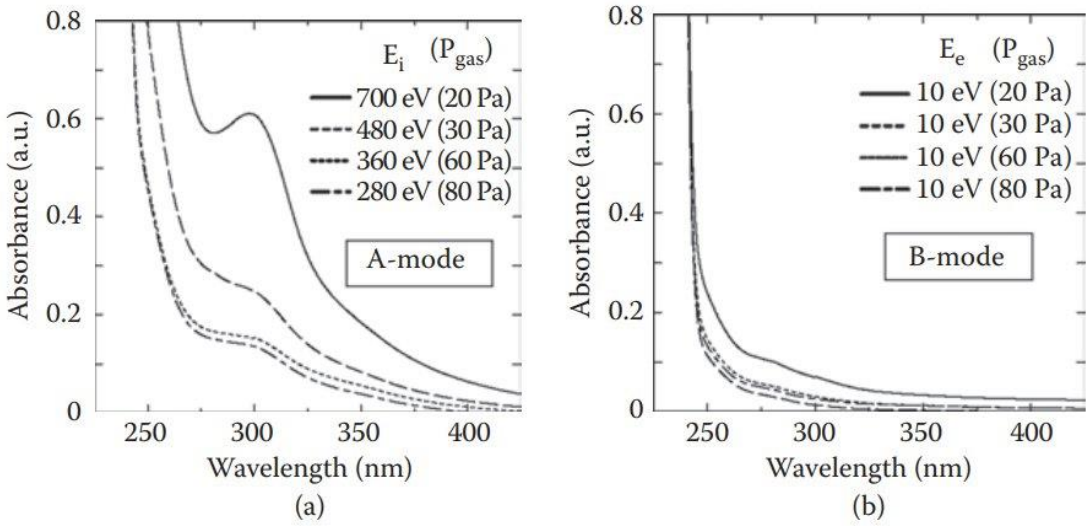

Figure 15. UV-vis absorption spectra of the plasma-treated ionic liquid $[C_8H_{15}N_2]^+[BF_4]^-$ (a) as a liquid cathode for different ion energy E_i and (b) as a liquid anode for electrons with an energy E_e of about 10 eV. The treatment was performed with Ar plasma at a pressure P_{gas} for 2 minutes. The sheath potential could be controlled by changing P_{gas} at a constant discharge current of 1 mA. Reproduced from [336] in Plasma Processing of Nanomaterials (2012) by permission of Taylor & Francis Group. Reproduced with permission of the Licensor through PLSclear.

Although electron bombardment seemed ineffective for this particular experiment, it may be effective in others. In fact, gaseous plasma has been proposed as a versatile cathode for electrochemical reactions that are unpractical or impossible with solid cathodes. Certain electron reactions namely require an activation energy inaccessible by conventional electrochemistry. An anode sheath at the liquid surface, in contrast, can accelerate the electrons towards the liquid, giving access to the reaction at its surface. In their review of 2011 [337], Mariotti and Sankaran elegantly describe how plasmas allow to decouple the reaction kinetics at a liquid surface from the overall system thermodynamics. According to their description, the principles behind electron-induced reactions in a gas phase plasma remain valid at a plasma-liquid interface. In other words, cross section data similar to the gas phase counterpart can be imagined for electron collisions with dissolved species at the liquid surface. As a well-known quantum mechanical effect, the excitation, dissociation, or ionization of a particle generally displays resonant regimes around certain electron energies, visible as a local maximum in the cross section. Applying this idea to the plasma-liquid interface, an anode sheath can be used to tune the incident electron energy, in order to stimulate one specific reaction.

To illustrate this, Mariotti and Sankaran elaborated on dissociative electron attachment by means of the model for a hypothetical diatomic system AB in Figure 16 by Krishnakumar et al. The latter authors explained the dissociation process as a sequence of resonant electron attachment to the excited state AB^{-*} and dissociation along its repulsive potential energy curve (purple line) [338]. In order to obtain the AB^{-*} state, only energy in a narrow interval can be added to the AB ground state, next to the attachment of the electron. The width of this interval is indicated by the blue peak in Figure 16. Such resonant electron

capture by the molecule can be realized from a vibrationally or electronically excited intermediate AB^* before the electron attachment, or directly from the AB ground state through the appropriate kinetic energy of the colliding electron [338, 339]. In other words, a specific dissociative electron attachment process can be selectively initiated by means of the electron energy. At a liquid anode, this energy can on its turn be tuned with the anode sheath properties. This permits a strategy to selectively synthesize nanomaterials with plasma-liquid interaction.

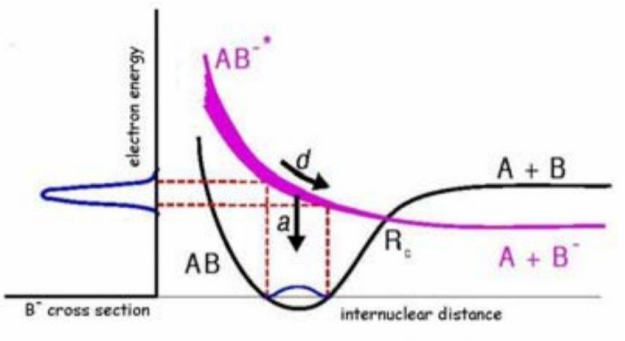

Figure 16. Schematic model of dissociative electron attachment of a hypothetical diatomic system AB. The attachment occurs in the Franck-Condon region to form the resonant state AB^{-*}, which has a repulsive potential energy curve indicated by the purple line. The width of this curve represents the finite lifetime of AB^{-*} against auto-detachment, i.e. spontaneous electron ejection, denoted with the arrow **a**. The more likely dissociative path is shown by means of the arrow **d**. If the repulsive state survives against auto-detachment until the internuclear distance R_c, it dissociates to give the stable neutral fragment A and the negative ion B^-. Reprinted from [338]: E. Krishnakumar, et al., XXV International Conference on Photonic, Electronic and Atomic Collisions, 2007; licensed under a Creative Commons Attribution (CC BY) license.

Nonetheless, we would like to put forward three points of caution about this hypothesis. First of all, reaction mechanisms like the one of Figure 16 are usually studied in the gas phase, instead of at the liquid surface. Prabhudesai et al., for instance, observed resonant electron capture directly from the AB ground state during the interaction of a molecular beam with a pulsed electron beam [339]. In the gas phase, the dissociation process along the repulsive potential curve (arrow **d** in Figure 16) mainly competes with the less likely auto-detachment process (arrow **a**). In the liquid phase, however, several other relaxation channels might become available. This *a priori* puts into question the mechanism's validity at the liquid surface. Yet, as pointed out by Mariotti and Sankaran, dissociative electron attachment has already been reported for electron beam excitation of various solutions from alcohols to water, demonstrating its validity *a posteriori* [337, 338, 340-342]. Even so, such confirmation is required for all other types of reactions, if one wishes to translate a gas phase mechanism to the liquid surface.

As a second point of caution, this still does not prove the mechanism's effectiveness at the plasma-liquid interface, because the strong local field may increase the probabilities of the various relaxation channels competing with the reaction. As a third point of caution, even if the reaction proceeds, the electric field may also interfere with its pathway. The field is namely expected to reorient the liquid surface species in an anisotropic manner, changing its direction relative to their bond and reaction axes, in agreement with

the chemical field effects discussed in Section 2.3. In fact, this could provoke reaction pathways inaccessible in conventional electron beam experiments, adding another dimension of selectivity to the plasma-liquid interfacial chemistry. Using electron energy as a control parameter, Krishnakumar et al. found dissociative electron attachment to selectively break the N-H and O-H bonds in carboxylic acids, without much damage to other bonds [338]. In contrast, the selectivity did not appear as good for C-H bonds. The local field of the sheath may provide a means to modify this pattern, allowing the synthesis of unique nanoparticles. As an important remark, the orientation of the bond to be broken relative to the incoming electron direction is also expected to be an important factor in the chemical control and anisotropy. Krishnakumar et al., for instance, observed this orientation to be decisive for the angular distribution of the ejected product anions, independent of the molecular orientation [338]. They termed this phenomenon *bond orientation dependent electron attachment*.

The plasma sheath can also influence the chemistry at the liquid surface with non-collisional processes. An example is given by Morishita et al., in a reaction route towards nanocarbons realized with bipolar pulsed spark-glow transition plasma in benzene [343]. According to their study, this route starts with the electronic excitation of benzene at the plasma-solution interface by the local field. The π-conjugated bonding and antibonding orbitals namely lie close to the Fermi level, giving the molecule a high reactivity. The electrons in the π-orbitals are therefore readily excited to π* orbitals by the plasma sheath potential, which plays a similar role as the electrical double layer potential in conventional electrochemical reactions. Subsequently, the excited electrons can be ejected by collisions of plasma particles at the interface. This produces benzene radical cations, which serve as important intermediates in the formation of polycyclic aromatic hydrocarbons, i.e. nanocarbons. In comparison to the other organic solvents (hexane, hexadecane and cyclohexane), benzene displayed the highest synthesis rate. Morishita et al. explained the lower efficiency for the linear molecules with a synthesis process in the gaseous plasma from small molecules such as C_2 under heat, similar to pyrolysis. For the saturated ring of cyclohexane, on the other hand, unsaturated ring molecules first needed to be formed through C-H dissociation, adding additional steps in the reaction pathway towards the nanocarbons. These different routes likely also underlie the lower degree of nanocarbon crystallinity obtained for the ring molecules relative to the linear ones. The proposed reaction schemes are in good agreement with the reactivity of the starting materials, as evaluated via *ab initio* molecular orbital calculations [343].

As another example of non-collisional interfacial chemistry that may be controllable by the sheath properties, reactions of solvated electrons are expected to strongly depend on their electronic state. Rumbach et al. investigated the solvation of electrons by a DC atmospheric pressure glow discharge into a water anode, finding an unexpected blue-shift of about 50 nm in the measured absorption spectrum relative to the well-known peak of the bulk solvated electron at 720 nm (Figure 17(a)) [131]. They attributed this blue-shift to the intense electric field in the interfacial Debye layer, which is closely related to the sheath features. If this is correct, the interfacial solvated electron reaction kinetics may be controllable by the sheath, forming another argument to intensify investigations on this topic. However, the origin of the blue-shift is speculative for now, because it might instead be an inherent property of the interface, independent of the plasma. Although several computational studies suggest the fully solvated electrons at the air-water interface to be almost or completely indistinguishable from their bulk

counterpart (see e.g. [54, 55, 58, 344, 345]), their findings do not contradict a possible blue-shift of 50 nm (or 0.13 eV) in the absorption spectrum. Figure 17(b) illustrates this with results from mixed quantum mechanics/molecular mechanics simulations combined with time-dependent density functional theory calculations, using the same protocol for the interfacial and bulk spectrum [345]. A blue-shift of about 1 eV can be seen for the interfacial variant, in agreement with a later analysis of the same data [55] and with the experimental observations by Rumbach et al. Yet, more investigations are required to provide a conclusive assessment about the origin of this blue-shift, since contradictive output has been obtained with other simulation methods. A red-shift of 0.5 eV and no shift at all in the interfacial absorption peak have been predicted by the respective TB and LGS models, named after their developers Turi and Borgis, and Larsen, Glover and Schwartz [57, 58, 346]. We also note that Figure 17(a) seems to be the first experimental absorption spectrum of the interfacial solvated electron reported in literature. Moreover, none of the mentioned models take into consideration the possible long-range quantum correlations between neighboring solvated electrons and negative ions, which may significantly affect their spectral features and underlie the experimental blue-shift as well.

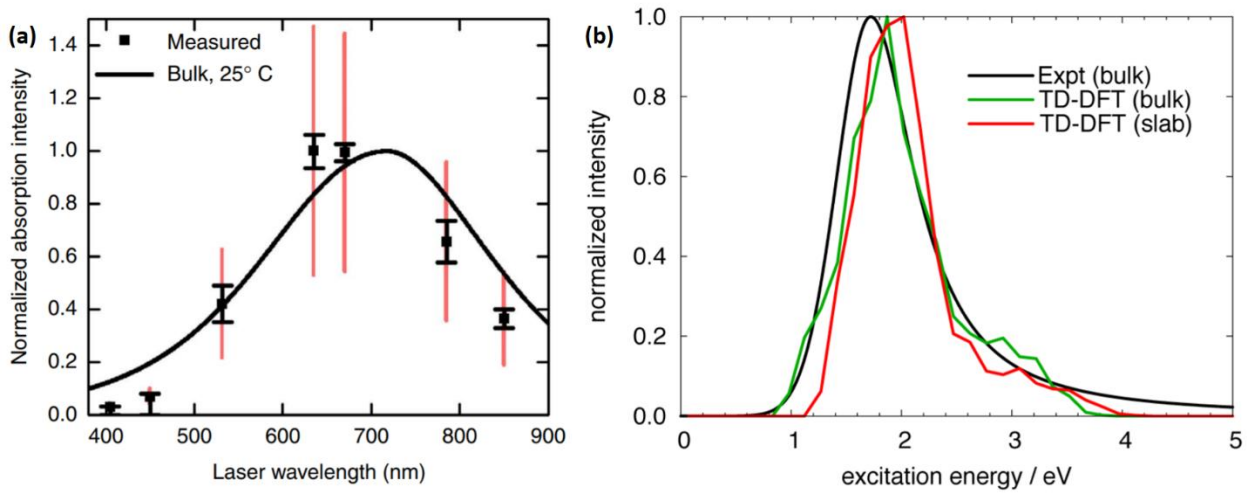

Figure 17. The optical absorption spectrum of the solvated electron (a) as measured at the plasma-solution interface using laser diodes at different wavelengths and (b) as computed at a gas-water interface using a mixed quantum and classical protocol with time-dependent density functional theory (TD-DFT). The black error bars with capped ends represent the root mean square variance in the raw measured data. The overlaid red error bars additionally account for the systematic uncertainty in the laser-plasma overlap. The simulated curve (in red) is compared with its counterpart in the liquid bulk, obtained with the same computation protocol. Further, the black solid lines in both graphs show the experimental spectrum for the solvated electron in the bulk liquid. (a) Reprinted from [131]: P. Rumbach, et al., Nature communications, Vol.6(1), p. 1-7, 2015; licensed under a Creative Commons Attribution 4.0 International License. (b) Reprinted with permission from [345] in The Journal of Physical Chemistry A 118(35): p. 7507-7515 (2014). Copyright 2014 American Chemical Society.

In principle, the sheath can also influence the solvated electron chemistry at the liquid surface in more indirect manners, by regulating the penetration depth or the local density of the species. According to

Mota-Lima, two additive contributions need to be distinguished in the penetration depth: (i) the thermalization penetration, i.e. the distance due to slowing the kinetic motion of the plasma-injected electrons, and (ii) the diffusion length of the solvated electrons, i.e. the range of the associated mass diffusion within a given time window [347]. In the presence of an electric field in the liquid, however, a third contribution needs to be considered as well, namely (iii) the drift of the solvated electrons along the field. The total penetration depth is therefore expected to depend on the sheath properties. As should be noted, the thermalization depth is often called the penetration depth in literature, so caution is required when interpreting the given values.

In the study by Rumbach et al., the average thermalization depth of the electrons was estimated to be 2.5 ± 1.0 nm, based on the aforementioned absorption measurements and the reaction kinetics [131]. From this value, the authors concluded the electrons to get fully solvated before reacting. Monte Carlo simulations by Meesungnoen et al. gave a thermalization penetration of 1 to 30 nm for electron energies between 1 and 100 eV [348]. Diffusion lengths as calculated by Mota-Lima ranged from 269 to 2084 nm [347]. Only rapidly changing sheath fields can penetrate the liquid down to such depths (see Section 3.3). Rumbach et al. determined a field strength of 10^4 V/m at the liquid side in the interfacial electrostatic Debye layer, by means of an analytic model [128]. Using this value, they disregarded the drift component in the solvated electron transport, finding a penetration depth ranging between 10 and 100 nm over a wide range of electron current densities j_e, inversely scaling with j_e and reaching 28 nm for a typical current density $j_e = 10^4 \mathrm{Am}^{-2}$ [349]. According to the model, the interfacial concentration of the solvated electrons increases with j_e, ranging between 0.02 and 1 mM. The increasing density and decreasing penetration depth with j_e was also observed in the model of Keniley and Curreli [350] and has recently been confirmed with experiments [351]. Further, these results are in good agreement with the simulation output from the particle-in-cell Monte Carlo collision (PIC-MCC) model with liquid chemistry developed by Gopalakrishnan et al., which provided an electric field strength in the liquid of 10^4 V/m, and a solvated electron density profile from almost 1 mM at the surface to around 0.1 mM at a depth of 20 nm, dropping to 10^{-3} mM around 90 nm [129]. The external electric field was found to only weakly influence the solvated electron density profile.

However, both the models from Gopalakrishnan et al., and Rumbach et al. have neglected the free electron penetration through thermalization upon impact. Their results therefore do not represent the conditions in the first molecular layers of the liquid. For instance, the calculated electric field strengths of 104 V/m at the liquid side cannot explain the aforementioned blue-shift in the absorption peak [128, 352], but stronger fields may still be present near the liquid surface due to such disregarded effects. The possible field-dependency of the observed blue-shift thus remains an open question. Next to that, the solvated electron chemistry may be regulated by the sheath in the upper region of the liquid, by means of the varying thermalization depth with the incident electron energy, as acquired with the Monte Carlo simulations by Meesungnoen et al. [348]. In this respect, Levko et al. performed another interesting modeling study of streamer penetration into the surface of a de-ionized water anode with a PIC-MCC method [130]. In contrast to other models, which ignore electron impact reactions, their simulations predict ionization of the water molecules at the surface due to the kinetic electrons from the plasma. Additionally, the simulations revealed an ion-rich sheath with positive space charge in the vicinity of the

water surface on the gas side, as already discussed in Section 2.4 and Figure 5. This forced plasma electrons back towards the plasma phase. Further in the plasma, the electric field reversed, strongly accelerating the plasma electrons towards the liquid surface to overcome this repulsion. At the surface, the electrons penetrated into the liquid to a depth of about 20 nm, producing solvated electrons with an average kinetic energy of 0.02 eV [130], i.e. thermal energies expected around room temperature. The striking differences with the other models regarding electron solvation form yet another reason to promote more fundamental work on the sheath properties in plasma-liquid interaction. In particular, more accurate information on the solvation dynamics of electrons and other plasma species for the unique conditions at the plasma-liquid interface is highly desirable.

Deeper towards the liquid bulk, below the thermalization depth, the chemistry likely becomes rather independent from the external field. Importantly, the solvated electron chemistry displays a strong selectivity on its own, making it particularly attractive for nanoparticle and chemical synthesis applications. Hawtof et al. recently reported a record-high faradaic efficiency approaching 100% for ammonia synthesis from nitrogen plasma and water, attributed to the selective production of hydrogen radicals from solvated electrons [353]. Rumbach et al. measured a faradaic efficiency close to 10% for CO_2 reduction in an aqueous solution by the solvated electrons injected from an argon plasma, and postulated it to reach 100% for an increasing CO_2 concentration [354]. Mota-Lima explained the obtained results with a theoretical framework, similarly predicting the reduction efficiency to become 98%, with 97% selectivity to oxalate generation, if a flow cell is used to refill the aqueous CO_2 in the reactor [347]. Using a computational model for silver reduction with plasma-produced solvated electrons, Zeng et al. found the relative electron and silver ion concentrations in the liquid phase to be decisive for the type of products being formed [355]. An excess of solvated electrons mainly resulted in neutral silver clusters, while ionic silver clusters were dominantly generated in the case of excess argon ions. Various studies have demonstrated the crucial role of the current density, plasma gas and scavenger concentration on the solvated electron density and chemistry (see e.g. [129, 353, 355-357]). In addition to the selection of these parameters, a more profound understanding of the plasma sheath will allow further fine-tuning of the species transport through the interface and thus of the aqueous chemistry accordingly.

If an electrolyte solution is used as a liquid cathode to obtain a plasma-induced liquid chemistry, the system is often referred to as glow discharge electrolysis (GDE) [144, 358-360]. This configuration has been intensively investigated for various applications, including chemical and nanomaterial synthesis, water treatment, surface modification and functional polymer preparation [358-360]. As we will illustrate in Section 6.1, the ions bombarding the electrolytic cathode induce several competing reaction pathways in the liquid phase, some of which involve excess electrons. Correspondingly, electron emission may occur, or the electrons react further in the solution, perhaps with additional energy before getting fully solvated. Therefore, the above discussions on dissociative electron attachment and solvated electrons at a liquid anode may also apply to a liquid cathode to a certain extent. It would thus be interesting to investigate in future research the prevalence of solvated electrons at a liquid cathode and to compare the related chemical mechanisms with the opposite electrode polarity.

6. Towards a fundamental understanding of the liquid-related sheath properties

6.1 Electron emission mechanisms for a liquid surface

As indicated already in Figure 1, one of the most crucial material features affecting the plasma sheath involves its ability to emit electrons. While the electron emission mechanisms from a solid surface are relatively well understood, the situation for a liquid surface remains more obscure. A significant part of our previous review paper has been devoted to this topic [35], so we will only give a short overview here, with a few additions. On the timescale of a single plasma species interaction with the surface, the liquid appears frozen in time to a good approximation. Physical sputtering by an incident ion, for instance, can take place in a few to tens of femtoseconds [361, 362]. Local heating effects due to the transfer of the ion kinetic energy occur on a subpicosecond timescale up to a few ps [361, 363, 364]. During this entire event, the liquid can be considered very similar to a solid, which permits to adopt the electron emission mechanisms for solid electrodes. More precisely, electrons may be released from a liquid surface via the photoelectric effect, or through secondary electron emission by bombardment with ions, hot neutrals, metastables or electrons, as long as the energetic conditions allow it. In the case of ion bombardment, the electron to be emitted can absorb both the kinetic and potential energy of the ion. As should be noted, insulating dielectric solids are known to display a generally higher secondary electron emission yield in comparison with metals [365]. This also counts for water ice, of which the emission yield has been measured to be significantly higher than the one of aluminum [35, 366]. Additionally, a strong local electric field can cause band bending and the shifting of surface levels, aiding the escape of the electron. Thermionic emission, on the other hand, is only expected to be relevant for liquids that do not decompose or evaporate below the high temperatures needed for it.

On the atomic scale, the electron emission mechanism of a liquid surface can therefore be identical to the ones described for solids. However, dielectric liquids possess a few characteristics that may counteract these effects. In the first place, the charge transport between their surface and bulk transpires through diffusion, drift and convection, in contrast to solids. Accordingly, the overall electron emission is likely transport-limited. Such limitation may explain the relatively low secondary electron emission coefficient frequently measured for electrolyte solutions. For example, Delgado et al. recently obtained a value below 10^{-5} from their experiments, meaning that only one electron is emitted by bombardment with more than 100,000 ions [53]. In the second place, the electron solvation dynamics in liquids often involve the rotational or librational reorientation of the composing particles. In principle, these effects do not necessarily prevent the emission of electrons, but they affect the charge organization and microscopic structure of the liquid surface. As a central question, one may ask where emitted electrons from this distinct structure exactly come from.

In this context, several mechanisms have been proposed involving the individual liquid constituents, such as solvated electrons or negative ions residing in the liquid phase. For example, Cserfalvi and Mezei postulated a four-step process for a water surface, where incident ions generate solvated electrons, which react to produce aqueous hydrogen atoms that on their turn diffuse towards the gas phase, where they get ionized and emit secondary electrons [150]. Gaisin and Son instead assumed electrons to be released by negative ions in the gas or liquid side of the interface [367]. Polyakov et al. went further by considering

the electron emission from the liquid phase to be a competitive process with solvation and scavenging of quasi-free electrons [368]. Delgado et al. recently extended this idea with the scheme of Figure 18, and by specifying the energetic state of the quasi-free electron [53]. According to their model, the electron resides at the bottom of the conduction band of the liquid, about 1 eV below the vacuum level, before rapid localization into a pre-solvated state would take place. This is a more favorable state for electron emission than the solvated electron, which has a vertical binding energy of about 3.7 eV in the liquid bulk [55, 58, 369]. Delgado et al. suggested that the required emission energy of 1 eV for the conduction band electron may originate from the kinetic energy of the incident ion, although they did not exclude the possible contribution of other mechanisms, such as field emission [53].

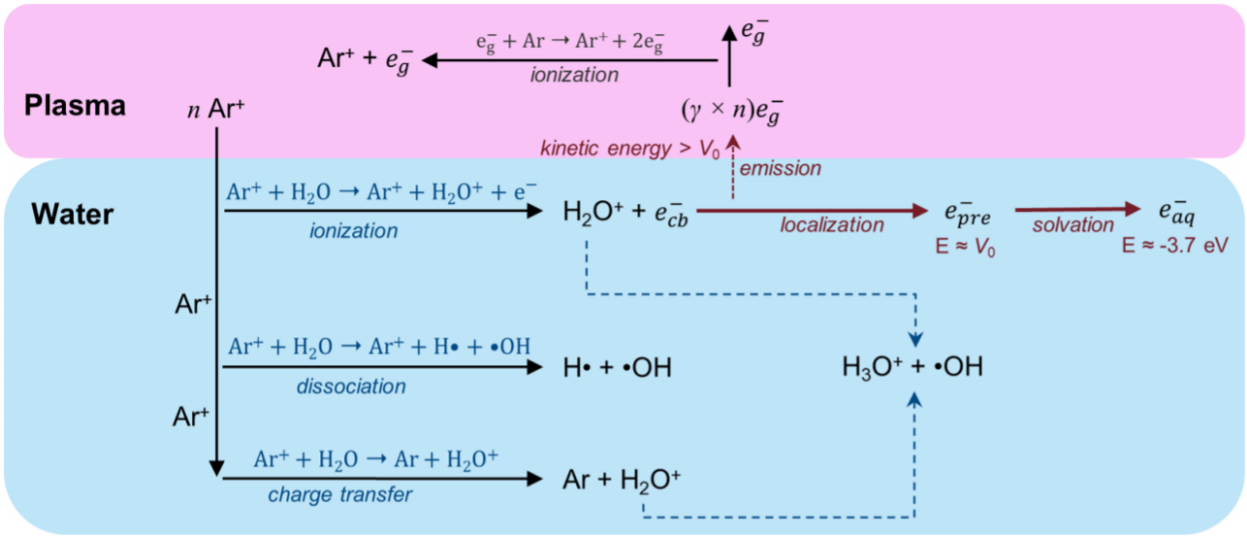

Figure 18. Scheme of the ion-induced secondary electron emission mechanism proposed by Delgado et al. For n argon ions bombarding the surface, $\gamma \times n$ emitted electrons e_g^- are produced. The argon ions interact with a water molecule in the liquid phase near the surface, which may ionize the molecule in competition with other reactions. In the case of ionization, the resulting conduction band electron e_{cb}^- either is emitted if it has sufficient kinetic energy or relaxes into a pre-solvated state e_{pre}^- to subsequently become a solvated electron e_{aq}^-. The electron levels are indicated relative to the vacuum level. Reprinted with permission from [53] in Langmuir 36(5), p. 1156-1164 (2020). Copyright 2020 American Chemical Society.

We support the idea behind this model, but propose a further extension and refinement. First of all, Delgado et al. assumed the mechanism for incident Ar^+ ions, while electron emission is likely favored for H^+ ions and hot H atoms. As already pointed out by Polyakov et al., protons are the major fragmentation product of water molecules under electron and ion impact [368]. Moreover, they have an order of magnitude higher mean free path in water vapor than heavier ions, such as Ar^+ and H_2O^+. Therefore, they can accelerate to a substantially higher kinetic energy in the sheath before colliding with the liquid surface. Intermediate charge transfer reactions can transform them into hot H atoms, which have an even higher cross section for liquid water ionization [368, 370, 371]. Such details are important, considering the low secondary electron emission yield of 10^{-5} measured by Delgado et al. [53].

Secondly, envisioning a more universal look on plasma-liquid interaction, the time-dependence of the plasma features needs to be taken into consideration as well. Babaeva et al., for example, simulated the interaction of a positive streamer in atmospheric air with dry and wet wounds [198]. During the first few nanoseconds when the plasma filament struck the surface, they found an electric field strength in the sheath significantly surpassing 10^7 V/m. Assuming an ion mean free path of half a micron at atmospheric pressure, they deduced incident ion energies in excess of 20 to 30 eV on dry wounds, and even beyond 60 to 70 eV on wet wounds with high permittivity [198]. Such a brief pulse of energetic ions likely induces effective secondary electron emission and distinct aqueous reaction pathways.

Thirdly, the water surface is expected to be a complex quantum mechanical environment, with a more convoluted electronic structure than the one presented in Figure 18. As already discussed in Section 5, the blue-shift in the optical absorption peak of the interfacial solvated electron by Rumbach et al. still remains an open question. It seems to imply a larger energy between the ground state and the first excited state of the solvated electron, but may also be related to a smaller vertical binding energy of the latter, and perhaps significantly longer lifetimes of the excited states. The energy scheme will display local variations, due to the presence of other charged species at the interface and surface deformations (see also below). Moreover, the electronic structure of the interface can be further modified by long-range quantum correlations between excess electrons, which are extremely hard to capture even with the most advanced modern ab initio computational quantum mechanical techniques.

Fourthly, the ionization and electron emission processes may involve excitation mechanisms characteristic to the condensed phase. For instance, two neighboring electronically excited species or solvated electrons may transfer energy between each other, to generate an Auger or Auger-like electron emission event. Alternatively, the ensemble of such species at the interface may acquire excitations of a more collective nature. It is worth noting that Polyakov et al. already suggested the possible contribution of pre-existing collective excitations of water molecules in electron emission at the liquid surface [368]. However, they did not further specify the nature and mechanisms behind these phenomena. Collective excitations and their interactions are well-known in condensed matter physics, often expressed in terms of quasi-particles. They might therefore play a crucial role at the plasma-liquid interface too. In theory, electronic excitations of individual interfacial aqueous species can form plasmonic waves. If the energy of such surface plasmons exceeds the binding energy of an electron, electron emission may occur. To our knowledge, such quasi-particle-based electron emission mechanism has not been proposed before in the scientific literature. It can be more generally described for any plasma-liquid interface by means of the multi-plasma model, a quasi-particle-based theoretical framework that we recently introduced for the excitation and thermalization processes in laser-excited matter [77]. Similarly, the multi-plasma model could serve as a useful toolbox to describe excitation and relaxation mechanisms at a plasma-liquid or plasma-solid interface in general.

Nevertheless, the applicability of these models and mechanisms to plasma-liquid interaction is still speculative, because several other processes complicate the interfacial structure. The surface of volatile liquids is continuously covered by a vapor layer, which may effectively shield the surface from incident ions. Taking into account the relatively low latent energy of 0.4 eV to evaporate a water molecule on average from the bulk liquid, the heat flux caused by the ion bombardment may even enhance this effect,

counteracting the ion-induced electron emission. This invokes another question, whether electron emission predominantly occurs at the main liquid surface or in the plasma sheath itself. Indeed, negative charge can also be transferred from the liquid to the gas phase in the form of negative ions, clusters or droplets. Strong local field enhancement at such clusters and droplets, as well as modifications in the solvated electron state, perhaps permit a more favorable electron emission process in comparison to at the main surface in contact with the bulk liquid (see also Section 6.2). Additionally, droplets adjacent to the main liquid surface can enhance the local electric field there too [372]. Closely related is the explosive electron emission mechanism proposed by Mesyats, where electrons are released in an explosive event at the sharp tip of Taylor cones formed on the surface under influence of the sheath field and local field enhancement [373, 374]. Note in this regard that electron emission may transpire as discrete events, limited in time by surface deformation and droplet formation, rather than through stochastics in the individual interactions of ions with the surface. Accordingly, each of the processes depicted in Figure 1 are relevant to the discussion of electron emission from a liquid surface. Which of these mechanisms dominates the electron emission remains an open question, requiring more fundamental experimental and computational studies.

6.2 Origin of droplets in the plasma sheath

In principle, droplets over a liquid surface can originate from either droplet ejection or nucleation in the vapor phase. At the plasma-liquid interface, several mechanisms of droplet ejection can be thought of. Electrospray ionization serves as a famous example with a rich research history, where charged droplets are emitted from a Taylor cone, under influence of the local electric field [375]. In general, droplet ejection may be expected as a product of extreme deformations of the liquid surface. Fuchs et al., for instance, proposed field-induced electrospray processes and the break-up of microjets by capillary waves, to explain microdroplet formation during the operation of a floating water bridge [376]. Similar effects may be at work at a plasma-liquid interface, where conditions are expected to be even more violent. Plasma can even penetrate through the surface into the liquid bulk, as observed in experiments [377, 378]. Next to that, boiling and electrolysis enable the generation and collapse of microbubbles at the liquid surface, also leading to possible microdroplet ejection [35]. When the charged droplets enter the sheath, they can reduce in size by evaporation, fission processes and sputtering, similar to the mechanisms in electrospray ionization [375]. Still, droplets ejected from the liquid have the potential to be comparable in size to the sheath thickness. Since a sheath also forms around them, they can significantly alter the sheath properties.

Nucleation in the vapor phase, on the other hand, results in molecular clusters and droplets of a much smaller size. Many useful insights on this phenomenon have been reported in aerosol science, for the study of the atmosphere [379, 380], for nanoparticle synthesis [381] and various industrial processes. These insights often seem to directly apply to the plasma sheath at a volatile liquid, but will likely need to get revised to the conditions specific to the considered interface, such as the field strength and ion densities. This forms a challenging task, considering the experimental and computational difficulties encountered in research on vapor nucleation outside a plasma environment. Detection of nucleating

clusters requires highly sensitive instrumentation that minimize cluster fragmentation during measurement [382]. The transient nature of the nucleation poses another challenge, especially when rapid nucleation rates demand a high time-resolution of the measuring device. Next to that, nucleation often occurs in complex chemical environments with numerous species as possible participants. In a plasma sheath, the presence of the liquid surface further complicates the cluster detection. Still, the detection technology has advanced tremendously in the past decades, currently allowing the observation of nucleation on the molecular level, e.g. by means of mass spectrometry. A complementary source of information is provided by modeling techniques. For this purpose, the most commonly applied atomistic methods are quantum chemistry calculations, Monte Carlo and molecular dynamics simulations [382]. The former relies on first principles of quantum mechanics, by which cluster energy is obtained with the highest level of accuracy, but at a high computational cost. The latter two, in contrast, are mostly based on atomic force fields, and enable the simulation of larger clusters with decreased accuracy. Despite the advancement of these methods and the large research efforts in this domain, finding agreement between experimental and simulation output regarding the nucleation rates remains problematic [383-385].

To the best of our knowledge, investigations on vapor nucleation at the plasma-liquid interface have not been performed yet *in situ* on the molecular level. In this sense, the mechanism remains speculative for now in this system. However, the wide interest of plasma-liquid interaction for nanomaterial synthesis implies that this hypothesis is not new. Moreover, vapor nucleation in laser ablation is a well-known effect with a clear resemblance [381]. At the plasma-liquid interface, its occurrence is expected to depend on various local factors, such as the temperature, pressure and their spatial and temporal variation, the oversaturation degree of the vapor, and the presence of nucleation precursors. As should be noted, ions serve as effective initiators of nucleation [379, 381], strengthening the hypothesis. For an atmospheric air plasma containing humidity, for instance, H_2O molecules attach to O_2^- through cascade reactions, to form $O_2^-(H_2O)_3$ as the most probable cluster [386]. An analogous process is observed for positive ions, but in a less pronounced manner [387]. Another open question is the subsequent growth of the clusters into microdroplets and how the electric field influences this process. According to the classical thermodynamic nucleation theory, clustering of vapor molecules needs to overcome an energy barrier, in order to obtain a cluster size above which further growth is spontaneous (see Figure 19) [382, 383]. This energy barrier depends on the vapor saturation ratio S. If S is less than 1, the Gibbs free energy keeps rising with cluster size, and no spontaneous growth can be reached. If it is much higher than 1, the energy barrier disappears, and spontaneous clustering is immediate [382].

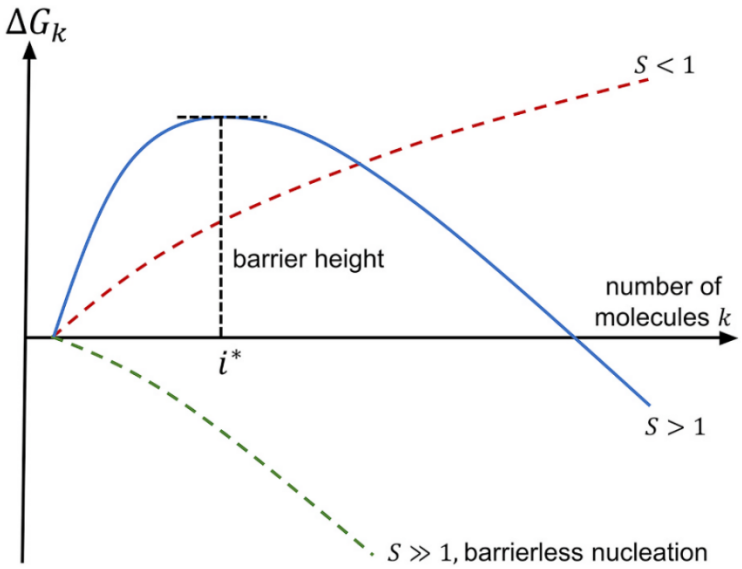

Figure 19. The Gibbs free energy ΔG_k of cluster formation as a function of cluster size for three examples of the vapor saturation ratio S. Reprinted from [382] in Journal of Aerosol Science 153, p. 105676 (2020), with permission from Elsevier.

However, classical thermodynamics is known to break down at the quantum scale, so this picture is likely oversimplified. We refer here to the analogy with nanobubbles in the liquid phase, which were thought for a long time to be thermodynamically impossible, but still turned out to exist with a remarkable stability [35, 388-390]. Likewise, various subtle quantum mechanical effects may need to be taken into account for an accurate calculation of the cluster free energy. A strongly related point to consider is the local electric field at a microdroplet surface, and the effect of an external field on the stability and growth rate. As the state-of-the-art in aerosol science indicates, vapor nucleation in the plasma sheath will likely remain a topic plagued with persistent uncertainties in the first years to come. New fundamental experimental and computational investigations will likely not only increase our understanding on this process, but also provide insight in how to optimize its effect for specific applications, especially with regard to cluster and microdroplet chemistry. As an interesting motivation for such research, Lee et al. recently observed spontaneous H_2O_2 generation on aqueous microdroplets [391]. They attributed this phenomenon to autoionization at the air-water interface, causing a strong electric field that subsequently generates an intermediate solvated electron.

7. Summary and outlook

In this Perspective, we gave multiple arguments on why investigating the plasma sheath at the plasma-liquid interface is not only recommended, but also essential, both for an accurate understanding of plasma-liquid interactions and for making progress in the related applications. On a fundamental level, the sheath plays an active role in the fluid dynamics continuity equations and the electrical coupling between the plasma and the liquid phase (see Section 2.1). The sheath models developed for the plasma-solid interface may not be applied at a liquid surface without taking into account several liquid-specific

aspects. These additional effects include fluid dynamical processes, such as evaporation, surface deformations and droplet ejection, as well as electrical factors, such as the formation of an electric double layer, an ion drift-mediated liquid resistivity and the yet unclear mechanisms behind secondary electron emission. More basic research is required to investigate these processes on a microscopic level, in order to assess their influence on the sheath properties. As a possible experimental strategy, different types of liquids can be compared in their effect on the plasma properties and the liquid surface charging for fixed reactor conditions. Ionic liquids and molten salts, for instance, display a negligible evaporation, which makes them a useful reference when investigating the effect of vapor in the sheath. Metallic liquids form an interesting reference with regard to the influence of the electrical liquid properties.

Detailed knowledge on the sheath is crucial to understand the bidirectional mass transfer across the plasma-liquid interface (Section 2.2), which is of prime importance to most applications. Throughout scientific literature, the focus heavily lies on the injection of reactive species from the plasma into the liquid phase. However, also for applications mainly relying on this principle, the emission of liquid species into the gas phase affects the sheath and plasma properties, and thus the entire plasma treatment process. Accordingly, the corresponding desorption, extraction and sputter mechanisms need to be included into the fundamental study of the plasma sheath. With a deeper understanding of such mechanisms, the sheath can be employed as a selective filter for plasma and liquid species, as illustrated in Section 4 for the liquid walls in a fusion reactor. Next to that, the bidirectional mass transfer across the plasma-liquid interface is not simply expected to be influenced by the chemistry in the sheath, but largely based on it for many plasma-liquid systems. The dominance of the sheath chemistry in the species transfer depends on the sheath size, the species lifetimes and mean-free paths, but there are strong reasons to deem it high even in collisionless or relatively thin sheaths, as discussed in Section 2.3. The number of publications on sheath chemistry is remarkably scarce, also for plasma-solid interaction. Therefore, we want to stimulate a higher awareness and more intense research on this topic, as one of the main purposes of this Perspective Article. Accordingly, Section 5 illustrated how the sheath can be used to tune specific chemical reactions for nanomaterial and chemical synthesis. Section 6 discussed electron emission mechanisms and droplet formation at the plasma-liquid interface, which are also expected to contribute to the interfacial chemistry. Another crucial aspect is the type of sheath formed at the liquid surface, in particular at a liquid anode, as we explained in Section 2.4.

A great part of this work deals with field-induced effects in the condensed phase, as we also believe this aspect deserves more attention. We selected biological materials as an example, because a large body of knowledge already exists about their stimulation by electric fields, and because the related applications in plasma medicine, plasma agriculture and food processing make up some of the strongest drivers in the plasma-liquid research domain. On a cellular level, electroporation and electrostatic disruption of the cell membrane are often considered as possible plasma-induced effects, which can underlie immediate cell death. According to a few recent experimental studies, endocytosis has been identified as the main transfection mechanism, indicating that the fields penetrating the condensed phase may be less intense than the threshold value for electroporation. For an accurate estimation of these fields for various plasma sources, a more profound insight into the sheath properties is required, both in terms of structure and dynamics. The rate of voltage fluctuations over the condensed phase relative to the charging times in the

liquid namely determines the extent to which the field can penetrate. In physiological tissue, this charging time lies around 1 µs, so sub-microsecond fluctuations are required for effective field penetration. Based on this knowledge and an accurate sheath model, specialized plasma sources can be engineered to obtain a desired effect, such as electroporation or electro-endocytosis. As should be emphasized, however, this principle also counts for applications of plasma-liquid systems in general. For example, the plasma-induced fields can regulate key processes in the liquid phase for nanomaterial synthesis. For this purpose, the field-induced effects on a cellular level can serve as inspiration for mechanisms on a nanoparticle level. Additionally, the field also influences the liquid on a molecular level, which is relevant to all applications. In this way, it can regulate in-liquid phase transitions or chemistry, with field intensity and frequency as control parameters, tuned by means of the sheath. The study of the plasma sheath at a liquid surface is therefore tightly linked to the investigation of electromagnetic field effects in the liquid phase.

ACKNOWLEDGMENTS

P. Vanraes wants to thank Dr. Angela Privat Maldonado (University of Antwerp) for the fruitful discussions on Section 3 and Prof. Mark J. Kushner (University of Michigan) for the interesting discussion on reference [198].

AUTHOR CONTRIBUTIONS

Patrick Vanraes: Conceptualization, Methodology, Investigation, Writing - Original Draft, Visualization.
Annemie Bogaerts: Writing - Review & Editing, Supervision.

DATA AVAILABILITY

Data sharing is not applicable to this article as no new data were created or analyzed in this study.

REFERENCES

1. Langmuir, I., *Oscillations in ionized gases.* Proceedings of the National Academy of Sciences of the United States of America, 1928. **14**(8): p. 627.
2. Langmuir, I., *Positive ion currents from the positive column of mercury arcs.* Science, 1923. **58**(1502): p. 290-291.
3. Robertson, S., *Sheaths in laboratory and space plasmas.* Plasma Physics and Controlled Fusion, 2013. **55**(9): p. 093001.
4. Pearton, S.J., et al., *Plasma etching of wide bandgap and ultrawide bandgap semiconductors.* Journal of Vacuum Science & Technology A: Vacuum, Surfaces, and Films, 2020. **38**(2): p. 020802.

5. Mändl, S. and D. Manova, *Modification of metals by plasma immersion ion implantation.* Surface and Coatings Technology, 2019. **365**: p. 83-93.
6. Foster, J.E., *Plasma-based water purification: Challenges and prospects for the future.* Physics of Plasmas, 2017. **24**(5): p. 055501.
7. Hijosa-Valsero, M., et al., *Decontamination of waterborne chemical pollutants by using atmospheric pressure nonthermal plasma: a review.* Environmental Technology Reviews, 2014. **3**(1): p. 71-91.
8. Vanraes, P., A.Y. Nikiforov, and C. Leys, *Electrical discharge in water treatment technology for micropollutant decomposition*, in *Plasma Science and Technology—Progress in Physical States and Chemical Reactions*, T. Mieno, Editor. 2016, IntechOpen. p. 429-478.
9. Magureanu, M., N.B. Mandache, and V.I. Parvulescu, *Degradation of pharmaceutical compounds in water by non-thermal plasma treatment.* Water research, 2015. **81**: p. 124-136.
10. Rezaei, F., et al., *Applications of Plasma-Liquid Systems: A Review.* Materials, 2019. **12**(17): p. 2751.
11. Kanitz, A., et al., *Review on experimental and theoretical investigations of the early stage, femtoseconds to microseconds processes during laser ablation in liquid-phase for the synthesis of colloidal nanoparticles.* Plasma Sources Science and Technology, 2019.
12. Kaushik, N.K., et al., *Plasma and nanomaterials: fabrication and biomedical applications.* Nanomaterials, 2019. **9**(1): p. 98.
13. Levchenko, I., et al., *Lightning under water: Diverse reactive environments and evidence of synergistic effects for material treatment and activation.* Applied Physics Reviews, 2018. **5**(2): p. 021103.
14. Colombo, V., et al., *Atmospheric Pressure Non-Equilibrium Plasma Treatment to Improve the Electrospinnability of Poly (L-Lactic Acid) Polymeric Solution.* Plasma Processes and Polymers, 2014. **11**(3): p. 247-255.
15. Grande, S., et al., *Atmospheric pressure plasma jet treatment of poly-ε-caprolactone polymer solutions to improve electrospinning.* ACS applied materials & interfaces, 2017. **9**(38): p. 33080-33090.
16. Rezaei, F., et al., *Investigation of plasma-induced chemistry in organic solutions for enhanced electrospun PLA nanofibers.* Plasma Processes and Polymers, 2018. **15**(6): p. 1700226.
17. He, Q., Z. Zhu, and S. Hu, *Flowing and nonflowing liquid electrode discharge microplasma for metal ion detection by optical emission spectrometry.* Applied Spectroscopy Reviews, 2014. **49**(3): p. 249-269.
18. Smoluch, M., P. Mielczarek, and J. Silberring, *Plasma-based ambient ionization mass spectrometry in bioanalytical sciences.* Mass spectrometry reviews, 2016. **35**(1): p. 22-34.
19. Pankaj, S.K. and K.M. Keener, *Cold plasma: Background, applications and current trends.* Current Opinion in Food Science, 2017. **16**: p. 49-52.
20. Pignata, C., et al., *A review on microbiological decontamination of fresh produce with nonthermal plasma.* Journal of applied microbiology, 2017. **122**(6): p. 1438-1455.
21. Sarangapani, C., et al., *Recent advances in the application of cold plasma technology in foods.* Annual review of food science and technology, 2018. **9**: p. 609-629.
22. Ohta, T., *Plasma in agriculture*, in *Cold Plasma in Food and Agriculture*. 2016, Elsevier. p. 205-221.
23. Puač, N., M. Gherardi, and M. Shiratani, *Plasma agriculture: A rapidly emerging field.* Plasma Processes and Polymers, 2018. **15**(2): p. 1700174.
24. Randeniya, L.K. and G.J. de Groot, *Non-Thermal Plasma Treatment of Agricultural Seeds for Stimulation of Germination, Removal of Surface Contamination and Other Benefits: A Review.* Plasma Processes and Polymers, 2015. **12**(7): p. 608-623.

25. Aryal, S. and G. Bisht, *New paradigm for a targeted cancer therapeutic approach: a short review on potential synergy of gold nanoparticles and cold atmospheric plasma.* Biomedicines, 2017. **5**(3): p. 38.
26. Bernhardt, T., et al., *Plasma Medicine: Applications of Cold Atmospheric Pressure Plasma in Dermatology.* Oxidative medicine and cellular longevity, 2019. **2019**.
27. Bogaerts, A., et al., *Plasma for cancer treatment: How can RONS penetrate through the cell membrane? Answers from computer modeling.* Frontiers of Chemical Science and Engineering, 2019. **13**(2): p. 253-263.
28. Boonyawan, D. and C. Chutsirimongkol, *Cold Atmospheric Plasma Sources—An Upcoming Innovation in Plasma Medicine*, in *Plasma Science and Technology for Emerging Economies*. 2017, Springer. p. 659-691.
29. Ranjan, R., et al., *Nonthermal plasma in dentistry: an update.* Journal of International Society of Preventive & Community Dentistry, 2017. **7**(3): p. 71.
30. Graves, D.B., *The emerging role of reactive oxygen and nitrogen species in redox biology and some implications for plasma applications to medicine and biology.* Journal of Physics D: Applied Physics, 2012. **45**(26): p. 263001.
31. Wang, Q., et al., *A comparative study of cold atmospheric plasma treatment, chemical versus physical strategy.* Journal of Physics D: Applied Physics, 2020.
32. Bauer, G., *Cold atmospheric plasma and plasma-activated medium: antitumor cell effects with inherent synergistic potential.* Plasma Medicine, 2019. **9**(1).
33. Klämpfl, T.G., et al., *Cold atmospheric air plasma sterilization against spores and other microorganisms of clinical interest.* Appl. Environ. Microbiol., 2012. **78**(15): p. 5077-5082.
34. Sakudo, A., Y. Yagyu, and T. Onodera, *Disinfection and Sterilization Using Plasma Technology: Fundamentals and Future Perspectives for Biological Applications.* International journal of molecular sciences, 2019. **20**(20): p. 5216.
35. Vanraes, P. and A. Bogaerts, *Plasma physics of liquids - a focused review.* Applied Physics Reviews, 2018. **5**(3): p. 031103.
36. Bogaerts, A. and R. Gijbels, *The ion- and atom-induced secondary electron emission yield: numerical study for the effect of clean and dirty cathode surfaces.* Plasma Sources Science and Technology, 2002. **11**(1): p. 27.
37. Cho, Y., et al., *First-principles study on secondary electron emission of MgO surface.* Journal of applied physics, 2007. **101**(8): p. 083710.
38. McCracken, G., *The behaviour of surfaces under ion bombardment.* Reports on Progress in Physics, 1975. **38**(2): p. 241.
39. Bohra, D., et al., *Modeling the electrical double layer to understand the reaction environment in a CO2 electrocatalytic system.* Energy & Environmental Science, 2019. **12**(11): p. 3380-3389.
40. Guriyanova, S., V.G. Mairanovsky, and E. Bonaccurso, *Superviscosity and electroviscous effects at an electrode/aqueous electrolyte interface: An atomic force microscope study.* Journal of colloid and interface science, 2011. **360**(2): p. 800-804.
41. Ji, Q., et al., *Electric double-layer effects induce separation of aqueous metal ions.* ACS nano, 2015. **9**(11): p. 10922-10930.
42. Starikovskiy, A., et al., *Non-equilibrium plasma in liquid water: dynamics of generation and quenching.* Plasma Sources Science and Technology, 2011. **20**(2): p. 024003.
43. Wexler, A.D., et al., *Non-equilibrium thermodynamics and collective vibrational modes of liquid water in an inhomogeneous electric field.* Physical Chemistry Chemical Physics, 2016. **18**(24): p. 16281-16292.
44. Kolb, J., et al. *The permittivity of water under high dielectric stress*. in *2005 IEEE Pulsed Power Conference*. 2005. IEEE.

45. Linz, N., et al., *Wavelength dependence of nanosecond infrared laser-induced breakdown in water: Evidence for multiphoton initiation via an intermediate state.* Physical Review B, 2015. **91**(13): p. 134114.
46. Lazic, V. and S. Jovićević, *Laser induced breakdown spectroscopy inside liquids: processes and analytical aspects.* Spectrochimica Acta Part B: Atomic Spectroscopy, 2014. **101**: p. 288-311.
47. Linz, N., et al., *Wavelength dependence of femtosecond laser-induced breakdown in water and implications for laser surgery.* Physical Review B, 2016. **94**(2): p. 024113.
48. Dharmadhikari, J., et al., *Optical control of filamentation-induced damage to DNA by intense, ultrashort, near-infrared laser pulses.* Scientific reports, 2016. **6**(1): p. 1-9.
49. Sacchi, C., *Laser-induced electric breakdown in water.* Josa b, 1991. **8**(2): p. 337-345.
50. Minardi, S., et al., *Energy deposition dynamics of femtosecond pulses in water.* Applied Physics Letters, 2014. **105**(22): p. 224104.
51. Ambrosio, F., G. Miceli, and A. Pasquarello, *Structural, dynamical, and electronic properties of liquid water: A hybrid functional study.* The Journal of Physical Chemistry B, 2016. **120**(30): p. 7456-7470.
52. Chen, W., et al., *Ab initio electronic structure of liquid water.* Physical review letters, 2016. **117**(18): p. 186401.
53. Delgado, H.E., et al., *Chemical analysis of secondary electron emission from a water cathode at the interface with a nonthermal plasma.* Langmuir, 2020. **36**(5): p. 1156-1164.
54. Coons, M.P., Z.-Q. You, and J.M. Herbert, *The hydrated electron at the surface of neat liquid water appears to be indistinguishable from the bulk species.* Journal of the American Chemical Society, 2016. **138**(34): p. 10879-10886.
55. Herbert, J.M. and M.P. Coons, *The hydrated electron.* Annual review of physical chemistry, 2017. **68**: p. 447-472.
56. Coons, M.P. and J.M. Herbert, *Quantum chemistry in arbitrary dielectric environments: Theory and implementation of nonequilibrium Poisson boundary conditions and application to compute vertical ionization energies at the air/water interface.* The Journal of chemical physics, 2018. **148**(22): p. 222834.
57. Casey, J.R., B.J. Schwartz, and W.J. Glover, *Free energies of cavity and noncavity hydrated electrons near the instantaneous air/water interface.* The journal of physical chemistry letters, 2016. **7**(16): p. 3192-3198.
58. Herbert, J.M., *Structure of the aqueous electron.* Physical Chemistry Chemical Physics, 2019. **21**(37): p. 20538-20565.
59. Doyle, C.C., Y. Shi, and T.L. Beck, *The importance of the water molecular quadrupole for estimating interfacial potential shifts acting on ions near the liquid–vapor interface.* The Journal of Physical Chemistry B, 2019. **123**(15): p. 3348-3358.
60. Cendagorta, J.R. and T. Ichiye, *The surface potential of the water–vapor interface from classical simulations.* The Journal of Physical Chemistry B, 2015. **119**(29): p. 9114-9122.
61. Leung, K., *Surface potential at the air− water interface computed using density functional theory.* The Journal of Physical Chemistry Letters, 2010. **1**(2): p. 496-499.
62. Kathmann, S.M., I.-F.W. Kuo, and C.J. Mundy, *Electronic effects on the surface potential at the vapor− liquid interface of water.* Journal of the American Chemical Society, 2008. **130**(49): p. 16556-16561.
63. Xiong, H., et al., *Strong electric field observed at the interface of aqueous microdroplets.* The Journal of Physical Chemistry Letters, 2020. **11**(17): p. 7423-7428.
64. Jirsak, J., et al., *Aqueous electrolyte surfaces in strong electric fields: molecular insight into nanoscale jets and bridges.* Molecular Physics, 2015. **113**(8): p. 848-853.

65. Bruggeman, P., et al., *DC electrical breakdown in a metal pin–water electrode system.* IEEE transactions on plasma science, 2008. **36**(4): p. 1138-1139.
66. Namin, R.M. and Z. Karimi, *Dynamics of a vertical water bridge.* arXiv preprint arXiv:1309.2222, 2013.
67. Bruggeman, P. and C. Leys, *Non-thermal plasmas in and in contact with liquids.* Journal of Physics D: Applied Physics, 2009. **42**(5): p. 053001.
68. Bruggeman, P.J., et al., *Plasma–liquid interactions: a review and roadmap.* Plasma sources science and technology, 2016. **25**(5): p. 053002.
69. Rifna, E., K.R. Ramanan, and R. Mahendran, *Emerging technology applications for improving seed germination.* Trends in food science & technology, 2019. **86**: p. 95-108.
70. Vancauwenberghe, V., P. Di Marco, and D. Brutin, *Wetting and evaporation of a sessile drop under an external electrical field: A review.* Colloids and Surfaces A: Physicochemical and Engineering Aspects, 2013. **432**: p. 50-56.
71. Zheng, D.-J., et al., *Investigation of EHD-enhanced water evaporation and a novel empirical model.* International Journal of Food Engineering, 2011. **7**(2).
72. Okuno, Y., et al., *Simulation study on the influence of an electric field on water evaporation.* Journal of Molecular Structure: THEOCHEM, 2009. **904**(1-3): p. 83-90.
73. Mezei, P. and T. Cserfalvi, *Electrolyte cathode atmospheric glow discharges for direct solution analysis.* Applied spectroscopy reviews, 2007. **42**(6): p. 573-604.
74. Webb, M.R., F.J. Andrade, and G.M. Hieftje, *Use of electrolyte cathode glow discharge (ELCAD) for the analysis of complex mixtures.* Journal of Analytical Atomic Spectrometry, 2007. **22**(7): p. 766-774.
75. Mottaleb, M.A., J.S. Yang, and H.-J. Kim, *Electrolyte-as-cathode glow discharge (ELCAD)/glow discharge electrolysis at the gas-solution interface.* Applied Spectroscopy Reviews, 2002. **37**(3): p. 247-273.
76. Mezei, P. and T. Cserfalvi, *A critical review of published data on the gas temperature and the electron density in the electrolyte cathode atmospheric glow discharges.* Sensors, 2012. **12**(5): p. 6576-6586.
77. Vanraes, P. and A. Bogaerts, *Laser-induced excitation mechanisms and phase transitions in spectrochemical analysis–Review of the fundamentals.* Spectrochimica Acta Part B: Atomic Spectroscopy, 2021. **179**: p. 106091.
78. Park, Y.S., et al., *Fundamental studies of electrolyte-as-cathode glow discharge-atomic emission spectrometry for the determination of trace metals in flowing water.* Spectrochimica Acta Part B: Atomic Spectroscopy, 1998. **53**(6-8): p. 1167-1179.
79. Roshan, M., A. Babazadeh, and S.S. Kiai, *Effect of impurities on the exclusive parameters of plasma-focus Dena.* IEEE transactions on plasma science, 2006. **34**(6): p. 2568-2571.
80. Fox-Lyon, N., G.S. Oehrlein, and V. Godyak, *Effect of surface derived hydrocarbon impurities on Ar plasma properties.* Journal of Vacuum Science & Technology A: Vacuum, Surfaces, and Films, 2014. **32**(3): p. 030601.
81. Lazarou, C., et al., *Numerical modeling of the effect of the level of nitrogen impurities in a helium parallel plate dielectric barrier discharge.* Plasma Sources Science and Technology, 2015. **24**(3): p. 035012.
82. Raniszewski, G., Z. Kolacinski, and L. Szymanski, *Influence of contaminants on arc properties during treatment of polluted soils in electric arc plasma.* Journal of Advanced Oxidation Technologies, 2012. **15**(1): p. 34-40.
83. Ognier, S., et al., *Analysis of mechanisms at the plasma–liquid interface in a gas–liquid discharge reactor used for treatment of polluted water.* Plasma Chemistry and Plasma Processing, 2009. **29**(4): p. 261-273.

84. Verlackt, C., W. Van Boxem, and A. Bogaerts, *Transport and accumulation of plasma generated species in aqueous solution.* Physical Chemistry Chemical Physics, 2018. **20**(10): p. 6845-6859.
85. Heirman, P., W. Van Boxem, and A. Bogaerts, *Reactivity and stability of plasma-generated oxygen and nitrogen species in buffered water solution: a computational study.* Physical Chemistry Chemical Physics, 2019. **21**(24): p. 12881-12894.
86. Lindsay, A.D., D.B. Graves, and S.C. Shannon, *Fully coupled simulation of the plasma liquid interface and interfacial coefficient effects.* Journal of Physics D: Applied Physics, 2016. **49**(23): p. 235204.
87. Liu, Z., et al., *Physicochemical processes in the indirect interaction between surface air plasma and deionized water.* Journal of Physics D: Applied Physics, 2015. **48**(49): p. 495201.
88. Lietz, A.M. and M.J. Kushner, *Air plasma treatment of liquid covered tissue: long timescale chemistry.* Journal of Physics D: Applied Physics, 2016. **49**(42): p. 425204.
89. Kruszelnicki, J., A.M. Lietz, and M.J. Kushner, *Atmospheric pressure plasma activation of water droplets.* Journal of Physics D: Applied Physics, 2019. **52**(35): p. 355207.
90. Nathanson, G.M., *Molecular beam studies of gas-liquid interfaces.* Annu. Rev. Phys. Chem., 2004. **55**: p. 231-255.
91. Benjamin, I., *Solute dynamics at aqueous interfaces.* Chemical Physics Letters, 2009. **469**(4-6): p. 229-241.
92. Brągiel, P., *Surface reactions in an external electrostatic field.* Surface science, 1992. **266**(1-3): p. 35-39.
93. Yabe, T., et al., *Role of electric field and surface protonics on low-temperature catalytic dry reforming of methane.* ACS Sustainable Chemistry & Engineering, 2019. **7**(6): p. 5690-5697.
94. Landolt, D. and P. Marcus, *Introduction to surface reactions: electrochemical basis of corrosion.* CORROSION TECHNOLOGY-NEW YORK AND BASEL-, 2002. **17**: p. 1-18.
95. Wang, C., et al., *Combining plasmonics and electrochemistry at the nanoscale.* Current Opinion in Electrochemistry, 2018. **7**: p. 95-102.
96. Muhl, S. and A. Pérez, *The use of hollow cathodes in deposition processes: A critical review.* Thin Solid Films, 2015. **579**: p. 174-198.
97. Franklin, R., *The plasma–sheath boundary region.* Journal of Physics D: Applied Physics, 2003. **36**(22): p. R309.
98. Landheer, K., et al., *Chemical sputtering by H2+ and H3+ ions during silicon deposition.* Journal of Applied Physics, 2016. **120**(5): p. 053304.
99. Stoffels, E., et al., *Near-surface generation of negative ions in low-pressure discharges.* Journal of Vacuum Science & Technology A: Vacuum, Surfaces, and Films, 2001. **19**(5): p. 2109-2115.
100. Stoffels, E., W. Stoffels, and G. Kroesen, *Plasma chemistry and surface processes of negative ions.* Plasma Sources Science and Technology, 2001. **10**(2): p. 311.
101. Conway, J., et al., *Using the resonance hairpin probe and pulsed photodetachment technique as a diagnostic for negative ions in oxygen plasma.* Plasma Sources Science and Technology, 2010. **19**(6): p. 065002.
102. von Keudell, A., *Surface processes during thin-film growth.* Plasma Sources Science and Technology, 2000. **9**(4): p. 455.
103. Stoffels, E., Y. Sakiyama, and D.B. Graves, *Cold atmospheric plasma: charged species and their interactions with cells and tissues.* IEEE Transactions on plasma science, 2008. **36**(4): p. 1441-1457.
104. Girod, M., et al., *Accelerated bimolecular reactions in microdroplets studied by desorption electrospray ionization mass spectrometry.* Chemical Science, 2011. **2**(3): p. 501-510.

105. Yan, X., R.M. Bain, and R.G. Cooks, *Organic reactions in microdroplets: Reaction acceleration revealed by mass spectrometry.* Angewandte Chemie International Edition, 2016. **55**(42): p. 12960-12972.
106. Cooks, R.G. and X. Yan, *Mass spectrometry for synthesis and analysis.* Annual Review of Analytical Chemistry, 2018. **11**: p. 1-28.
107. Zhang, W., et al., *Microdroplets as Microreactors for Fast Synthesis of Ketoximes and Amides.* The Journal of organic chemistry, 2018. **84**(2): p. 851-859.
108. Cheng, H., et al., *Accelerating Electrochemical Reactions in a Voltage-Controlled Interfacial Microreactor.* Angewandte Chemie International Edition, 2020. **59**(45): p. 19862-19867.
109. Ciampi, S., et al., *Harnessing electrostatic catalysis in single molecule, electrochemical and chemical systems: a rapidly growing experimental tool box.* Chemical Society Reviews, 2018. **47**(14): p. 5146-5164.
110. Shaik, S., et al., *Structure and reactivity/selectivity control by oriented-external electric fields.* Chemical Society Reviews, 2018. **47**(14): p. 5125-5145.
111. Liu, D.-X., et al., *Wall fluxes of reactive oxygen species of an rf atmospheric-pressure plasma and their dependence on sheath dynamics.* Journal of Physics D: Applied Physics, 2012. **45**(30): p. 305205.
112. Baalrud, S.D., et al., *Interaction of biased electrodes and plasmas: sheaths, double layers, and fireballs.* Plasma Sources Science and Technology, 2020. **29**(5): p. 053001.
113. Sternberg, N. and V. Godyak, *On asymptotic matching and the sheath edge.* IEEE transactions on plasma science, 2003. **31**(4): p. 665-677.
114. Sternberg, N. and V. Godyak, *Patching collisionless plasma and sheath solutions to approximate the plasma-wall problem.* IEEE transactions on plasma science, 2003. **31**(6): p. 1395-1401.
115. Sternberg, N. and V. Godyak, *Reply to comments on" On asymptotic matching and the sheath Edge".* IEEE Transactions on Plasma Science, 2004. **32**(6): p. 2271-2276.
116. Riemann, K.-U., *Comments on" On asymptotic matching and the sheath Edge".* IEEE Transactions on Plasma Science, 2004. **32**(6): p. 2265-2270.
117. Sternberg, N. and V. Godyak, *The Bohm plasma-sheath model and the Bohm criterion revisited.* IEEE transactions on plasma science, 2007. **35**(5): p. 1341-1349.
118. Riemann, K., *Plasma and sheath.* Plasma Sources Science and Technology, 2008. **18**(1): p. 014006.
119. Riemann, K., et al., *The plasma–sheath matching problem.* Plasma physics and controlled fusion, 2005. **47**(11): p. 1949.
120. Riemann, K.-U., *Plasma-sheath transition in the kinetic Tonks-Langmuir model.* Physics of plasmas, 2006. **13**(6): p. 063508.
121. Sternberg, N. *Plasma-Sheath Revisited*. in *APS Annual Gaseous Electronics Meeting Abstracts*. 2012.
122. Hobbs, G. and J. Wesson, *Heat flow through a Langmuir sheath in the presence of electron emission.* Plasma Physics, 1967. **9**(1): p. 85.
123. Guernsey, R.L. and J.H. Fu, *Potential distribution surrounding a photo-emitting, plate in a dilute plasma.* Journal of Geophysical Research, 1970. **75**(16): p. 3193-3199.
124. Cheng, G. and L. Liu, *Effect of surface produced secondary electrons on the sheath structure induced by high-power microwave window breakdown.* Physics of Plasmas, 2011. **18**(3): p. 033507.
125. Li, W., et al., *Measurement of virtual cathode structures in a plasma sheath caused by secondary electrons.* Physics of Plasmas, 2012. **19**(3): p. 030704.
126. Schweigert, I., et al., *Sheath structure transition controlled by secondary electron emission.* Plasma Sources Science and Technology, 2015. **24**(2): p. 025012.

127. Fang, M., D. Fraser, and J. Allen, *The dc properties of a thermally produced plasma.* Journal of Physics D: Applied Physics, 1969. **2**: p. 229-240.
128. Rumbach, P., J.P. Clarke, and D.B. Go, *Electrostatic Debye layer formed at a plasma-liquid interface.* Physical Review E, 2017. **95**(5): p. 053203.
129. Gopalakrishnan, R., et al., *Solvated electrons at the atmospheric pressure plasma–water anodic interface.* Journal of Physics D: Applied Physics, 2016. **49**(29): p. 295205.
130. Levko, D., A. Sharma, and L.L. Raja, *Kinetic modeling of streamer penetration into de-ionized water.* Physics of Plasmas, 2018. **25**(3): p. 033515.
131. Rumbach, P., et al., *The solvation of electrons by an atmospheric-pressure plasma.* Nature communications, 2015. **6**(1): p. 1-7.
132. Bruggeman, P., et al., *Dc excited glow discharges in atmospheric pressure air in pin-to-water electrode systems.* Journal of Physics D: Applied Physics, 2008. **41**(21): p. 215201.
133. Cserfalvi, T., P. Mezei, and P. Apai, *Emission studies on a glow discharge in atmospheric pressure air using water as a cathode.* Journal of Physics D: Applied Physics, 1993. **26**(12): p. 2184.
134. Verreycken, T., P. Bruggeman, and C. Leys, *Anode pattern formation in atmospheric pressure air glow discharges with water anode.* Journal of Applied Physics, 2009. **105**(8): p. 083312.
135. Shirai, N., S. Ibuka, and S. Ishii, *Self-organization pattern in the anode spot of an atmospheric glow microdischarge using an electrolyte anode and axial miniature helium flow.* Applied Physics Express, 2009. **2**(3): p. 036001.
136. Wilson, A., et al., *Self-rotating dc atmospheric-pressure discharge over a water-surface electrode: regimes of operation.* Plasma Sources Science and Technology, 2008. **17**(4): p. 045001.
137. Shirai, N., et al., *Self-organized anode pattern on surface of liquid or metal anode in atmospheric DC glow discharges.* IEEE Transactions on Plasma Science, 2011. **39**(11): p. 2652-2653.
138. Foster, J.E., et al., *Self-organization in 1 atm DC glows with liquid anodes: Current understanding and potential applications.* Plasma Sources Science and Technology, 2020. **29**(3): p. 034004.
139. Shutov, D., et al., *Comparison of the Characteristics of DC Discharges with a Liquid Anode and a Liquid Cathode over Aqueous Solutions of Zinc Nitrate.* Plasma Physics Reports, 2019. **45**(11): p. 997-1004.
140. Zhang, S. and T. Dufour, *Self-organized patterns by a DC pin liquid anode discharge in ambient air: Effect of liquid types on formation.* Physics of Plasmas, 2018. **25**(7): p. 073502.
141. Kovach, Y.E., M.C. García, and J.E. Foster, *Optical emission spectroscopy investigation of a 1-atm dc glow discharge with liquid anode and associated self-organization patterns.* IEEE Transactions on Plasma Science, 2019. **47**(7): p. 3214-3227.
142. Gaisin, A.F., R.S. Basyrov, and E. Son, *Model of glow discharge between an electrolytic anode and a metal cathode.* High Temperature, 2015. **53**(2): p. 188-192.
143. Mezei, P., T. Cserfalvi, and M. Janossy, *The gas temperature in the cathode surface-dark space boundary layer of an electrolyte cathode atmospheric glow discharge (ELCAD).* Journal of Physics D: Applied Physics, 1998. **31**(11): p. L41.
144. Hickling, A. and M. Ingram, *Glow-discharge electrolysis.* Journal of Electroanalytical Chemistry (1959), 1964. **8**(1): p. 65-81.
145. Kulentsan, A., et al. *Physical characteristics of atmospheric pressure glow discharge with liquid electrolyte cathode (water and CuCl2 solutions)*. in *Proc. 28th Int. Conf. on Phenomena in Ionized Gases (Prague, Czech Republic)*. 2007.
146. Smirnov, S.A., et al., *Physical parameters and chemical composition of a nitrogen DC discharge with water cathode.* Plasma chemistry and plasma processing, 2015. **35**(4): p. 639-657.
147. Bobkova, E.S., et al., *Phenol decomposition in water cathode of DC atmospheric pressure discharge in air.* Korean Journal of Chemical Engineering, 2016. **33**(5): p. 1620-1628.

148. Shutov, D.A., et al., *Kinetics and mechanism of Cr (VI) reduction in a water cathode induced by atmospheric pressure DC discharge in air.* Plasma Chemistry and Plasma Processing, 2016. **36**(5): p. 1253-1269.
149. Sirotkin, N., A. Khlyustova, and V. Titov, *Chemical Composition and Processes in the DC Discharge Plasma of Atmospheric Pressure with a Liquid Electrolyte Cathode.* Plasma Chemistry and Plasma Processing, 2020. **40**(1): p. 187-205.
150. Cserfalvi, T. and P. Mezei, *Operating mechanism of the electrolyte cathode atmospheric glow discharge.* Fresenius' journal of analytical chemistry, 1996. **355**(7): p. 813-819.
151. Rumbach, P. and D. Go, *Perspectives on plasmas in contact with liquids for chemical processing and materials synthesis.* Topics in Catalysis, 2017. **60**(12): p. 799-811.
152. André, P., et al., *Experimental study of discharge with liquid non-metallic (tap-water) electrodes in air at atmospheric pressure.* Journal of Physics D: Applied Physics, 2001. **34**(24): p. 3456.
153. Barinov, Y.A. and S. Shkol'nik, *Probe measurements in a discharge with liquid nonmetallic electrodes in air at atmospheric pressure.* Technical Physics, 2002. **47**(3): p. 313-319.
154. Mendis, D., M. Rosenberg, and F. Azam, *A note on the possible electrostatic disruption of bacteria.* IEEE transactions on plasma science, 2000. **28**(4): p. 1304-1306.
155. Gaunt, L.F., C.B. Beggs, and G.E. Georghiou, *Bactericidal action of the reactive species produced by gas-discharge nonthermal plasma at atmospheric pressure: a review.* IEEE Transactions on Plasma Science, 2006. **34**(4): p. 1257-1269.
156. Lunov, O., et al., *The interplay between biological and physical scenarios of bacterial death induced by non-thermal plasma.* Biomaterials, 2016. **82**: p. 71-83.
157. Laroussi, M., D. Mendis, and M. Rosenberg, *Plasma interaction with microbes.* New Journal of Physics, 2003. **5**(1): p. 41.
158. Martines, E., *Interaction of cold atmospheric plasmas with cell membranes in plasma medicine studies.* Japanese Journal of Applied Physics, 2019. **59**(SA): p. SA0803.
159. Park, C.W., et al., *Real-time monitoring of bioaerosols via cell-lysis by air ion and ATP bioluminescence detection.* Biosensors and Bioelectronics, 2014. **52**: p. 379-383.
160. Galván-D'Alessandro, L. and R.A. Carciochi, *Fermentation assisted by pulsed Electric field and ultrasound: a review.* Fermentation, 2018. **4**(1): p. 1.
161. Panagopoulos, D.J., A. Karabarbounis, and L.H. Margaritis, *Mechanism for action of electromagnetic fields on cells.* Biochemical and biophysical research communications, 2002. **298**(1): p. 95-102.
162. Donsì, F., G. Ferrari, and G. Pataro, *Applications of pulsed electric field treatments for the enhancement of mass transfer from vegetable tissue.* Food Engineering Reviews, 2010. **2**(2): p. 109-130.
163. Zimmermann, U. and G. Neil, *Electromanipulation of Cells CRC Press.* Boca Raton, FL, 1996.
164. Kotnik, T., et al., *Cell membrane electroporation-Part 1: The phenomenon.* IEEE Electrical Insulation Magazine, 2012. **28**(5): p. 14-23.
165. Esser, A.T., et al., *Towards solid tumor treatment by irreversible electroporation: intrinsic redistribution of fields and currents in tissue.* Technology in cancer research & treatment, 2007. **6**(4): p. 261-273.
166. Asavasanti, S., et al., *Critical electric field strengths of onion tissues treated by pulsed electric fields.* Journal of food science, 2010. **75**(7): p. E433-E443.
167. Pakhomova, O.N., et al., *Two modes of cell death caused by exposure to nanosecond pulsed electric field.* PloS one, 2013. **8**(7): p. e70278.
168. Yang, N., et al., *Pulsed electric field technology in the manufacturing processes of wine, beer, and rice wine: A review.* Food Control, 2016. **61**: p. 28-38.

169. Yogesh, K., *Pulsed electric field processing of egg products: a review.* Journal of food science and technology, 2016. **53**(2): p. 934-945.
170. Arshad, R.N., et al., *Electrical systems for pulsed electric field applications in the food industry: An engineering perspective.* Trends in Food Science & Technology, 2020.
171. Dymek, K., et al., *Effect of pulsed electric field on the germination of barley seeds.* Lwt-food science and technology, 2012. **47**(1): p. 161-166.
172. Su, B., et al., *Early growth effects of nanosecond pulsed electric field (nsPEFs) exposure on Haloxylon ammodendron.* Plasma Processes and Polymers, 2015. **12**(4): p. 372-379.
173. Starodubtseva, G.P., et al., *Process control of pre-sowing seed treatment by pulsed electric field.* Acta Technologica Agriculturae, 2018. **21**(1): p. 28-32.
174. Ahmed, Z., et al., *Impact of pulsed electric field treatments on the growth parameters of wheat seeds and nutritional properties of their wheat plantlets juice.* Food Science & Nutrition, 2020. **8**(5): p. 2490-2500.
175. Gibot, L. and M.-P. Rols, *Gene transfer by pulsed electric field is highly promising in cutaneous wound healing.* Expert Opinion on Biological Therapy, 2016. **16**(1): p. 67-77.
176. Golberg, A., et al., *Pulsed electric fields for burn wound disinfection in a murine model.* Journal of Burn Care & Research, 2015. **36**(1): p. 7-13.
177. Novickij, V., et al., *Low concentrations of acetic and formic acids enhance the inactivation of Staphylococcus aureus and Pseudomonas aeruginosa with pulsed electric fields.* BMC microbiology, 2019. **19**(1): p. 1-7.
178. Wu, M., et al., *High-voltage pulsed electric fields eliminate Pseudomonas aeruginosa stable infection in a mouse burn model.* Advances in Wound Care, 2020(ja).
179. Nuccitelli, R., et al., *Nanosecond pulsed electric fields cause melanomas to self-destruct.* Biochemical and biophysical research communications, 2006. **343**(2): p. 351-360.
180. Nuccitelli, R., *Application of pulsed electric fields to cancer therapy.* Bioelectricity, 2019. **1**(1): p. 30-34.
181. Frandsen, S.K., M. Vissing, and J. Gehl, *A comprehensive review of calcium electroporation—A novel cancer treatment modality.* Cancers, 2020. **12**(2): p. 290.
182. Steuer, A., et al., *Cell stimulation versus cell death induced by sequential treatments with pulsed electric fields and cold atmospheric pressure plasma.* PloS one, 2018. **13**(10): p. e0204916.
183. Wolff, C.M., et al., *Combination of cold plasma and pulsed electric fields–A rationale for cancer patients in palliative care.* Clinical Plasma Medicine, 2019. **16**: p. 100096.
184. Griseti, E., et al., *pulsed electric Field treatment enhances the Cytotoxicity of plasma-Activated Liquids in a three-Dimensional Human Colorectal Cancer Cell Model.* Scientific reports, 2019. **9**(1): p. 1-15.
185. Wolff, C.M., et al., *Combination Treatment with Cold Physical Plasma and Pulsed Electric Fields Augments ROS Production and Cytotoxicity in Lymphoma.* Cancers, 2020. **12**(4): p. 845.
186. Lin, A., et al., *Non-Thermal plasma as a unique delivery system of short-lived reactive oxygen and nitrogen species for immunogenic cell death in melanoma cells.* Advanced Science, 2019. **6**(6): p. 1802062.
187. Chung, T.-H., et al., *Cell electropermeabilisation enhancement by non-thermal-plasma-treated pbs.* Cancers, 2020. **12**(1): p. 219.
188. Krug, D.M., P.K. Diwakar, and A. Hassanein, *A temporal study of cell death signaling responses to cold atmospheric plasma and electroporation in human cancer cells.* IEEE Transactions on Plasma Science, 2019. **47**(6): p. 2868-2874.
189. Moreau, M., N. Orange, and M. Feuilloley, *Non-thermal plasma technologies: new tools for bio-decontamination.* Biotechnology advances, 2008. **26**(6): p. 610-617.

190. Graves, D.B., *Mechanisms of plasma medicine: coupling plasma physics, biochemistry, and biology.* IEEE Transactions on Radiation and Plasma Medical Sciences, 2017. **1**(4): p. 281-292.
191. Recek, N., et al., *Microplasma Induced Cell Morphological Changes and Apoptosis of Ex Vivo Cultured Human Anterior Lens Epithelial Cells–Relevance to Capsular Opacification.* PloS one, 2016. **11**(11): p. e0165883.
192. Babaeva, N.Y. and M.J. Kushner, *Intracellular electric fields produced by dielectric barrier discharge treatment of skin.* Journal of Physics D: Applied Physics, 2010. **43**(18): p. 185206.
193. Jansky, J., et al., *Experimental–modeling study of an atmospheric-pressure helium discharge propagating in a thin dielectric tube.* IEEE transactions on plasma science, 2012. **40**(11): p. 2912-2919.
194. Begum, A., M. Laroussi, and M.R. Pervez, *Atmospheric pressure He-air plasma jet: Breakdown process and propagation phenomenon.* AIP Advances, 2013. **3**(6): p. 062117.
195. Sretenović, G.B., et al., *Spatio-temporally resolved electric field measurements in helium plasma jet.* Journal of Physics D: Applied Physics, 2014. **47**(10): p. 102001.
196. Wang, X., et al., *Numerical modelling of mutual effect among nearby needles in a multi-needle configuration of an atmospheric air dielectric barrier discharge.* Energies, 2012. **5**(5): p. 1433-1454.
197. Barni, R., et al. *On the use of pulsed Dielectric Barrier Discharges to control the gas-phase composition of atmospheric pressure air plasmas*. in *Journal of Physics: Conference Series*. 2014. IOP Publishing.
198. Babaeva, N.Y., et al., *Ion activation energy delivered to wounds by atmospheric pressure dielectric-barrier discharges: sputtering of lipid-like surfaces.* Journal of Physics D: Applied Physics, 2012. **45**(11): p. 115203.
199. Luengo, E., et al., *Effects of millisecond and microsecond pulsed electric fields on red beet cell disintegration and extraction of betanines.* Industrial Crops and Products, 2016. **84**: p. 28-33.
200. Kempkes, M.A., *Industrial pulsed electric field systems.* Handbook of Electroporation, Springer International Publishing AG, 2017: p. 2-20.
201. Saulis, G. and R. Saulė, *Size of the pores created by an electric pulse: Microsecond vs millisecond pulses.* Biochimica et Biophysica Acta (BBA)-Biomembranes, 2012. **1818**(12): p. 3032-3039.
202. Luengo, E., et al., *A comparative study on the effects of millisecond-and microsecond-pulsed electric field treatments on the permeabilization and extraction of pigments from Chlorella vulgaris.* The Journal of membrane biology, 2015. **248**(5): p. 883-891.
203. Wang, H.-Y. and C. Lu, *Electroporation of mammalian cells in a microfluidic channel with geometric variation.* Analytical chemistry, 2006. **78**(14): p. 5158-5164.
204. Chu, G., H. Hayakawa, and P. Berg, *Electroporation for the efficient transfection of mammalian cells with DNA.* Nucleic acids research, 1987. **15**(3): p. 1311-1326.
205. Ouf, S.A., A.A.H. Mohamed, and W.S. El-Sayed, *Fungal decontamination of fleshy fruit water washes by double atmospheric pressure cold plasma.* CLEAN–Soil, Air, Water, 2016. **44**(2): p. 134-142.
206. Devi, Y., et al., *Influence of cold plasma on fungal growth and aflatoxins production on groundnuts.* Food Control, 2017. **77**: p. 187-191.
207. Jinno, M., et al., *Investigation of plasma induced electrical and chemical factors and their contribution processes to plasma gene transfection.* Archives of biochemistry and biophysics, 2016. **605**: p. 59-66.
208. Tero, R., et al., *Plasma irradiation of artificial cell membrane system at solid–liquid interface.* Applied Physics Express, 2014. **7**(7): p. 077001.
209. Rajapaksha, S.P., et al., *Protein-fluctuation-induced water-pore formation in ion channel voltage-sensor translocation across a lipid bilayer membrane.* Physical Review E, 2015. **92**(5): p. 052719.

210. Zhan, Y., et al., *Low-frequency ac electroporation shows strong frequency dependence and yields comparable transfection results to dc electroporation.* Journal of controlled release, 2012. **160**(3): p. 570-576.
211. Marszalek, P., D. Liu, and T.Y. Tsong, *Schwan equation and transmembrane potential induced by alternating electric field.* Biophysical journal, 1990. **58**(4): p. 1053-1058.
212. Tsong, T.Y., *On electroporation of cell membranes and some related phenomena.* Bioelectrochemistry and Bioenergetics, 1990. **24**(3): p. 271-295.
213. Weaver, J.C., *Electroporation of cells and tissues.* IEEE transactions on plasma science, 2000. **28**(1): p. 24-33.
214. Heinz, V., et al., *Preservation of liquid foods by high intensity pulsed electric fields—basic concepts for process design.* Trends in food science & technology, 2001. **12**(3-4): p. 103-111.
215. Huang, K., et al., *A comparison of pulsed electric field resistance for three microorganisms with different biological factors in grape juice via numerical simulation.* Food and Bioprocess technology, 2014. **7**(7): p. 1981-1995.
216. Yusupov, M., et al., *Synergistic effect of electric field and lipid oxidation on the permeability of cell membranes.* Biochimica et Biophysica Acta (BBA)-General Subjects, 2017. **1861**(4): p. 839-847.
217. Zerrouki, A., et al., *Monte Carlo poration model of cell membranes for application to plasma gene transfection.* Plasma Processes and Polymers, 2016. **13**(6): p. 633-648.
218. Reuter, S., T. Von Woedtke, and K.-D. Weltmann, *The kINPen—a review on physics and chemistry of the atmospheric pressure plasma jet and its applications.* Journal of Physics D: Applied Physics, 2018. **51**(23): p. 233001.
219. Bussiahn, R., et al., *Spatially and temporally resolved measurements of argon metastable atoms in the effluent of a cold atmospheric pressure plasma jet.* Journal of Physics D: Applied Physics, 2010. **43**(16): p. 165201.
220. Yoon, S.-Y., et al., *Bullet-to-streamer transition on the liquid surface of a plasma jet in atmospheric pressure.* Physics of Plasmas, 2017. **24**(1): p. 013513.
221. Yang, Y., et al., *OH Radicals Distribution and Discharge Dynamics of an Atmospheric Pressure Plasma Jet Above Water Surface.* IEEE Transactions on Radiation and Plasma Medical Sciences, 2018. **2**(3): p. 223-228.
222. Wagner, H.-E., et al., *The barrier discharge: basic properties and applications to surface treatment.* Vacuum, 2003. **71**(3): p. 417-436.
223. Kogelschatz, U., *Filamentary, patterned, and diffuse barrier discharges.* IEEE Transactions on plasma science, 2002. **30**(4): p. 1400-1408.
224. Babaeva, N.Y., W. Tian, and M.J. Kushner, *The interaction between plasma filaments in dielectric barrier discharges and liquid covered wounds: electric fields delivered to model platelets and cells.* Journal of Physics D: Applied Physics, 2014. **47**(23): p. 235201.
225. Babaeva, N.Y. and M.J. Kushner, *Reactive fluxes delivered by dielectric barrier discharge filaments to slightly wounded skin.* Journal of Physics D: Applied Physics, 2012. **46**(2): p. 025401.
226. Vanraes, P., et al., *Study of an AC dielectric barrier single micro-discharge filament over a water film.* Scientific reports, 2018. **8**(1): p. 1-11.
227. Laroussi, M., et al., *The resistive barrier discharge.* IEEE Transactions on Plasma Science, 2002. **30**(1): p. 158-159.
228. Wang, X., et al., *Study on an atmospheric pressure glow discharge.* Plasma Sources Science and Technology, 2003. **12**(3): p. 358.
229. Wen, X., et al., *Applications of cold atmospheric plasma for transdermal drug delivery: a review.* Drug Delivery and Translational Research, 2020: p. 1-7.

230. Banga, A.K., S. Bose, and T.K. Ghosh, *Iontophoresis and electroporation: comparisons and contrasts.* International journal of pharmaceutics, 1999. **179**(1): p. 1-19.
231. Shimizu, K., K. Hayashida, and M. Blajan, *Novel method to improve transdermal drug delivery by atmospheric microplasma irradiation.* Biointerphases, 2015. **10**(2): p. 029517.
232. Gelker, M., C.C. Müller-Goymann, and W. Viöl, *Permeabilization of human stratum corneum and full-thickness skin samples by a direct dielectric barrier discharge.* Clinical Plasma Medicine, 2018. **9**: p. 34-40.
233. Liu, X., et al., *A comparative study on the transdermal penetration effect of gaseous and aqueous plasma reactive species.* Journal of Physics D: Applied Physics, 2018. **51**(7): p. 075401.
234. Gratieri, T., D. Kalaria, and Y.N. Kalia, *Non-invasive iontophoretic delivery of peptides and proteins across the skin.* Expert opinion on drug delivery, 2011. **8**(5): p. 645-663.
235. Abla, N., et al., *Contributions of electromigration and electroosmosis to peptide iontophoresis across intact and impaired skin.* Journal of controlled release, 2005. **108**(2-3): p. 319-330.
236. Bakshi, P., et al., *Iontophoretic skin delivery systems: Success and failures.* International Journal of Pharmaceutics, 2020: p. 119584.
237. Wallace, M.S., et al., *Topical delivery of lidocaine in healthy volunteers by electroporation, electroincorporation, or iontophoresis: an evaluation of skin anesthesia.* Regional Anesthesia & Pain Medicine, 2001. **26**(3): p. 229-238.
238. Priya, B., T. Rashmi, and M. Bozena, *Transdermal iontophoresis.* Expert opinion on drug delivery, 2006. **3**(1): p. 127-138.
239. Gratieri, T. and Y.N. Kalia, *Mathematical models to describe iontophoretic transport in vitro and in vivo and the effect of current application on the skin barrier.* Advanced drug delivery reviews, 2013. **65**(2): p. 315-329.
240. Pikal, M.J. and S. Shah, *Transport mechanisms in iontophoresis. III. An experimental study of the contributions of electroosmotic flow and permeability change in transport of low and high molecular weight solutes.* Pharmaceutical research, 1990. **7**(3): p. 222-229.
241. Pikal, M.J., *Transport mechanisms in iontophoresis. I. A theoretical model for the effect of electroosmotic flow on flux enhancement in transdermal iontophoresis.* Pharmaceutical research, 1990. **7**(2): p. 118-126.
242. Pikal, M.J. and S. Shah, *Transport mechanisms in iontophoresis. II. Electroosmotic flow and transference number measurements for hairless mouse skin.* Pharmaceutical research, 1990. **7**(3): p. 213-221.
243. Pikal, M.J., *The role of electroosmotic flow in transdermal iontophoresis.* Advanced drug delivery reviews, 2001. **46**(1-3): p. 281-305.
244. Jadoul, A., J. Bouwstra, and V. Preat, *Effects of iontophoresis and electroporation on the stratum corneum: review of the biophysical studies.* Advanced drug delivery reviews, 1999. **35**(1): p. 89-105.
245. Sugár, I.P., *A theory of the electric field-induced phase transition of phospholipid bilayers.* Biochimica et Biophysica Acta (BBA)-Biomembranes, 1979. **556**(1): p. 72-85.
246. Ruddy, S.B. and B.W. Hadzija, *The role of stratum corneum in electrically facilitated transdermal drug delivery. I. Influence of hydration, tape-stripping and delipidization on the DC electrical properties of skin.* Journal of controlled release, 1995. **37**(3): p. 225-238.
247. Kaneko, T., et al., *Improvement of cell membrane permeability using a cell-solution electrode for generating atmospheric-pressure plasma.* Biointerphases, 2015. **10**(2): p. 029521.
248. Canton, I. and G. Battaglia, *Endocytosis at the nanoscale.* Chemical Society Reviews, 2012. **41**(7): p. 2718-2739.
249. Mettlen, M., et al., *Regulation of clathrin-mediated endocytosis.* Annual review of biochemistry, 2018. **87**: p. 871-896.

250. Jinno, M., et al., *Synergistic effect of electrical and chemical factors on endocytosis in micro-discharge plasma gene transfection.* Plasma Sources Science and Technology, 2017. **26**(6): p. 065016.
251. Vijayarangan, V., et al., *Cold atmospheric plasma parameters investigation for efficient drug delivery in HeLa cells.* IEEE Transactions on Radiation and Plasma Medical Sciences, 2017. **2**(2): p. 109-115.
252. He, Z., et al., *Cold atmospheric plasma induces ATP-dependent endocytosis of nanoparticles and synergistic U373MG cancer cell death.* Scientific reports, 2018. **8**(1): p. 1-11.
253. Mahrour, N., et al., *In vitro increase of the fluid-phase endocytosis induced by pulsed radiofrequency electromagnetic fields: importance of the electric field component.* Biochimica et Biophysica Acta (BBA)-Biomembranes, 2005. **1668**(1): p. 126-137.
254. Moisescu, M.G., et al., *900 MHz modulated electromagnetic fields accelerate the clathrin-mediated endocytosis pathway.* Bioelectromagnetics: Journal of the Bioelectromagnetics Society, The Society for Physical Regulation in Biology and Medicine, The European Bioelectromagnetics Association, 2009. **30**(3): p. 222-230.
255. Baluška, F. and Y.-L. Wan, *Physical control over endocytosis*, in *Endocytosis in Plants*. 2012, Springer. p. 123-149.
256. Kolosnjaj-Tabi, J., et al., *Electric field-responsive nanoparticles and electric fields: physical, chemical, biological mechanisms and therapeutic prospects.* Advanced drug delivery reviews, 2019. **138**: p. 56-67.
257. Chang, C.-C., M. Wu, and F. Yuan, *Role of specific endocytic pathways in electrotransfection of cells.* Molecular Therapy-Methods & Clinical Development, 2014. **1**: p. 14058.
258. Rosazza, C., et al., *Endocytosis and endosomal trafficking of DNA after gene electrotransfer in vitro.* Molecular Therapy-Nucleic Acids, 2016. **5**: p. e286.
259. Wu, M. and F. Yuan, *Membrane binding of plasmid DNA and endocytic pathways are involved in electrotransfection of mammalian cells.* PloS one, 2011. **6**(6): p. e20923.
260. Jørgensen, I.L., G.C. Kemmer, and T.G. Pomorski, *Membrane protein reconstitution into giant unilamellar vesicles: a review on current techniques.* European Biophysics Journal, 2017. **46**(2): p. 103-119.
261. Has, C. and P. Sunthar, *A comprehensive review on recent preparation techniques of liposomes.* Journal of liposome research, 2020. **30**(4): p. 336-365.
262. Morshed, A., et al., *Mechanical characterization of vesicles and cells: A review.* Electrophoresis, 2020. **41**(7-8): p. 449-470.
263. Dimova, R., et al., *Vesicles in electric fields: some novel aspects of membrane behavior.* Soft Matter, 2009. **5**(17): p. 3201-3212.
264. Portet, T., et al., *Destabilizing giant vesicles with electric fields: an overview of current applications.* The Journal of membrane biology, 2012. **245**(9): p. 555-564.
265. Perrier, D.L., L. Rems, and P.E. Boukany, *Lipid vesicles in pulsed electric fields: fundamental principles of the membrane response and its biomedical applications.* Advances in colloid and interface science, 2017. **249**: p. 248-271.
266. Vlahovska, P.M., *Electrohydrodynamics of drops and vesicles.* Annual Review of Fluid Mechanics, 2019. **51**: p. 305-330.
267. Schubert, T. and W. Römer, *How synthetic membrane systems contribute to the understanding of lipid-driven endocytosis.* Biochimica et Biophysica Acta (BBA)-Molecular Cell Research, 2015. **1853**(11): p. 2992-3005.
268. Madl, J., S. Villringer, and W. Römer, *Delving into lipid-driven endocytic mechanisms using biomimetic membranes*, in *Chemical and synthetic approaches in membrane biology*. 2016, Springer. p. 17-36.

269. Schmid, S.L., *Reciprocal regulation of signaling and endocytosis: Implications for the evolving cancer cell.* Journal of Cell Biology, 2017. **216**(9): p. 2623-2632.
270. Stein, H., et al., *Production of isolated giant unilamellar vesicles under high salt concentrations.* Frontiers in physiology, 2017. **8**: p. 63.
271. Stacey, M., et al., *Differential effects in cells exposed to ultra-short, high intensity electric fields: cell survival, DNA damage, and cell cycle analysis.* Mutation Research/Genetic Toxicology and Environmental Mutagenesis, 2003. **542**(1-2): p. 65-75.
272. Chen, N., et al., *Nanosecond electric pulses penetrate the nucleus and enhance speckle formation.* Biochemical and biophysical research communications, 2007. **364**(2): p. 220-225.
273. Zhang, M., et al., *Intense picosecond pulsed electric fields inhibit proliferation and induce apoptosis of HeLa cells.* Molecular medicine reports, 2013. **7**(6): p. 1938-1944.
274. Hua, Y.-Y., et al., *Intense picosecond pulsed electric fields induce apoptosis through a mitochondrial-mediated pathway in HeLa cells.* Molecular medicine reports, 2012. **5**(4): p. 981-987.
275. Zhao, S., A.S. Mehta, and M. Zhao, *Biomedical applications of electrical stimulation.* Cellular and Molecular Life Sciences, 2020. **77**: p. 2681–2699.
276. Nakano, A. and A. Ros, *Protein dielectrophoresis: advances, challenges, and applications.* Electrophoresis, 2013. **34**(7): p. 1085-1096.
277. Viefhues, M. and R. Eichhorn, *DNA dielectrophoresis: Theory and applications a review.* Electrophoresis, 2017. **38**(11): p. 1483-1506.
278. Kim, D., M. Sonker, and A. Ros, *Dielectrophoresis: From molecular to micrometer-scale analytes.* Analytical chemistry, 2018. **91**(1): p. 277-295.
279. Hölzel, R. and R. Pethig, *Protein Dielectrophoresis: I. Status of Experiments and an Empirical Theory.* Micromachines, 2020. **11**(5): p. 533.
280. Zhao, W., R. Yang, and H.Q. Zhang, *Recent advances in the action of pulsed electric fields on enzymes and food component proteins.* Trends in Food Science & Technology, 2012. **27**(2): p. 83-96.
281. Zhao, W., et al., *Pulsed electric fields processing of protein-based foods.* Food and Bioprocess Technology, 2014. **7**(1): p. 114-125.
282. Alirezalu, K., et al., *Pulsed electric field and mild heating for milk processing: a review on recent advances.* Journal of the Science of Food and Agriculture, 2020. **100**(1): p. 16-24.
283. Rodrigues, R.M., et al., *Electric field effects on proteins–Novel perspectives on food and potential health implications.* Food Research International, 2020. **137**: p. 109709.
284. Hammadi, Z. and S. Veesler, *New approaches on crystallization under electric fields.* Progress in Biophysics and Molecular Biology, 2009. **101**(1-3): p. 38-44.
285. Weaver, J.C., et al., *A brief overview of electroporation pulse strength–duration space: A region where additional intracellular effects are expected.* Bioelectrochemistry, 2012. **87**: p. 236-243.
286. Evans, D., et al., *Electric field interactions and aggregation dynamics of ferroelectric nanoparticles in isotropic fluid suspensions.* Physical Review B, 2011. **84**(17): p. 174111.
287. Selyshchev, P., et al., *Non-uniform distribution of ferrofluids spherical particles under external electric field: Theoretical description.* Journal of Molecular Liquids, 2019. **278**: p. 491-495.
288. Kwaadgras, B.W., et al., *Polarizability and alignment of dielectric nanoparticles in an external electric field: Bowls, dumbbells, and cuboids.* The Journal of chemical physics, 2011. **135**(13): p. 134105.
289. Zijlstra, P., et al., *Rotational diffusion and alignment of short gold nanorods in an external electric field.* Physical Chemistry Chemical Physics, 2012. **14**(13): p. 4584-4588.
290. Azari, A., et al., *Directed Self-Assembly of Polarizable Ellipsoids in an External Electric Field.* Langmuir, 2017. **33**(48): p. 13834-13840.

291. Liu, Y., et al., *Manipulation of nanoparticles and biomolecules by electric field and surface tension.* Computer Methods in Applied Mechanics and Engineering, 2008. **197**(25-28): p. 2156-2172.
292. M'hamed, B., et al., *A review on why researchers apply external magnetic field on nanofluids.* International Communications in Heat and Mass Transfer, 2016. **78**: p. 60-67.
293. Li, Q., Y. Xuan, and J. Wang, *Experimental investigations on transport properties of magnetic fluids.* Experimental Thermal and Fluid Science, 2005. **30**(2): p. 109-116.
294. Schulten, K., *Magnetic field effects in chemistry and biology*, in *Festkörperprobleme 22*. 1982, Springer. p. 61-83.
295. Rodgers, C.T., *Magnetic field effects in chemical systems.* Pure and Applied Chemistry, 2009. **81**(1): p. 19-43.
296. Leonard, A.W., *Edge-localized-modes in tokamaks.* Physics of Plasmas, 2014. **21**(9): p. 090501.
297. Tabarés, F.L., *Present status of liquid metal research for a fusion reactor.* Plasma Physics and Controlled Fusion, 2015. **58**(1): p. 014014.
298. Rapp, J., *The challenges of plasma material interactions in nuclear fusion devices and potential solutions.* Fusion Science and Technology, 2017. **72**(3): p. 211-221.
299. Evans, T., *ELM mitigation techniques.* Journal of Nuclear Materials, 2013. **438**: p. S11-S18.
300. Kondo, M. *Forefront of liquid metal technologies for fusion reactors*. in *IOP Conference Series: Earth and Environmental Science*. 2019. IOP Publishing.
301. Andruczyk, D., et al., *A Domestic Program for Liquid Metal PFC Research in Fusion.* Journal of Fusion Energy, 2020. **39**: p. 441–447.
302. Cheng-Yue, L., J.P. Allain, and D. Bai-Quan, *Effects of a liquid lithium curtain as the first wall in a fusion reactor plasma.* Chinese Physics, 2007. **16**(11): p. 3312.
303. Krstic, P., et al., *Unraveling the surface chemistry processes in lithiated and boronized plasma material interfaces under extreme conditions.* Matter and Radiation at Extremes, 2018. **3**(4): p. 165-187.
304. Kondo, M., et al., *Compatibility of reduced activation ferritic martensitic steel JLF-1 with liquid metals Li and Pb–17Li.* Fusion Engineering and Design, 2012. **87**(10): p. 1777-1787.
305. Tabarés, F., et al., *Reactor plasma facing component designs based on liquid metal concepts supported in porous systems.* Nuclear Fusion, 2016. **57**(1): p. 016029.
306. Allain, J.P., M. Coventry, and D. Ruzic, *Collisional and thermal effects on liquid lithium sputtering.* Physical Review B, 2007. **76**(20): p. 205434.
307. Mirnov, S., et al., *Experiments with lithium limiter on T-11M tokamak and applications of the lithium capillary-pore system in future fusion reactor devices.* Plasma Physics and Controlled Fusion, 2006. **48**(6): p. 821.
308. Allain, J.P., D.G. Whyte, and J. Brooks, *Lithium erosion experiments and modelling under quiescent plasma conditions in DIII-D.* Nuclear fusion, 2004. **44**(5): p. 655.
309. Brooks, J., et al., *PSI modeling of liquid lithium divertors for the NSTX tokamak.* Journal of nuclear materials, 2005. **337**: p. 1053-1057.
310. Brooks, J., et al., *Erosion/redeposition analysis of lithium-based liquid surface divertors.* Journal of nuclear materials, 2001. **290**: p. 185-190.
311. Vasileska, I., D. Tskhakaya, and L. Kos, *ITER plasma sheath characteristics during ELMs*, in *46th EPS Conference on Plasma Physics*, S.B. C. Riconda, K. McCarty, K. Lancaster, D. Burgess, P. Brault, D. Farina, Editor. 2019, European Physical Society: Milan, Italy. p. P5.3011.
312. Moritz, J., et al., *The plasma-wall transition layers in the presence of collisions with a magnetic field parallel to the wall.* Physics of Plasmas, 2018. **25**(1): p. 013534.
313. Moritz, J., et al., *Plasma sheath properties in a magnetic field parallel to the wall.* Physics of Plasmas, 2016. **23**(6): p. 062509.

314. Li, D. and S. Wang, *Particle simulation of a magnetized plasma sheath with the magnetic field parallel to the wall.* Physics of Plasmas, 2018. **25**(9): p. 092104.
315. Theilhaber, K. and C. Birdsall, *Kelvin-Helmholtz vortex formation and particle transport in a cross-field plasma sheath.* Physical review letters, 1989. **62**(7): p. 772.
316. Krasheninnikova, N.S., X. Tang, and V.S. Roytershteyn, *Scaling of the plasma sheath in a magnetic field parallel to the wall.* Physics of Plasmas, 2010. **17**(5): p. 057103.
317. Stangeby, P., *The Bohm–Chodura plasma sheath criterion.* Physics of plasmas, 1995. **2**(3): p. 702-706.
318. Chodura, R., *Plasma–wall transition in an oblique magnetic field.* The Physics of Fluids, 1982. **25**(9): p. 1628-1633.
319. Khoramabadi, M., H. Ghomi, and P.K. Shukla, *Numerical investigation of the ion temperature effects on magnetized DC plasma sheath.* Journal of Applied Physics, 2011. **109**(7): p. 073307.
320. Liu, J., F. Wang, and J. Sun, *Properties of plasma sheath with ion temperature in magnetic fusion devices.* Physics of Plasmas, 2011. **18**(1): p. 013506.
321. Pandey, B.P., A. Samarian, and S. Vladimirov, *Plasma sheath in the presence of an oblique magnetic field.* Plasma Physics and Controlled Fusion, 2008. **50**(5): p. 055003.
322. Wang, T.-T., J. Ma, and Z.-A. Wei, *Effect of electron reflection on magnetized plasma sheath in an oblique magnetic field.* Physics of Plasmas, 2015. **22**(9): p. 093505.
323. Chalise, R. and R. Khanal, *A kinetic trajectory simulation model for magnetized plasma sheath.* Plasma Physics and Controlled Fusion, 2012. **54**(9): p. 095006.
324. He, J.-H., Y. Liu, and L. Xu, *Apparatus for preparing electrospun nanofibres: a comparative review.* Materials Science and Technology, 2010. **26**(11): p. 1275-1287.
325. Huang, W., et al., *Effect of magnetic field on stability of jet motion in electrospinning.* Materials and Manufacturing Processes, 2016. **31**(12): p. 1603-1607.
326. Jayaseelan, D. and P. Biji, *Finite element analysis of in-situ alignment of nanoparticles in polymeric nanofibers using magnetic field assisted electrospinning.* Materials Research Express, 2015. **2**(9): p. 095014.
327. Madden, A., et al., *Effect of a homogeneous magnetic field on the electrospraying characteristics of sulfolane ferrofluids.* Journal of Fluid Mechanics, 2017. **833**: p. 430.
328. Zakharov, L.E., *Magnetic propulsion of intense lithium streams in a tokamak magnetic field.* Physical review letters, 2003. **90**(4): p. 045001.
329. Wang, Z. and T. Lei, *Liquid metal MHD effect and heat transfer research in a rectangular duct with micro-channels under a magnetic field.* International Journal of Thermal Sciences, 2020. **155**: p. 106411.
330. Levich, V. and V. Krylov, *Surface-tension-driven phenomena.* Annual Review of Fluid Mechanics, 1969. **1**(1): p. 293-316.
331. Shercliff, J., *Thermoelectric magnetohydrodynamics.* Journal of fluid mechanics, 1979. **91**(2): p. 231-251.
332. Jaworski, M., N. Morley, and D. Ruzic, *Thermocapillary and thermoelectric effects in liquid lithium plasma facing components.* Journal of nuclear materials, 2009. **390**: p. 1055-1058.
333. Jaworski, M., et al., *Thermoelectric magnetohydrodynamic stirring of liquid metals.* Physical review letters, 2010. **104**(9): p. 094503.
334. Bormashenko, E., *Moses effect: Physics and applications.* Advances in colloid and interface science, 2019. **269**: p. 1-6.
335. Laumann, D., *Even liquids are magnetic: observation of the Moses effect and the inverse Moses Effect.* The Physics Teacher, 2018. **56**(6): p. 352-354.
336. Kaneko, T. and R. Hatakeyama, *Plasma–Liquid Interactions for Fabrication of Nanobiomaterials.* in Plasma Processing of Nanomaterials, 2012.

337. Mariotti, D. and R.M. Sankaran, *Perspectives on atmospheric-pressure plasmas for nanofabrication.* Journal of Physics D: Applied Physics, 2011. **44**(17): p. 174023.
338. Krishnakumar, E., V. Prabhudesai, and N. Bhargava Ram. *Controlling molecular fragmentation using low energy electrons*. in *XXV International Conference on Photonic, Electronic and Atomic Collisions*. 2007. Freiburg, Germany.
339. Prabhudesai, V.S., et al., *Functional group dependent site specific fragmentation of molecules by low energy electrons.* Physical review letters, 2005. **95**(14): p. 143202.
340. Orzol, M., et al., *Bond and site selectivity in dissociative electron attachment to gas phase and condensed phase ethanol and trifluoroethanol.* Physical chemistry chemical physics, 2007. **9**(26): p. 3424-3431.
341. Ibănescu, B.C. and M. Allan, *A dramatic difference between the electron-driven dissociation of alcohols and ethers and its relation to Rydberg states.* Physical Chemistry Chemical Physics, 2008. **10**(34): p. 5232-5237.
342. Prabhudesai, V.S., et al., *Functional group dependent dissociative electron attachment to simple organic molecules.* The Journal of chemical physics, 2008. **128**(15): p. 154309.
343. Morishita, T., et al., *Fastest formation routes of nanocarbons in solution plasma processes.* Scientific reports, 2016. **6**: p. 36880.
344. Sagar, D., C.D. Bain, and J.R. Verlet, *Hydrated electrons at the water/air interface.* Journal of the American Chemical Society, 2010. **132**(20): p. 6917-6919.
345. Uhlig, F., et al., *Optical spectroscopy of the bulk and interfacial hydrated electron from ab initio calculations.* The Journal of Physical Chemistry A, 2014. **118**(35): p. 7507-7515.
346. Madarász, Á., P.J. Rossky, and L. Turi, *Excess electron relaxation dynamics at water/air interfaces.* The Journal of chemical physics, 2007. **126**(23): p. 234707.
347. Mota-Lima, A., *The Electrified Plasma/Liquid Interface as a Platform for Highly Efficient CO2 Electroreduction to Oxalate.* The Journal of Physical Chemistry C, 2020. **124**(20): p. 10907-10915.
348. Meesungnoen, J., et al., *Low-energy electron penetration range in liquid water.* Radiation research, 2002. **158**(5): p. 657-660.
349. Rumbach, P., D.M. Bartels, and D.B. Go, *The penetration and concentration of solvated electrons and hydroxyl radicals at a plasma-liquid interface.* Plasma Sources Science and Technology, 2018. **27**(11): p. 115013.
350. Keniley, S. and D. Curreli, *Modeling solvated electron penetration depth and aqueous chemistry at the humid air plasma-water interface.* Bulletin of the American Physical Society, 2020.
351. Martin, D.C., et al., *Experimental confirmation of solvated electron concentration and penetration scaling at a plasma–liquid interface.* Plasma Sources Science and Technology, 2021. **30**(3): p. 03LT01.
352. Go, D.B. *Electrolysis with Plasma Cathodes: Modeling and Experiments to Understand the Electrochemical Interface*. in *ECS Meeting Abstracts*. 2017. IOP Publishing.
353. Hawtof, R., et al., *Catalyst-free, highly selective synthesis of ammonia from nitrogen and water by a plasma electrolytic system.* Science advances, 2019. **5**(1): p. eaat5778.
354. Rumbach, P., R. Xu, and D.B. Go, *Electrochemical production of oxalate and formate from CO2 by solvated electrons produced using an atmospheric-pressure plasma.* Journal of The Electrochemical Society, 2016. **163**(10): p. F1157.
355. Zheng, Y., L. Wang, and P. Bruggeman, *Modeling of an atmospheric pressure plasma-liquid anodic interface: Solvated electrons and silver reduction.* Journal of Vacuum Science & Technology A: Vacuum, Surfaces, and Films, 2020. **38**(6): p. 063005.
356. Gonçalves, I.A., et al., *Reduction of aqueous Ag+ steered by electrochemical plasma: Connecting the bulk pH variation with the reaction pathways for hydrated electrons.* Journal of the Brazilian Chemical Society, 2019. **30**(6): p. 1252-1265.

357. Rumbach, P., et al., *The effect of air on solvated electron chemistry at a plasma/liquid interface.* Journal of Physics D: Applied Physics, 2015. **48**(42): p. 424001.
358. Kareem, T.A. and A.A. Kaliani, *Glow discharge plasma electrolysis for nanoparticles synthesis.* Ionics, 2012. **18**(3): p. 315-327.
359. Ren, J., et al., *Recent progress in the application of glow-discharge electrolysis plasma.* Open Chemistry, 2014. **12**(12): p. 1213-1221.
360. Wang, X., M. Zhou, and X. Jin, *Application of glow discharge plasma for wastewater treatment.* Electrochimica Acta, 2012. **83**: p. 501-512.
361. Harafuji, K. and K. Kawamura, *Sputtering yield as a function of incident ion energy and angle in wurtzite-type GaN crystal.* Japanese journal of applied physics, 2008. **47**(3R): p. 1536.
362. Betz, G. and W. Husinsky, *Molecular dynamics studies of cluster emission in sputtering.* Nuclear Instruments and Methods in Physics Research Section B: Beam Interactions with Materials and Atoms, 1995. **102**(1-4): p. 281-292.
363. Harafuji, K. and K. Kawamura, *Molecular Dynamics of Ion Incident Angle Dependence of Sputtering Yield in Chlorine-Adsorbed GaN Crystal.* Japanese Journal of Applied Physics, 2011. **50**(8S1): p. 08JG03.
364. Harafuji, K. and K. Kawamura, *Chemical Sputtering of GaN Crystal with a Chlorine-Adsorbed Layer.* Japanese Journal of Applied Physics, 2010. **49**(8S1): p. 08JE03.
365. Winter, H., *Scattering of atoms and ions from insulator surfaces.* Progress in surface science, 2000. **63**(7-8): p. 177-247.
366. Shi, M., et al., *Particle emission induced by ionization tracks in water ice.* Nuclear Instruments and Methods in Physics Research Section B: Beam Interactions with Materials and Atoms, 1995. **96**(3-4): p. 524-529.
367. Gaisin, A.F. and E.E.e. Son, *Vapor-air discharges between electrolytic cathode and metal anode at atmospheric pressure.* High temperature, 2005. **43**(1): p. 1-7.
368. Polyakov, O., A. Badalyan, and L. Bakhturova, *The yields of radical products in water decomposition under discharges with electrolytic electrodes.* High Energy Chemistry, 2003. **37**(5): p. 322-327.
369. Glover, W.J. and B.J. Schwartz, *Short-range electron correlation stabilizes noncavity solvation of the hydrated electron.* Journal of chemical theory and computation, 2016. **12**(10): p. 5117-5131.
370. Uehara, S., et al., *Calculations of electronic stopping cross sections for low-energy protons in water.* Radiation Physics and Chemistry, 2000. **59**(1): p. 1-11.
371. Dingfelder, M., M. Inokuti, and H.G. Paretzke, *Inelastic-collision cross sections of liquid water for interactions of energetic protons.* Radiation physics and chemistry, 2000. **59**(3): p. 255-275.
372. Kornev, J., et al., *Generation of active oxidant species by pulsed dielectric barrier discharge in water-air mixtures.* Ozone: Science and Engineering, 2006. **28**(4): p. 207-215.
373. Mesyats, G., *Ecton mechanism of the vacuum arc cathode spot.* IEEE transactions on plasma science, 1995. **23**(6): p. 879-883.
374. Mesyats, G.A., *Ecton mechanism of the cathode spot phenomena in a vacuum arc.* IEEE Transactions on Plasma Science, 2013. **41**(4): p. 676-694.
375. Luedtke, W., et al., *Nanojets, electrospray, and ion field evaporation: Molecular dynamics simulations and laboratory experiments.* The Journal of Physical Chemistry A, 2008. **112**(40): p. 9628-9649.
376. Fuchs, E.C., et al., *Investigation of the mid-infrared emission of a floating water bridge.* Journal of Physics D: Applied Physics, 2012. **45**(47): p. 475401.
377. Vanraes, P., et al. *Time-resolved characterization of a pulsed discharge in a stationary bubble*. in *Journal of Physics: Conference Series*. 2012. IOP Publishing.

378. Hoffer, P., et al., *Penetration of gas discharge through the gas–liquid interface into the bulk volume of conductive aqueous solution.* IEEE Transactions on Plasma Science, 2015. **43**(11): p. 3868-3875.
379. Zhang, R., et al., *Nucleation and growth of nanoparticles in the atmosphere.* Chemical reviews, 2012. **112**(3): p. 1957-2011.
380. Ghan, S.J., et al., *Droplet nucleation: Physically-based parameterizations and comparative evaluation.* Journal of Advances in Modeling Earth Systems, 2011. **3**(4).
381. Kim, M., et al., *Synthesis of nanoparticles by laser ablation: A review.* KONA Powder and Particle Journal, 2017: p. 2017009.
382. Li, C. and R. Signorell, *Understanding vapor nucleation on the molecular level: A review.* Journal of Aerosol Science, 2020: p. 105676.
383. Wyslouzil, B.E. and J. Wölk, *Overview: Homogeneous nucleation from the vapor phase—The experimental science.* The Journal of chemical physics, 2016. **145**(21): p. 211702.
384. Holmes, N., *A review of particle formation events and growth in the atmosphere in the various environments and discussion of mechanistic implications.* Atmospheric Environment, 2007. **41**(10): p. 2183-2201.
385. Anisimov, M.P., et al., *Vapor–gas/liquid nucleation experiments: A review of the challenges.* Journal of aerosol science, 2009. **40**(9): p. 733-746.
386. Gallimberti, I., *The mechanism of the long spark formation.* Le Journal de Physique Colloques, 1979. **40**(C7): p. C7-193-C7-250.
387. Brodskaya, E., A.P. Lyubartsev, and A. Laaksonen, *Molecular dynamics simulations of water clusters with ions at atmospheric conditions.* The Journal of chemical physics, 2002. **116**(18): p. 7879-7892.
388. Alheshibri, M., et al., *A history of nanobubbles.* Langmuir, 2016. **32**(43): p. 11086-11100.
389. Liu, Y. and X. Zhang, *A review of recent theoretical and computational studies on pinned surface nanobubbles.* Chinese Physics B, 2018. **27**(1): p. 014401.
390. Sun, Y., et al., *Stability theories of nanobubbles at solid–liquid interface: A review.* Colloids and Surfaces A: Physicochemical and Engineering Aspects, 2016. **495**: p. 176-186.
391. Lee, J.K., et al., *Spontaneous generation of hydrogen peroxide from aqueous microdroplets.* Proceedings of the National Academy of Sciences, 2019. **116**(39): p. 19294-19298.